



Automatic Torque and Speed Control of a Robotic Gripper

Sheffield Hallam University

Department of Engineering and Mathematics

Faculty of Arts, Computing, Engineering and Science



Report author: Matthew Whelan

Report author ID: 22017112

Module name & code: Individual Project 16-6080-00L

Course name: BEng Mechanical Engineering

Date: 22nd April 2016

Supervisor: Dr Tim Breikin

Preface

This report describes project work carried out within the Engineering Programme at Sheffield Hallam University between September 2015 to May 2016.

The submission of the report is in accordance with the requirements for the award of the degree of Bachelor of Mechanical Engineering under the auspices of the University.

Abstract

This report details the design of a robotic two-fingered gripping machine. The main objective of the project was to develop an automated machine that could output a large range of speeds and forces to a robotic gripper. To achieve this, a DC motor powered, automatic gearbox has been designed, having two gear ratios of 140 and 243, and an Arduino Uno microcontroller incorporated for controlling gripper speed and direction of travel, and later for automatic shifting of the gearbox.

The gear ratio of 140 was designed specifically to optimize the speed of rotation of the gripper fingers. The selected DC motor could output a max no-load speed of 5330rpm at 12V input voltage. With the gearbox, the speed reached at the gripper was 38rpm – fast enough to achieve desirable gripping closing times, yet slow enough to manage accurate control of gripper positioning.

The gear ratio of 243 was designed to multiply the torque reached at the gripper in order to achieve large desirable gripping forces. DC motor voltage source was limited to 6V to avoid motor overheating in stall, and testing showed that the max stall torque at 6V was 1.2Nm giving a max torque at the gripper of 292Nm. This translated to a gripping force of approx. 240N.

A design has been proposed to achieve automatic gear shifting between these two ratios, using the design solutions found in automotive synchronizers, but with some differences. The proposed gear shift mechanism utilises an electric linear motor that is able to actuate a sleeve. The sleeve locks mechanically between two output shafts – the outputs of the two gear ratios. These output shafts are concentric to one another, saving space and removing the need for bearings to be used on the two gear ratios as is the case in traditional transmission synchronizer designs. This improves the reliability of the shift mechanism. Calculations show that a gear change should fully complete in 0.67s using the selected linear motor.

Simulations were run in Simulink for the open-loop model of the machine's transfer function, and gripper output responses showed to be acceptable, with gripper closure times of 0.378s at 12V input voltage. Further simulations were performed for a negative feedback closed-loop model of the system having a proportional only controller. The closed-loop model gave highly desirable gripper positioning control, as well as DC motor source voltage control and slightly less energy consumption than the open-loop system. Gripper closure time was still acceptable, at 1.12s, but slower than the open-loop system. However, the time could be reduced to less than the time taken in the open-loop system but at the cost of additional energy consumption.

A model was developed using Simscape physical modelling software in order to verify the mathematical transfer functions obtained. The model agreed very well with the results from the transfer function, with only a 1.3% discrepancy between transfer function results and the Simscape model results.

Acknowledgements

I'd like to offer many thanks to my supervisor, Dr Tim Breikin, who was there to offer constant support and advice throughout the whole project period.

I would also like to show my deepest appreciation and love to my Grandma, Auntie, and Brother, who I so sadly lost in tragic circumstances midway through my second semester of my final year. Only through the kindness of my Grandma in offering me accommodation in her home during my degree was I able to study in a relaxed, congenial environment. I dedicate this report to her.

Contents

Preface	i
Abstract.....	ii
Acknowledgements.....	iii
List of Figures	vii
List of Tables	viii
Nomenclature	ix
1 Introduction	1
1.1 Rationale	1
1.2 Aim and Objectives	1
1.2.1 Project Objectives	1
1.3 Approach.....	2
2 Background.....	4
2.1 Background Theory.....	4
2.1.1 Theory on Gears.....	4
2.1.2 Theory on Induction Motors	6
2.1.3 Motor Speed Control	7
2.1.4 Theory on Synchronizers.....	8
2.2 Literature Survey.....	10
3 System Design	12
3.1 Project Design Specification.....	12
3.2 Robotic Gripper Design	14
3.3 DC Motor Selection.....	16
3.4 Gearbox Design	19
3.4.1 Motor Gear	19
3.4.2 Head Gear	19
3.4.3 Speed Gears	20
3.4.4 Torque Gears.....	20
3.4.5 Gearbox Layout.....	20
3.5 Gear Shift Mechanism.....	23
3.5.1 Initial Concept	23
3.5.2 Chosen design	25
3.6 Machine Assembly	28
3.7 Electronic Circuitry.....	29

3.8 Software Development	31
4 Simulation and Analysis	32
4.1 Assumptions.....	32
4.2 Development of the Gearbox Mathematical Model.....	32
4.2.1 Finding the Motor Constants	33
4.2.2 System Transfer Function	34
4.3 Gearbox Performance Simulations	34
4.3.1 Method.....	35
4.3.2 Open-Loop Simulation	35
4.3.3 Closed-Loop Simulation	38
4.3.4 Stability	39
4.3.5 Physical Modelling in Simscape	40
5 Discussion.....	43
5.1 Gearbox Performance.....	43
5.1.1 Open-Loop.....	44
5.1.2 Closed-Loop.....	44
5.2 Evaluation of Energy Consumption.....	45
5.2.1 Open-Loop.....	45
5.2.2 Closed-Loop.....	45
5.3 Further Applications.....	46
6 Manufacturing and Costing.....	47
6.1 Gearbox Engineering Drawings.....	47
6.1.1 3D Model, Parts List, General Arrangement and Cross-section	47
6.2 Gripper General Arrangement.....	50
6.3 Estimated Cost to Manufacture.....	51
7 Conclusions	52
7.1 Comparison to the Project Design Specification.....	53
7.2 Further work	53
8 Reflection	55
9 References.....	56
Appendices.....	60
A1. Gripper Vector Analysis.....	60
A2.1 CIM Motor Efficiency Data and Locked Motor Test.....	62
A2.2 Full Motor Test Data.....	64

A3. Gearbox and Gripper Component Inertias.....	67
A4. Arduino Code for DC Motor Control	71
A5. Closed Loop Control Signal Trendline Fitting Using Excel's "Trendline" Tool	72
A6. Bode Plots for the TF of the System.....	73
A7. Engineering Drawings.....	74
A8. CL Response Plots for Increased Proportional Gain.....	90
A9. Gripper Angle at Full Closure.....	91

List of Figures

Figure 1.1: Flowchart displaying the procedure taken in the design of the gearbox	2
Figure 2.1.1: Two gears in mesh	4
Figure 2.1.2: The critical parameters involved in the design of gears.....	5
Figure 2.1.3: Three methods used to obtain variable-voltage output from constant voltage source ...	7
Figure 2.1.4: Assembly sketch of a standard, single-cone synchronizer	8
Figure 2.1.5: Schematic of the process of synchronization	9
Figure 2.2.1: H-Bridge Chopper with mechanical switches	10
Figure 3.2.1: 3D sketch of the finger gripper	14
Figure 3.2.2: Free-body diagram for one half of the gripper.....	15
Figure 3.2.3: Final design of the robotic gripper.....	15
Figure 3.3.1: Current vs Torque for the CIM VEX Motor	17
Figure 3.3.2: Torque vs Speed for the CIM VEX Motor	17
Figure 3.3.3: Motor Output Power vs Motor Current for the CIM VEX Motor.....	18
Figure 3.3.4: Stall Torque vs Source Voltage for the CIM VEX Motor.....	19
Figure 3.4.1: Final Design for the gearbox	21
Figure 3.5.1: Sketch of the initial concept	24
Figure 3.5.2: Gear shift mechanism chosen design	25
Figure 3.5.3: Close up of the inner section of the sleeve, and the torque output shaft	26
Figure 3.5.4: Free Body Diagram for sleeve and shaft teeth	27
Figure 3.6.1: Complete assembly for the machine	28
Figure 3.6.1: Schematic of the circuit used for controlling the DC motor	30
Figure 3.8.1: Flowchart displaying the logic used for controlling the DC Motor	31
Figure 4.2.1: Schematic of the DC permanent magnet armature circuit.....	32
Figure 4.2.2: Schematic of a rotational, mechanical system	33
Figure 4.3.1: Open-loop model representing the machine	35
Figure 4.3.2: Plot of continuous voltage input vs time taken for full closure of gripper.....	36
Figure 4.3.3: Open-loop model with pulse generated input	36
Figure 4.3.4: Example output responses for open-loop	37
Figure 4.3.4: Closed-loop model having a continuous input of 6V.....	38
Figure 4.3.5: Gripper response for a displacement of 1.5 rad in the closed-loop system.....	39
Figure 4.3.6: Output response for OL TF vs the Simscape model.....	42
Figure 4.3.7: Simscape physical model representing the whole machine.....	43

List of Tables

Table 3.6.1: Logic for controlling the direction of rotation of the DC motor	29
Table 4.3.1: Time taken in open-loop for gripper to close fully for a range of input voltages	35
Table 4.3.2: Time taken in open-loop for gripper to close fully for a range of PWM duty cycles	36
Table 4.3.3: Settling time in closed-loop for proportional gains of 1 (unity) and 8.....	39
Table 4.3.4: Values for gains to achieve fastest settling times for varying displacements in CL.....	39
Table 4.3.5: Times taken for gripper to displace from fully open to closed for Simscape model	40

Nomenclature

Roman

\bar{A}	Motor specific electric loading, A/m
B	Rotational damping, Nm/(rad/s)
\bar{B}	Motor specific magnetic loading, Wb/m ²
D	Diameter, m
E	Motor e.m.f, V
e_a	Motor armature back e.m.f, V
F	Force, N
$F_{C,x}$	Force vector of point C in the x-direction, N
I	Electrical current, A
i_a	Motor armature electrical current, A
J	Mass moment of inertia, kg.m ²
J_e	Reflected mass moment of inertia, kg.m ²
K	Control gain
k_b	Motor speed constant
k_t	Motor torque constant
L	Length, m
L_a	Motor armature inductance, H
N	Transmission ratio
n	Number of gear teeth
P	Power, W
P	Controller proportional gain
P_O	Motor output power, W
P_S	Motor supply power, W
R	Electrical resistance, Ω
R_a	Motor armature electrical resistance, Ω
$R(s)$	Reference signal in s-domain
T	Torque, Nm
t	Time, s
$U(s)$	Control signal in s-domain
u	Gear tooth ratio
V	Electrical voltage, V
$V_{C,x}$	Velocity vector of point C in the x-direction, m/s
W	Gear tooth normal force, N

Greek

α	Angular acceleration, rad/s ²
α	Sleeve roof angle, rad
η	Efficiency
θ	Angular displacement, rad or deg
ω	Angular velocity, rad/s

Abbreviations

e.m.f.	Electromotive force
CL	Closed-loop
LTF	Laplace Transfer Function
OL	Open-loop
PS	Physical Signal
PWM	Pulse-Width Modulation
S	Simulink
TF	Transfer Function

1 Introduction

1.1 Rationale

Automation, and specifically the automation of mechanical parts, has proven to be effective for many requirements, certainly in the field of manufacturing but also in many other areas – elevators, personal computers and automated transmissions are just a few examples of automated consumer products. In manufacturing, automation can speed up repetitive tasks and therefore increase production rates, reduce errors and therefore improve quality, reduce waste as well as having many other benefits [1].

A significant proportion of mechanical automation is used in the field of robotics. One aspect of developing effective robotics is in the control of power. Gear boxes serve to appropriately give torque multiplication where required, but power is unaffected (if somewhat diminished due to mechanical efficiencies). To control power, it is necessary to control the power source, in this case an electric motor. With the recent introduction of open-source mini-computers, such as the Raspberry Pi and the Arduino, automatic control has become more readily available and accessible to non-experts. Besides the control of the power input, it is necessary that a machine must be capable of multiplying torque (or dividing speed) if greater magnitudes of torque are required above that in which the motor can provide. Transmissions are the primary machine in many systems for managing the system's powertrain. As discussed by Behrooz Mashadi and David Crolla in Vehicle Powertrain Systems (2011), the "overall powertrain system...defines the dynamic performance and character" of vehicles [2]. Synchronizers (also known as clutches) enable power to be transferred relatively effectively from one gear set to another whilst limiting the damage done to the gearbox's components or the power source (engine). Through the use of computers, the mechanisms that control the synchronizers can be actuated automatically, allowing the control of forces, and therefore governing the time taken for the synchronization process. Similarly, computers can be used to control motor speeds using Pulse Width Modulation (PWM), essential for the purposes of controlling the dynamical behaviour of systems powered by such motors.

Although the control and manipulation of speeds and torques could be applied to many problems, this project shall focus solely on that of a robotic arm gripper. Development for this project shall be based on the RA1-PRO robot arm, developed by AREXX Engineering [3]. The RA1-PRO gripper is originally powered by a servomotor, but for this purpose an electric motor shall be used. A servomotor directly connected to the robotic gripper can only offer torques and speeds within the range of the servomotor. Using a DC motor with a gearbox allows torques and speeds to be delivered to the gripper that are outside the range of the motor.

1.2 Aim and Objectives

To design a machine that can offer high output torques when necessary, and high output speeds when necessary.

1.2.1 Project Objectives

- Determination of the required speeds and torques from the gripper that the machine must output.
- Selection of a suitable DC electric motor.
- Development of a transmission system to automatically transfer the power path between two gear sets.

- Perform simulations of the machine to verify design decisions and analyse gripper performance.

1.3 Approach

The process through which the design of the gearbox was undertaken is laid out in Figure 1.1.

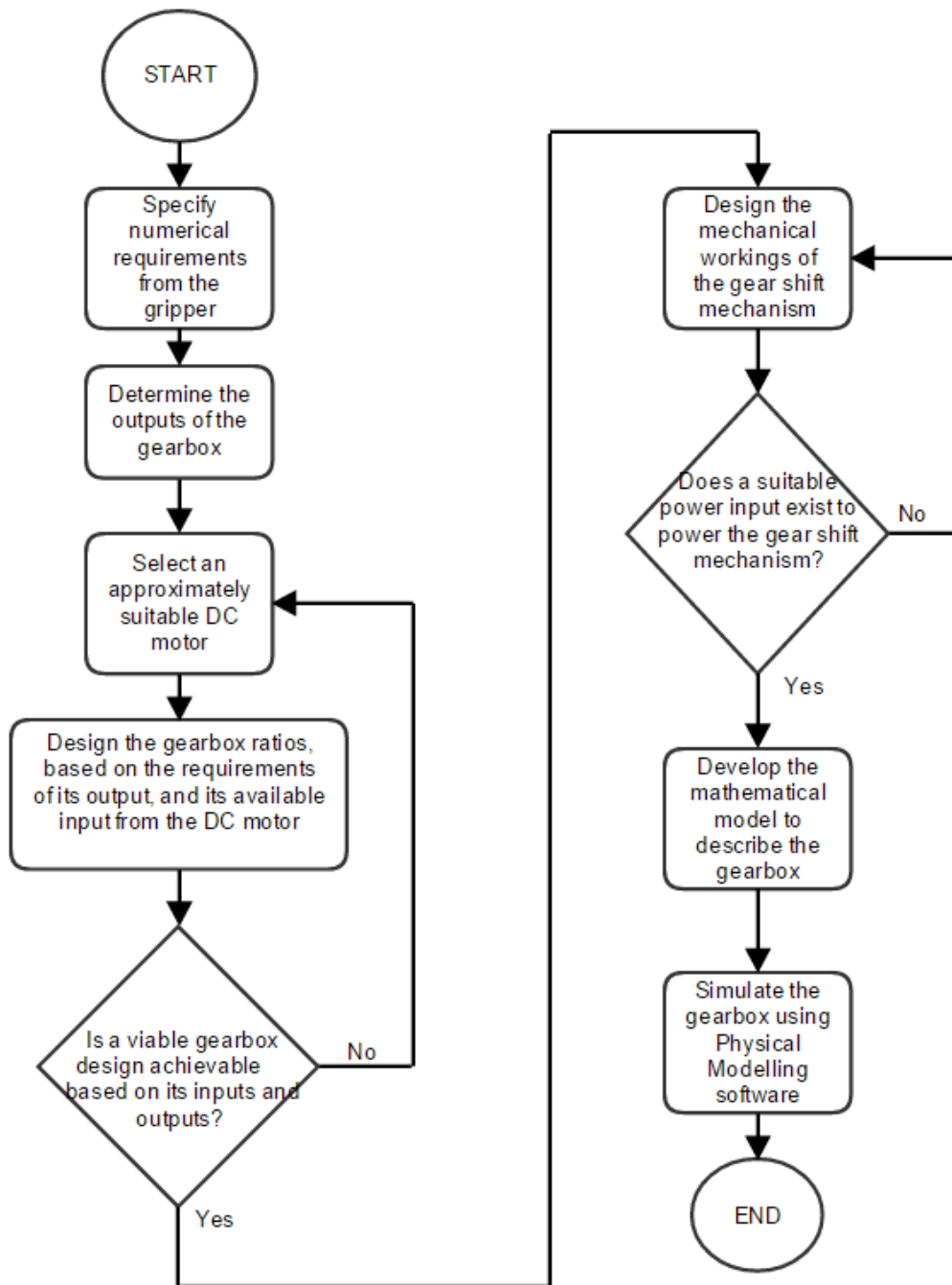


Figure 1.1: Flowchart displaying the procedure taken in the design of the gearbox

The numerical requirements of the gripper are used to determine the characteristics of the gearbox. However, this design approach may also be used for other machines that require the development of a suitable gearbox.

The above flowchart gives only a top level summary of the design approach taken. Within each stage, a more detailed description of the approaches used is discussed in the appropriate design sections (Section 3) of the report.

In order to verify the final design of the gearbox, the following approach was taken:

1. The mathematical model describing the gearbox was Laplace transformed from its differential form, to acquire the model in the s-domain.
2. The relationship between voltage input and angular displacement of the gearbox output shaft was determined.
3. Using Simulink, the model was constructed in open-loop, and simulations run for angular displacement vs time.
4. The same model was re-constructed as a closed-loop system, in order to compare the system response in closed-loop vs open-loop.
5. The gearbox was then modelled via Physical Modelling using Simscape. A comparison of the model could be made against the analytical model in order to verify and add confidence to the results.

Some of the design work undertaken for this project has involved a trial and error and iterative approach, but it was essential that the correct decisions were made and that the final design would fulfil the requirements of the project design specification. A lot of effort was put into the design stages before simulating the system, as a flaw that shows up in the simulations would have taken a lot of time to rectify.

2 Background

2.1 Background Theory

2.1.1 Theory on Gears

D. Jelaska, in his text on Gears and Gear Drives [4] notes that “mechanical power transmissions are units which transfer power from the prime mover to the actuator with the assistance of *rotary motion*”. These units are called mechanical drives, and are positioned between the prime mover (in this case an electric motor) and the actuator (which would be the gripper). Although Jelaska points out a number of reasons as to why mechanical drives are often used, the two functions related most closely to this project are that; 1) the required speed of the machine operating member is very different to that of the prime mover; 2) the driven side requires torques that cannot be achieved from the prime mover alone.

A fundamental parameter of mechanical drives is the transmission ratio, N , given as,

$$N = \frac{D_1}{D_2} = \frac{\omega_1}{\omega_2} \quad (2.1.1)$$

Where,

D = diameter of the respective driving wheels (m)

ω = rotational speed (rad/s)

Radzevich [5] mentions that, for gear pairs, the tooth ratio is often more convenient, since the rotation vectors for each gear can be represented as the summa of two components for each gear. Thus, tooth ratio, u , is defined as,

$$u = \frac{n_1}{n_2} \quad (2.1.2)$$

Where n is the respective number of teeth on each gear.

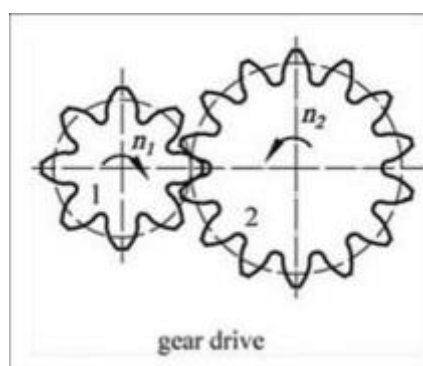


Figure 2.1.1: Two gears in mesh. Image source Jelaska, Gears and Gear Drives, Chapter 1, p. 5

It is also noted by J. Bird and C. Ross [6] that for any arbitrary gear, the torque, T , at that gear is given as the power divided by the gear's rotational speed,

$$T = \frac{P}{\omega} \quad (2.1.3)$$

And hence, from Eqtns. 2.1.1, 2.1.2 and 2.1.3,

$$N = \frac{P_1 T_2}{P_2 T_1} = \frac{T_2}{T_1} \frac{1}{\eta} \quad (2.1.4)$$

Where η is the efficiency of the geartrain.

As discussed by L. Kren [7], the mass moment of inertia of a driver gear can be reflected to its driven gear as follows,

$$J_{reflected} = \frac{J_1}{N^2} \eta \quad (2.1.5)$$

Where,

J = mass moment of inertia (kg.m^2)

And hence, the total effective mass moment of inertia at the driven gear is,

$$J_{2,e} = J_2 + \frac{J_1}{N^2} \eta \quad (2.1.6)$$

Gear Design

Literature on the design of gears is extensive and detailed. But for the purposes of this design, the most important concepts are considered. These are the circular pitch, module and the no. of teeth. Figure 2.1.2 gives an overview of the key dimensions considered when designing gears.

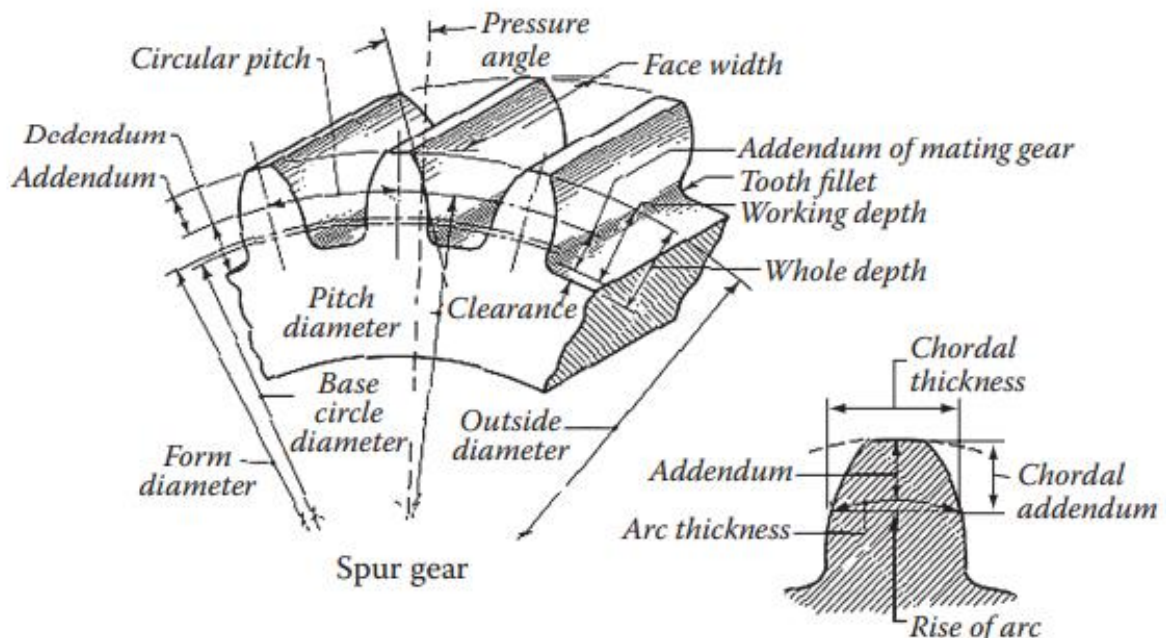


Figure 2.1.2: The critical parameters involved in the design of gears is shown. Image source: Stephen P. Radzevich, Dudley's Handbook of Practical Gear Design and Manufacture, 2012.

The relationships between circular pitch, module, and no. of teeth are given by [8],

$$\text{Circular pitch} = \pi \times \text{module} \quad (2.1.7)$$

$$\text{Pitch diameter} = \text{no. of teeth} \times \text{module} \quad (2.1.8)$$

It should be noted that once values for circular pitch and module are selected, these values will be the same for all gears meshed within the gearbox.

2.1.2 Theory on Induction Motors

The produced torque of a rotor having diameter, D, and length, L, is given as [9],

$$T = (\bar{B}\bar{A})\frac{\pi}{2}D^2L \quad (2.1.9)$$

Where,

\bar{B} = Specific magnetic loading (Wb/m^2)

\bar{A} = Specific electric loading (A/m)

The specific magnetic loading can also be described as the average flux density over the cylindrical surface of the rotor. The specific electric loading is defined as the axial current per unit length of circumference on the rotor. Multiplying the specific magnetic loadings and electric loadings gives the force per unit area on the surface of the rotor.

The power of the rotor can then be determined, by rearranging Eqtn 2.1.3, and substituting into Eqtn 2.1.9,

$$P = T\omega = (\bar{B}\bar{A})\frac{\pi}{2}D^2L\omega \quad (2.1.10)$$

Since $\bar{A} \propto I$ that is passing through the conductor [10], then if \bar{B}, D and L are fixed, Eqtn 2.1.9 becomes,

$$T = C_1I \quad (2.1.11)$$

Where C_1 is a constant for the motor.

This relationship is given in other sources [11] and will be a highly important relationship for this project.

Notice also in Eqtns 2.1.9 and 2.1.10 that the term D^2L is directly proportional to the volume of the rotor. Therefore, as a general rule of thumb, the torque production and power rating of most 'BIL' type motors is proportional to the size of the motor [12].

2.1.3 Motor Speed Control

Hughes [13] discusses that the control of a DC machine relies on controlling the torque, which, as shown in Eqtn 2.1.11, can be controlled by varying the current. To do this, it is necessary to vary the voltage that is outputted from the voltage source. Hughes and Drury detail three methods that can be used to vary the voltage, and can be seen in Figure 2.1.3.

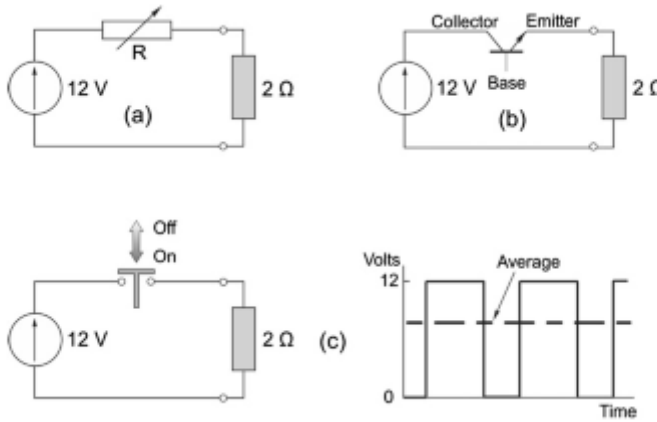


Figure 2.1.3: Three methods that can be used to obtain variable-voltage output from a constant voltage source. Image source: Hughes & Drury, Electric Drives and Motors, p. 41

Method (a) in Figure 2.1.3 simply involves a variable resistor. Ohm's Law [14] states that the current in a circuit is directly proportional to the applied source voltage, but inversely proportional to the resistance,

$$I = \frac{V}{R} \quad (2.1.12)$$

Where resistance, R , is measured in ohms, Ω .

Therefore, including a variable resistor in the circuit will alter the current flowing through the circuit, and hence will vary the voltage drop across the 2Ω resistor shown in Figure 2.1.3(a). It is obvious however, that if, for example, the load voltage at the 2Ω resistor was to be 3V, then the variable resistor must drop 9V, and most of the power would be lost in the variable resistor. Therefore, this method can be very ineffective.

Method (b) works on a similar principle to method (a), but instead makes use of a transistor. The major problem with this method is that lots of the power is burned off inside the transistor, and so efficiency is rather low.

Method (c) is the most efficient. It uses a switch to vary the amount of on/off time, and the average voltage can be taken as the effective voltage across the load. So a voltage of 6V across the load would mean a ratio of 1:1 for on:off time. This method is in theory 100% efficient. Varying the on/off time in this means is known as 'pulse-width modulation' (PWM).

2.1.4 Theory on Synchronizers

Synchronizers for gearboxes can most commonly be found in automotive transmissions. The main components for a single-cone synchronizer can be seen below [15].

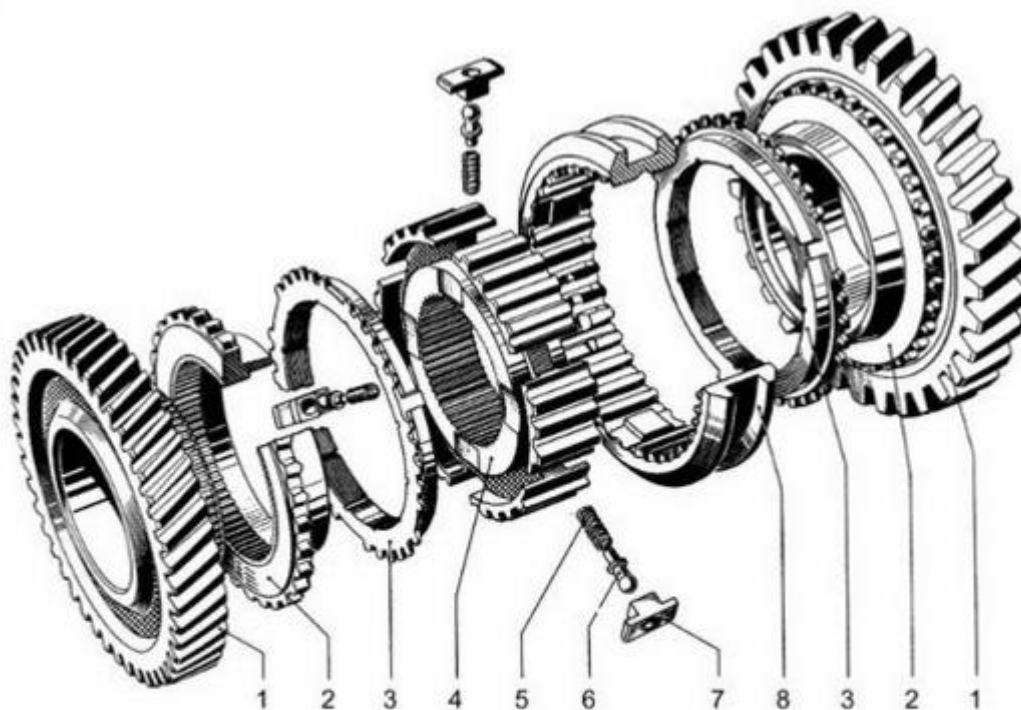


Fig. 9.12. Borg-Warner system single-cone synchronizer (ZF). 1 Idler gear running on needle roller bearings; 2 synchronizer hub with selector teeth and friction cone; 3 main functional element, synchronizer ring with counter-cone and locking toothings; 4 synchronizer body with internal toothings for positive locking with the transmission shaft and external toothings for the gearshift sleeve; 5 compression spring; 6 ball pin; 7 thrust piece; 8 gearshift sleeve with internal dog gearing

Figure 2.1.4: Assembly sketch of a standard, single-cone synchronizer. Image source: Naunheimer et al, Automotive Transmissions: Fundamentals, Selection, Design and Application, p. 316

Both the Idler gear gears (1) rotate independent of the shaft about which the synchronizer body (4) rotates. By locking the idler gears to the synchronizer body, locking of the idler gear to the synchronizer shaft can be achieved.

The synchronizer ring is pushed against the friction cone (2), which acts to synchronize the speeds of the idler and synchronizer. Once the speeds are synchronized, the sleeve can continue through and lock mechanically with the idler gear.

9.2 Layout and Design of Synchronizers 317

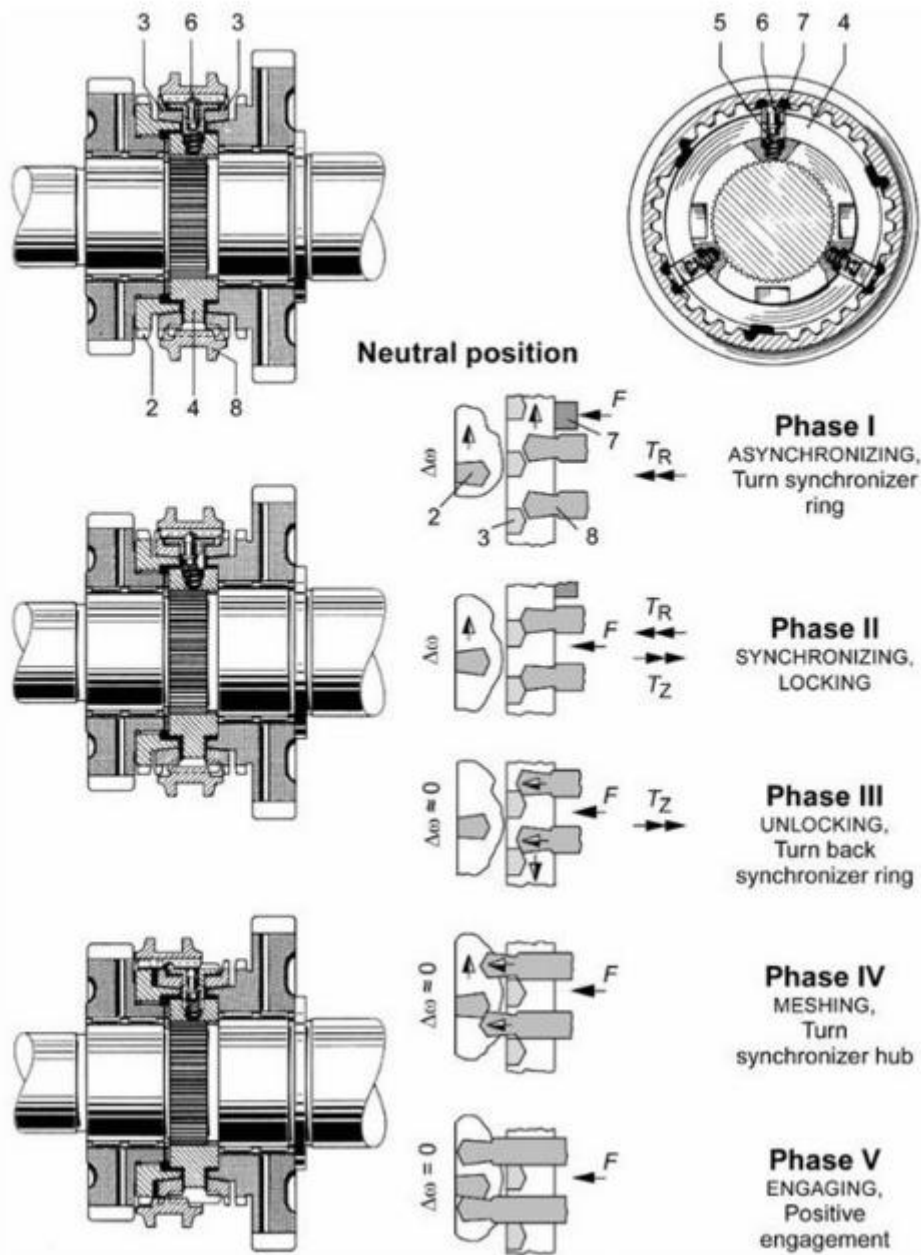


Figure 2.1.5: Schematic of the process of synchronization. Notice there are five distinct phases in the synchronization process. Image source: Naunheimer et al, *Automotive Transmissions: Fundamentals, Selection, Design and Application*, p. 317

For this project, there will be no speed differential between the two gears to be engaged. Thus, the process of synchronizing the speeds can be ignored. However, the mechanism through which a sleeve engages the idler gear to the mainshaft (phases 4 and 5 in Figure 2.1.5) is the fundamental design principle used for the gear shift mechanism in this project.

2.2 Literature Survey

Akhilendra Yadav et al [16] developed an open-loop speed control system for DC motors. The reason open-loop control was used was that closed-loop was deemed to be too complex and unnecessary for simple applications. Again, PWM was used for motor control, due to the loss of power in resistive power control. The DC motor's direction was able to be altered by employing a H-Bridge Chopper, as shown in Figure 2.2.1.

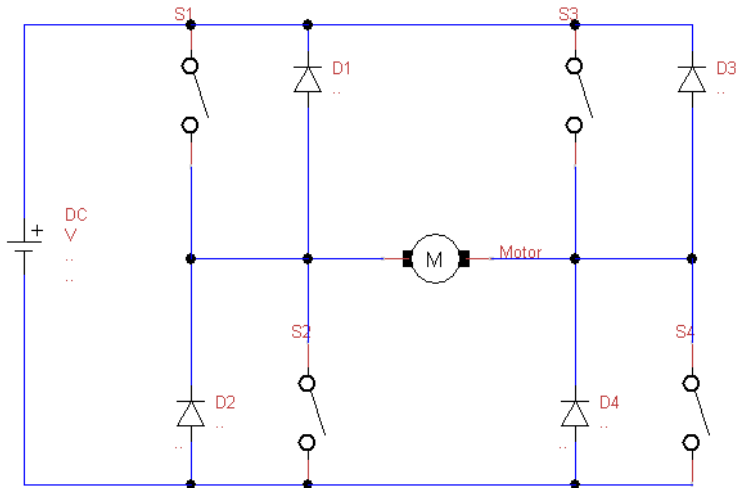


Figure 2.2.1: H-Bridge Chopper with mechanical switches. Diodes protect back current from damaging the circuit.

The logic can be displayed as,

S1 – ON & S4 – ON	CW rotation of motor
S2 – ON & S3 – ON	ACW rotation of motor

However, not having closed-loop feedback for a robotic gripper is unfeasible. Venkataramana Naik and Singh [17] were able to get good torque performance for a DC motor, again by using PWM, but they used space vector PWM. They discussed that conventional PI controllers are difficult for responding to sudden changes in load or speed, and hence employed a fuzzy-based controller.

Weize Liu et al [18] take a similar control approach for the torque control of a brushless DC motor used for an electric vehicle, but they use a fuzzy controller alongside a PID controller. They argue that the fuzzy controller has faster response, smaller overshoot and is more robust.

Fuzzy logic is also employed widely in the control of robotic grippers. Fotios Dimeas et al [19] use a fuzzy controller to regulate the force exerted by their gripper. The gripper is used to harvest strawberries. Using pressure profile sensors, the hardness of the objects is measured.

Shiu-Jer Huang et al [20] described a detailed method of sensing hardness. By applying an initial force to the object of 0.1N, then initiating 5 pulses of 0.1mm interval change, the hardness could be predicted by taking the difference in force required between each interval change. The average of the forces divided by the position difference of 0.1mm would predict the hardness, based on Hooke's law.

Hardness was used in the above two examples so that the max amount of force without deforming the objects could be applied and thus hopefully prevent slip. However, Glossas and Aspragathos [21] take a different approach to preventing slip. Rather than measuring hardness and subsequently using the max allowable force, they instead calculate the minimum required force. By using a rubber material on the gripper, the force is slowly incremented until the gripper can lift without slippage occurring. However, this method could at times be extremely slow.

The most advanced methods of object manipulation through gripper control is through evolutionary algorithms, as is the approach taken by Krenich [22]. Krenich mentions that, generally, most mechanisms use sequential or random search methods to solve the object manipulation problem, as discussed in the above papers. Krenich tested the random search method (RSM), gradient based method, and the evolutionary algorithm (EA) method. EA proved to satisfy all the requirements where the other methods could not.

In terms of designing a gripper, Chiari Lanni and Marco Ceccarelli [23] were able to analyse different mechanisms used for two-finger grippers in order to formulate the most optimum design procedure. The main objective functions used in the design process were grasping index, encumbrance of mechanism, acceleration and velocity of the fingers.

3 System Design

There were two key, distinct systems that were designed. The first is the gearbox, including an automatic gear shift mechanism. The second is the robotic gripper. The design process and the justifications for decisions made in the design shall be discussed in this section.

3.1 Project Design Specification

A Project Design Specification (PDS) was completed before the design process began. A lot of the specifications laid out for the gripper requirements were based on the AREXX RA1-PRO gripper, with the aim to improving on the widest gripper distance, gripper speed and force.

SPECIFICATION FOR: Automatic Torque and Speed Control of a Robotic Gripper				D = demand, W = wish
Date: 08/02/2016 Author: Matthew Whelan				
No.	D/W	Design requirement	Implications, comments and potential design features/concepts	
1	D	FUNCTIONS: <ul style="list-style-type: none"> To vary the forces and speeds of a robotic gripper. To automatically change gear between two differing gear ratios. 		
2		PERFORMANCE		
a	D	Power: Minimum 210W DC motor power output	Power output at gripper is an estimation based on an approx. torque of 60Nm at 3.5rad/s (the required gripper speed defined below).	
b	D	Force: Each gripper finger should be able to apply a max force of greater or equal to 120N.	This includes a coefficient of friction for steel on steel of 0.8, gripping a 10kg mass and including a safety factor of 3	
c	D	Speed: Gripper to move from fully open to fully closed in at least 1.5 seconds during speed operation. Optimum speed is within 0.5 seconds.	Therefore, if the gripper dimensions change, the speed of the gripper must change in order to compensate and offer the necessary closing time.	

	d	W	Timing: Full engagement of gear to be completed in less than 0.6 seconds.	
e		W	Dimensions: Gear box net size should be no larger than 80 x 80 x 50 mm. Gripper's widest distance to be 130mm + 10mm	Gear box will be housed with the gripper, as one unit.
	f	W	Weight: Gear box max weight of 200g	If this machine was connected to a robotic arm, the gear box weight should have as little an impact as possible on the arms performance, hence low weight.

3.2 Robotic Gripper Design

The design of the gripper is based heavily on the AREXX RA1-PRO gripper [3]. The main working principle behind the RA1-PRO gripper is that both fingers can be powered by only powering one finger, through meshing both fingers to each other. This mechanism is illustrated in Figure 3.2.1.

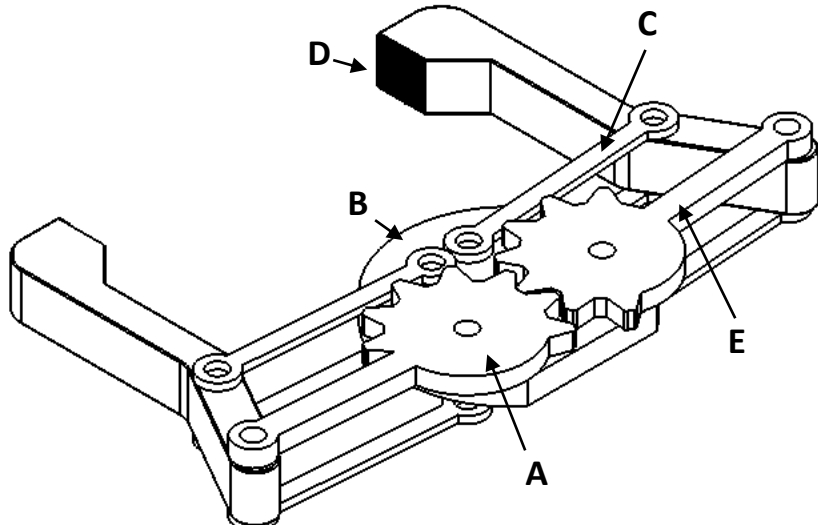


Figure 3.2.1: 3D sketch of the finger gripper. Both fingers are mechanically connected through the meshing of gear teeth (A), and therefore, only one of the fingers needs power. A base plate (B) grounds the second set of links (C) with the first set (E). Grooves on the finger tips (D) add additional friction to the fingers for lifting objects.

The arrangement of the two linkages, (C) and (E), is a common type of linkage known as a parallelogram linkage. Here, the two linkages must be of the same length. It ensures the orientation of the coupler (the finger) does not change during motion [24]. This principle is also proved via vector analysis (see Appendix A1). It is important the finger does not rotate, as the finger tips must remain parallel to one another at all times.

The design of the gripper was modified twice during its design – once because the teeth on the finger gears (A) touched the two linkages (C), and another occasion due to the widest gripper distance not performing to specification, and hence the linkage lengths were increased.

The finger gripper is displayed in vector analysis form in Figure 3.2.2. It can be shown from the vector analysis that the linear velocity in the x-direction of the fingertip, point C, is,

$$V_{C,x} = \omega_1 AO_1 \sin \theta_1 \quad (3.2.1)$$

And the x-component of the force is given as,

$$F_{C,x} = \frac{T_1 \sin \theta_1}{AO_1} \quad (3.2.2)$$

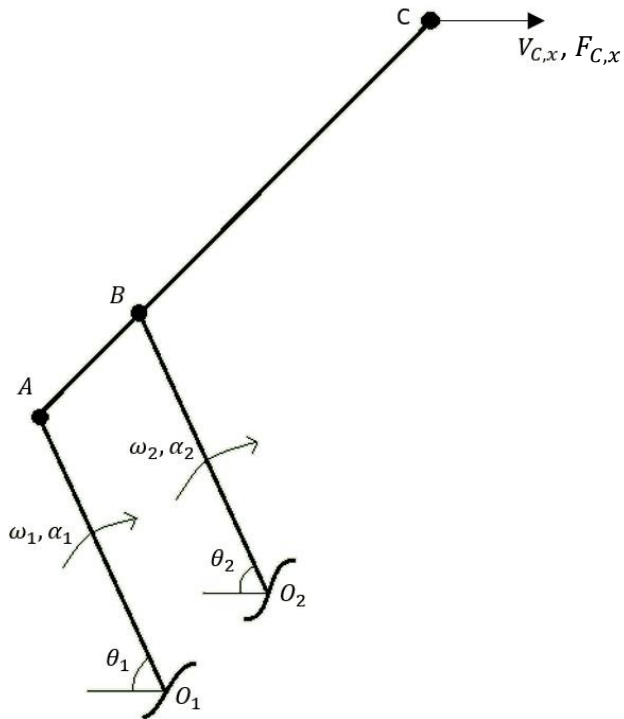


Figure 3.2.2: Free-body diagram for one half of the gripper. The gripper is symmetrical on both sides.

A schematic of the final design is shown in Figure 3.2.3, with key dimensions displayed. In the final design, the power is sent to the gripper through gear (A), the gear on the left in Figure 3.2.3.

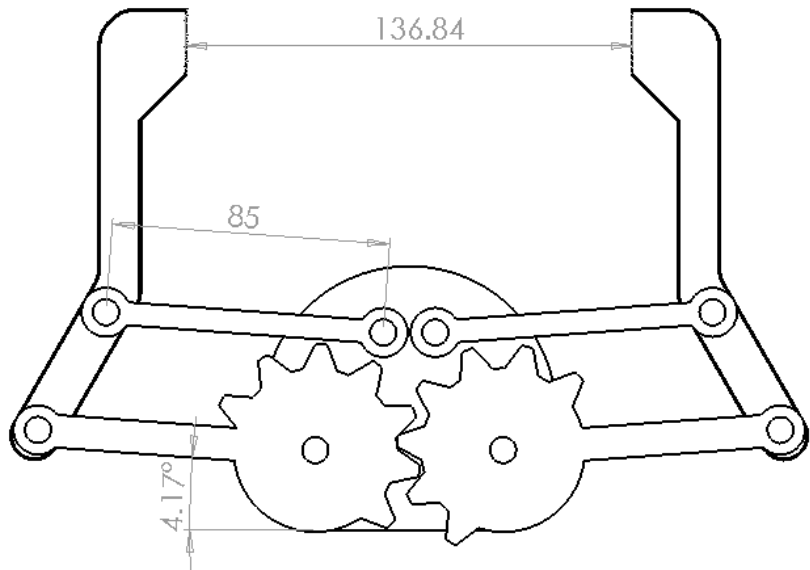


Figure 3.2.3: Final design of the robotic gripper. All dimensions are given in mm. Notice the widest distance of 136.84mm.

In order to facilitate the design of the gearbox, the average rotational speed of linkage AO₁ is determined, as the rotational speed of this linkage is proportional to the speed of the DC motor and will depend on the gear ratio chosen.

It is assumed that angle θ₁ has a range of 0° to 90°, or 0 to 0.5π rad. From the PDS, the closing time of the gripper should be equal to or less than 0.5s as an optimum. Choosing a value slightly less than 0.5s, at 0.45s, gives,

$$\omega_1 \approx \frac{0.5\pi}{0.45} \approx 3.49 \text{ rad/s}$$

The reason 0.45s is chosen is due to the fact that when the gearbox is designed, having an angular velocity of 3.49 rad/s at the gripper gives a manageable, integer ratio of 140 for the gearbox. This is not strictly necessary. However, it also acts as a small safety margin. See Section 3.4 for further detail.

Then, from the specification, each gripper finger should apply 120N of force giving a total gripping force of 240N. From Eqtn 3.2.2, the torque at the gripper, assuming the gripper is fully open so that sinθ₁ is smallest, is,

$$T_1 = \frac{F_{C,x}AO_1}{\sin \theta_1} = \frac{240 \times 0.085}{\sin 4^\circ} = 292 \text{ Nm}$$

These values serve as the output requirements necessary from the gearbox.

3.3 DC Motor Selection

As demanded in the PDS, Section 3.1, the power rating of the DC motor should be at a minimum 210W. A number of motors were considered, but the chosen motor was VEXRobotics' CIM Permanent Magnet Motor [25]. Not only did this motor fulfil the power requirements, with a max power of 337W, but VEXRobotics also provided comprehensive test data. This saved time in the testing of the motor. From this data, the torque vs speed, current vs torque and output power vs current can be seen plotted in Figures 3.3.1, 3.3.2 and 3.3.3 respectively.

But also important was the efficiency. The efficiency of the motor is given by the simple relationship,

$$\text{Efficiency (\%)} = \frac{P_O}{P_S} \times 100 \quad (3.3.1)$$

Where,

P_O = Motor Output Power (W)

P_S = Motor Supplied Power (W)

And from Eqtn 2.1.3, motor output power is given by,

$$P_O = T\omega \quad (3.3.2)$$

Both torque and rotational speed were measured in VEXRobotics' motor test (See Appendix A2.1 for efficiency data).

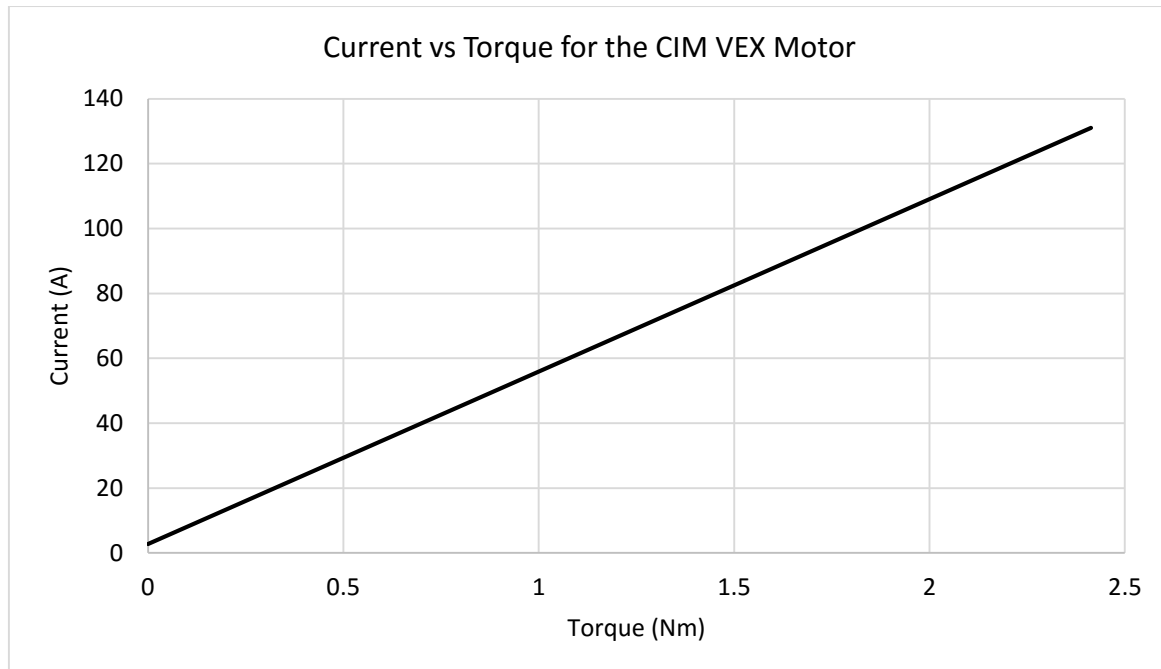


Figure 3.3.1: Current vs Torque for the CIM VEX Motor. Notice there is no motor torque until a current of approx. 3A.

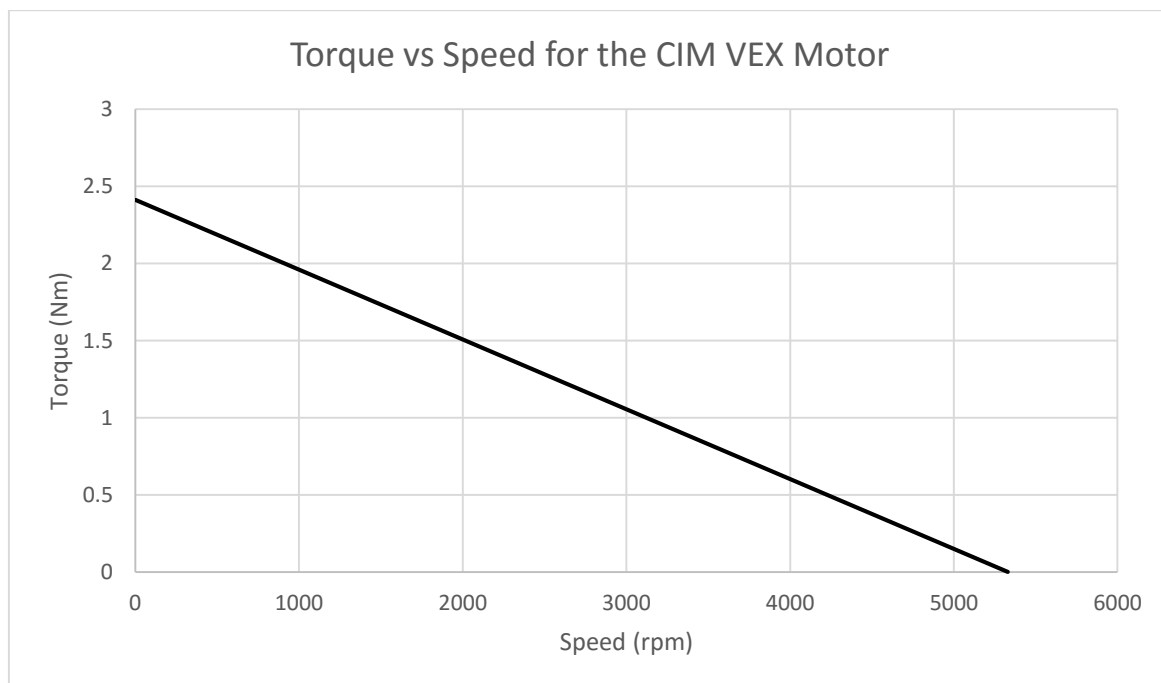


Figure 3.3.2: Torque vs Speed for the CIM VEX Motor. The no load speed has a value of 5330rpm at 12V source voltage.

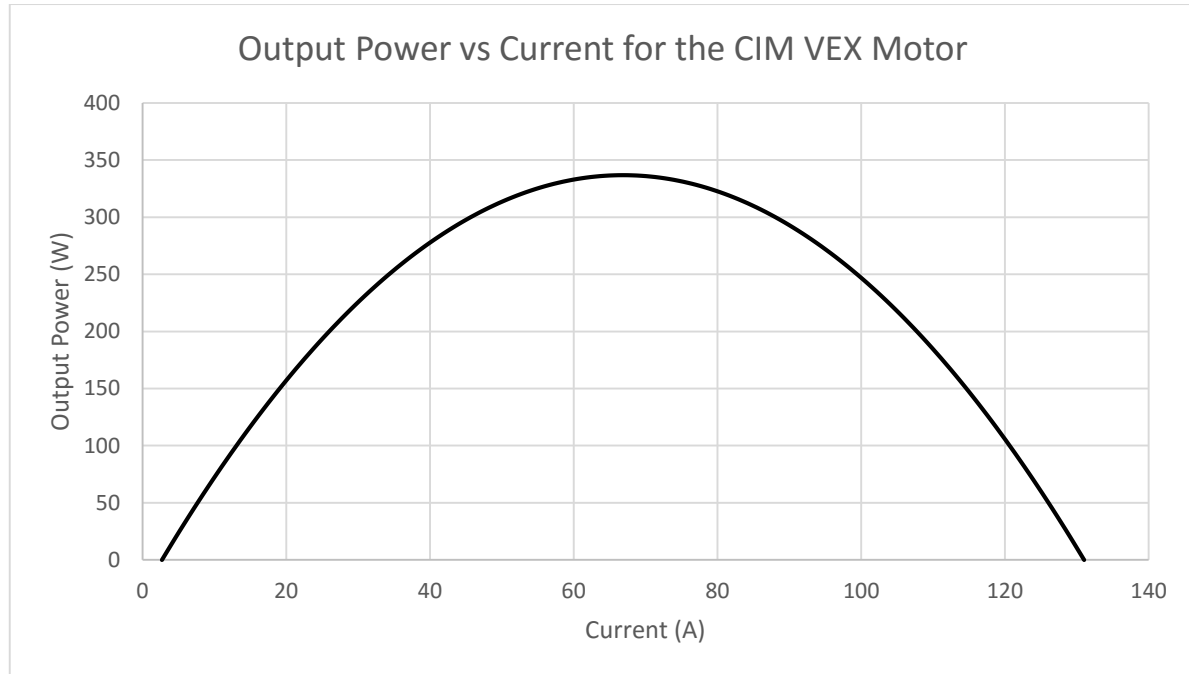


Figure 3.3.3: Motor Output Power vs Motor Current for the CIM VEX Motor.

If the gripper were to grip the object tightly, and essentially seize to move, then the motor would be in a stall situation. However, it is not safe to keep a motor in stall for a long period of time. The relationship between source voltage and back e.m.f. is given as [26],

$$V = E + I_a R_a \quad (3.3.3)$$

And if it is in stall, then the back e.m.f is zero, and hence,

$$V = I_a R_a \quad (3.3.4)$$

Thus the motor will be receiving max current, and the heat energy (I^2R) will be high, having the potential of damaging the motor. Mitigation of this is discussed in the further work section of this report, Section 7.2. However, assume for now that it is safe to run current through the motor during stall.

For high torque applications, it is wise to use a lower source voltage to limit the aforementioned problems. The locked motor test showed that the motor ran best at 6V, in that there was high motor stall torque without burning of the motor (see Appendix A2.1). Unfortunately, data does not exist for the torque vs. current plot at 6V. However, the motor would be running at stall anyway in this application, so the data for the locked rotor test at 6V will be sufficient.

At 6V, the stall torque is 1.29Nm. This should be the max torque. Then, by altering the voltage, the stall torque can steadily be decreased in order to vary the torque output. Figure 3.3.4 displays the relationship between voltage source and stall torque.

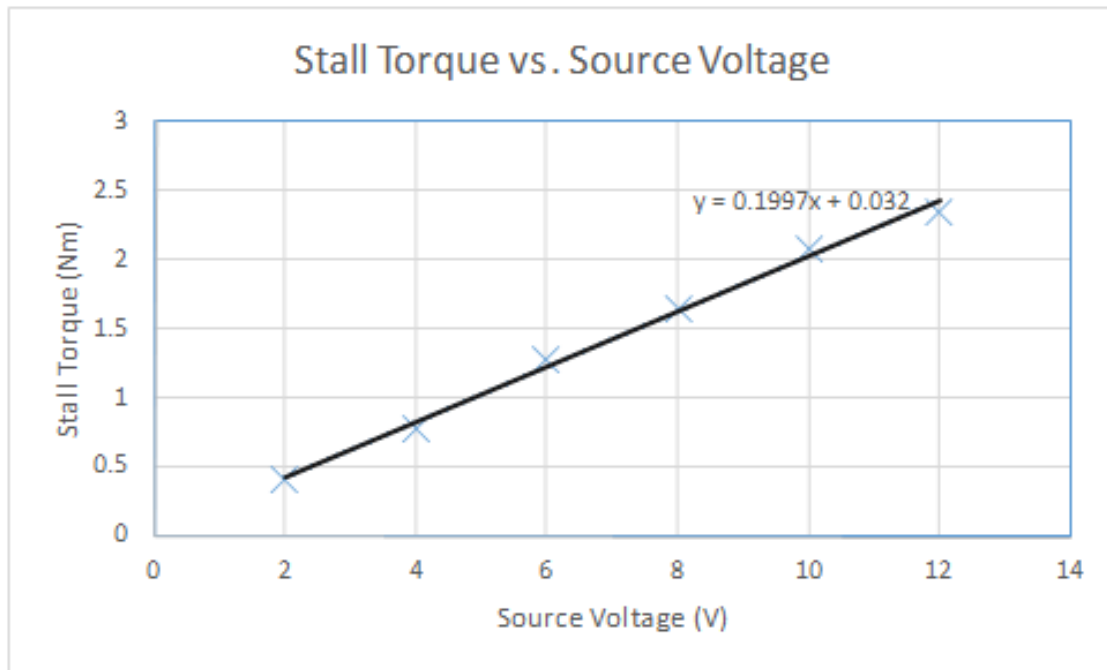


Figure 3.3.4: Stall Torque vs Source Voltage for the CIM VEX Motor. As expected from Eqtn 2.1.11, there is a linear relationship between stall torque and source voltage. Neglecting the small constant of 0.032 in the trendline Eqtn, the stall torque can then be predicted to be one fifth of the magnitude of the source voltage.

The data given for the CIM VEX Permanent Magnet Motor was then used in the designing of the gearbox.

3.4 Gearbox Design

It was necessary for the gearbox to be designed with two gear ratios. As shall be discussed in this section, the ratio needed from the gearbox to achieve the required gearbox output speed was 140. But at this ratio, only a max torque of 180.6Nm could be attained, whereas a torque of 292Nm was needed from the gearbox (see Section 3.2). Therefore, a ratio of 243 was required for torque. An automatic shift mechanism was designed to switch between these two ratios (see Section 3.5).

3.4.1 Motor Gear

The gear to be attached to the motor is designed first. Since the motor shaft has a diameter of 8mm, the gear pitch diameter was set at 20mm, to allow 6mm of material between gear inner radius and outer radius. Number of teeth was set at 40. There is no reason to this, other than it gave a satisfactory circular pitch of 1.5708mm which allowed for acceptable gear teeth thickness (using Eqtn 2.1.7). From Eqtn 2.1.8, the module is calculated to be 0.5 mm per pitch diameter. Module and circular pitch remains the same for all gears.

3.4.2 Head Gear

The head gear meshes with the motor gear, and is the input to the gearbox. The head gear was given 160 teeth. The ratio between motor gear and head gear, from Eqtn 2.1.2, is,

$$N_H = \frac{160}{40} = 4$$

Pitch diameter, from Eqtn 2.1.8 is,

$$Pitch = 160 \times 0.5 = 80\text{mm}$$

3.4.3 Speed Gears

Now, using the data from the DC Motor, the most efficient speeds for the motor to run at is 3250 – 5170 rpm, or 340.34 – 541.40 rad/s. Between these speeds, the motor efficiency is > 50% (see Appendix A2.1). The motor is most efficient at 4640rpm, or 485.90 rad/s. The average speed required from the gripper was 3.49 rad/s. Therefore, the total gearbox ratio for speed should be,

$$N_S = \frac{485.9}{3.49} = 140$$

Taking into account the headset ratio of 4, the ratio for the speed gears should be $140/4 = 35$. This ratio is large, so it was stepped down twice. Each step was through a ratio of $\sqrt{35}$ for easier fitting of the gearbox.

For each gear set, the driver gear was given 10 teeth, thus having a pitch diameter of 5mm.

Therefore, the no. of teeth for the driven gear = $\sqrt{35} \times 10 = 59$, thus having a pitch diameter of 29.5mm.

3.4.4 Torque Gears

From Figure 3.3.4, the stall torque at 6V voltage source is 1.2Nm. The torque required at the gripper is 292Nm. The total torque ratio is therefore,

$$N_T = \frac{292}{1.2} = 243$$

Again, accounting for the headset ratio of 4, the ratio of the torque gears should be $243/4 = 60.75$. Stepping down twice, each ratio is equal to $\sqrt{60.75}$.

For each gear set, the driver gear again was given 10 teeth, thus having a pitch diameter of 5mm.

Therefore, the no. of teeth for the driven gear = $\sqrt{60.75} \times 10 = 78$, having a pitch diameter of 39mm.

3.4.5 Gearbox Layout

The gearbox layout can be seen in Figures 3.4.1, showing both power paths for the Speed (a) and Torque (b) optimised gear ratios.

The output shafts for the two gear ratios have been design to be concentric to each other. I.e. the ‘speed’ output shaft passes through the hollowed ‘torque’ output shaft. This design solution provides the possibility of sliding a sleeve between the two shafts, in the same way synchronizers slide a sleeve between two gear sets to lock them to a second output. This design consideration was made in line with the gear shift mechanism design. For more detail, see Section 3.5.

More detailed engineering drawings for components, including a general assembly, cross-sectional view of the gearbox, and a parts list, can be found in Section 6. See Appendix A7 for all drawings.

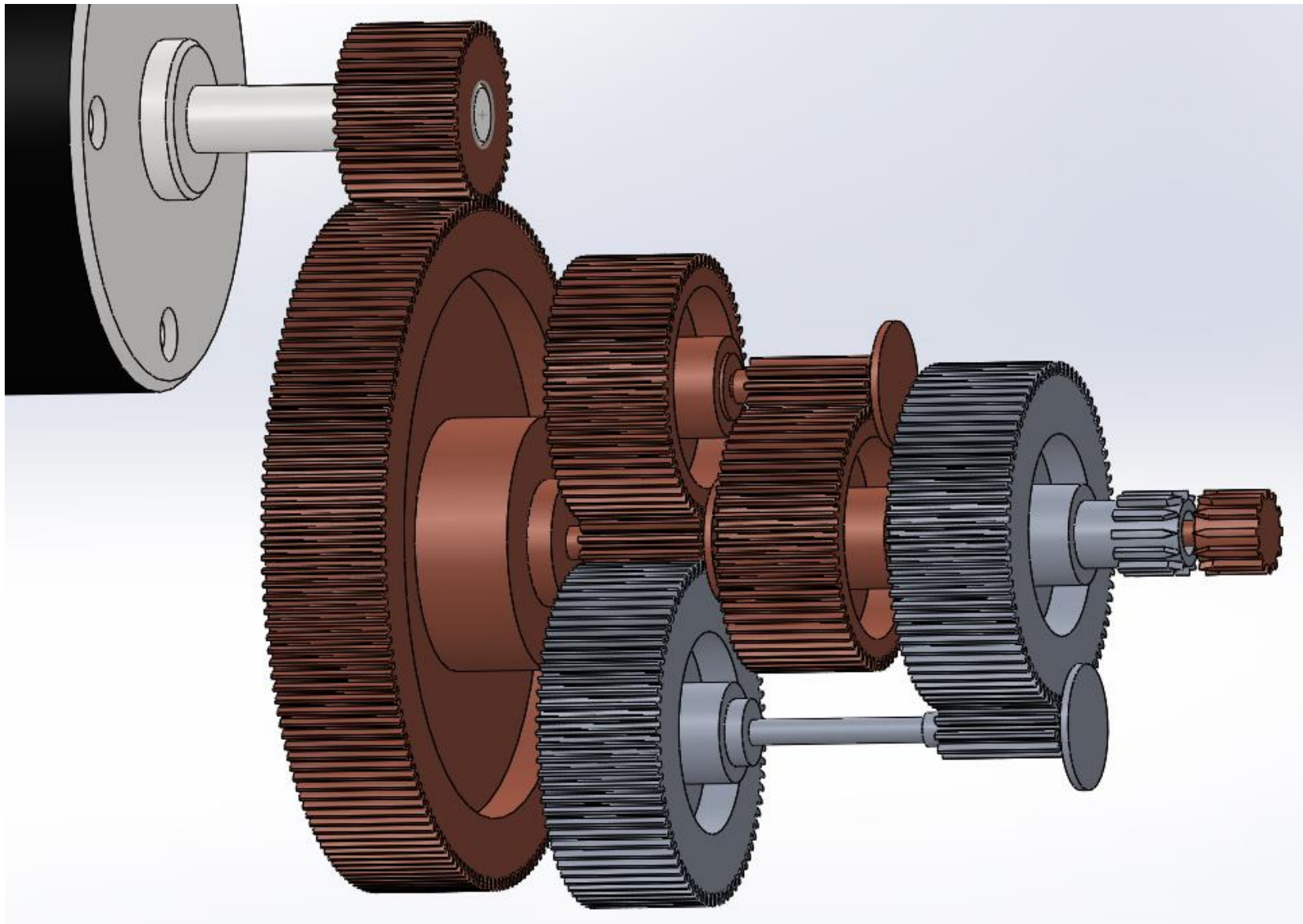


Figure 3.4.1a: Final Design for the gearbox. The power path for the 'speed' ratio can be seen highlighted, having a total ratio from output to input of 140. Notice that the output shaft for this gear ratio is concentric to the 'torque' output shaft. Teeth on the output shaft allow the gear-shift mechanism to mechanically lock with the shaft (see Section 3.5).

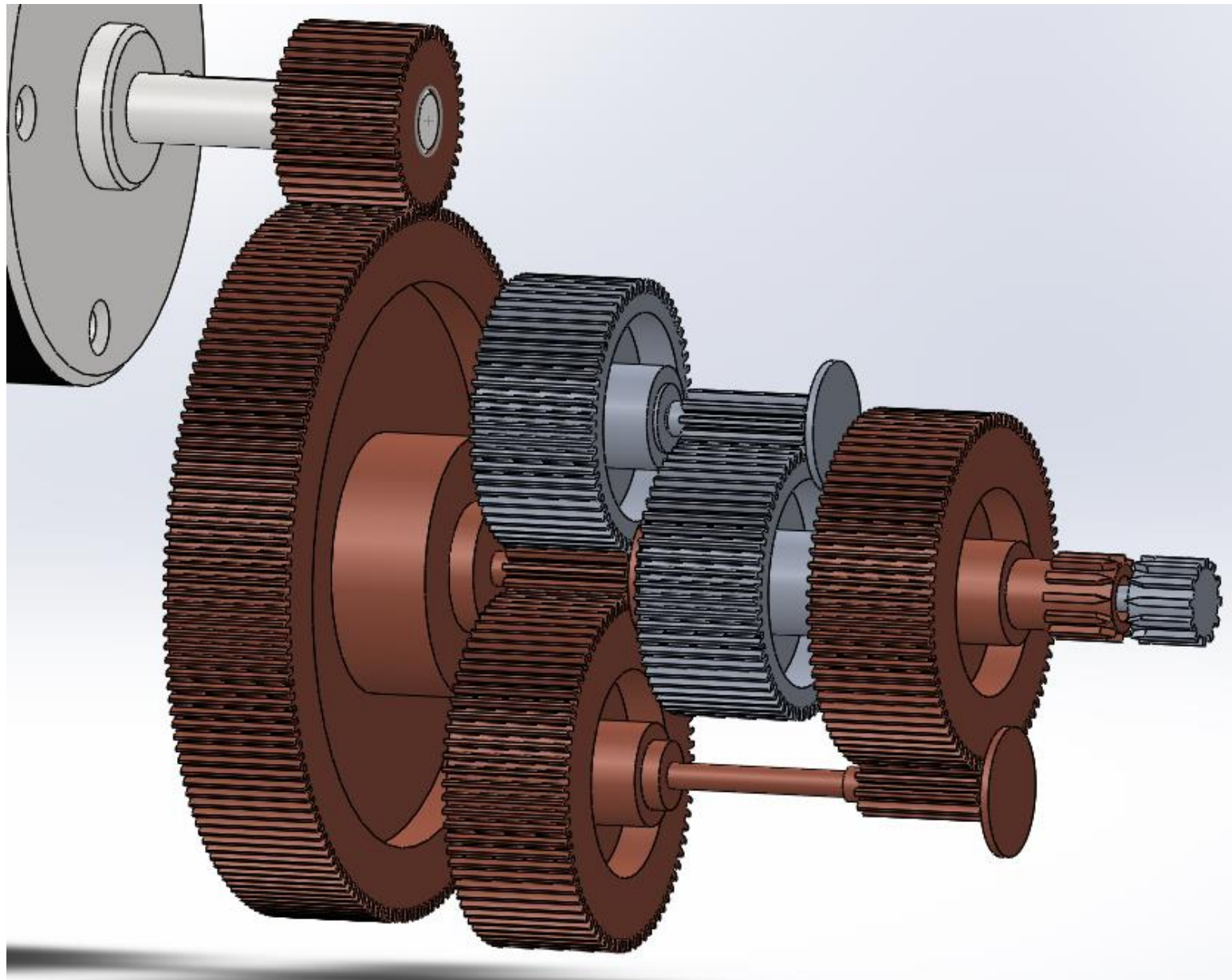


Figure 3.4.1b: Final Design for the gearbox. The power path for the 'torque' ratio can be seen highlighted, having a total output to input ratio of 243. Notice in this instance that the output shaft is on the outside of the 'speed' output shaft.

3.5 Gear Shift Mechanism

The design for the gear shift mechanism was heavily influenced by the principle of transmission synchronizers, but more specifically by the sleeve locking mechanism of synchronizers. An initial concept was proposed, but after analysing the advantages and disadvantages of the concept, it was deemed unfeasible for the required task.

3.5.1 Initial Concept

See Figure 3.5.1 for the sketch of the initial concept.

The working principle for this concept is very similar to a standard synchronizer sleeve. The mainshaft gear (A) is permanently locked against the mainshaft. A sleeve is also meshed permanently onto the mainshaft gear. The sleeve is wide enough that it can mesh both the mainshaft gear and an idler gear simultaneously.

The idler gears (B) are both positioned either side of the mainshaft gear. In neutral, the sleeve is unmeshed with either of the idler gears. Then, in order to mesh the idler gear onto the mainshaft, a servomotor (F) is able to actuate the sleeve in the direction of the required idler gear, causing it to mesh with the idler gear.

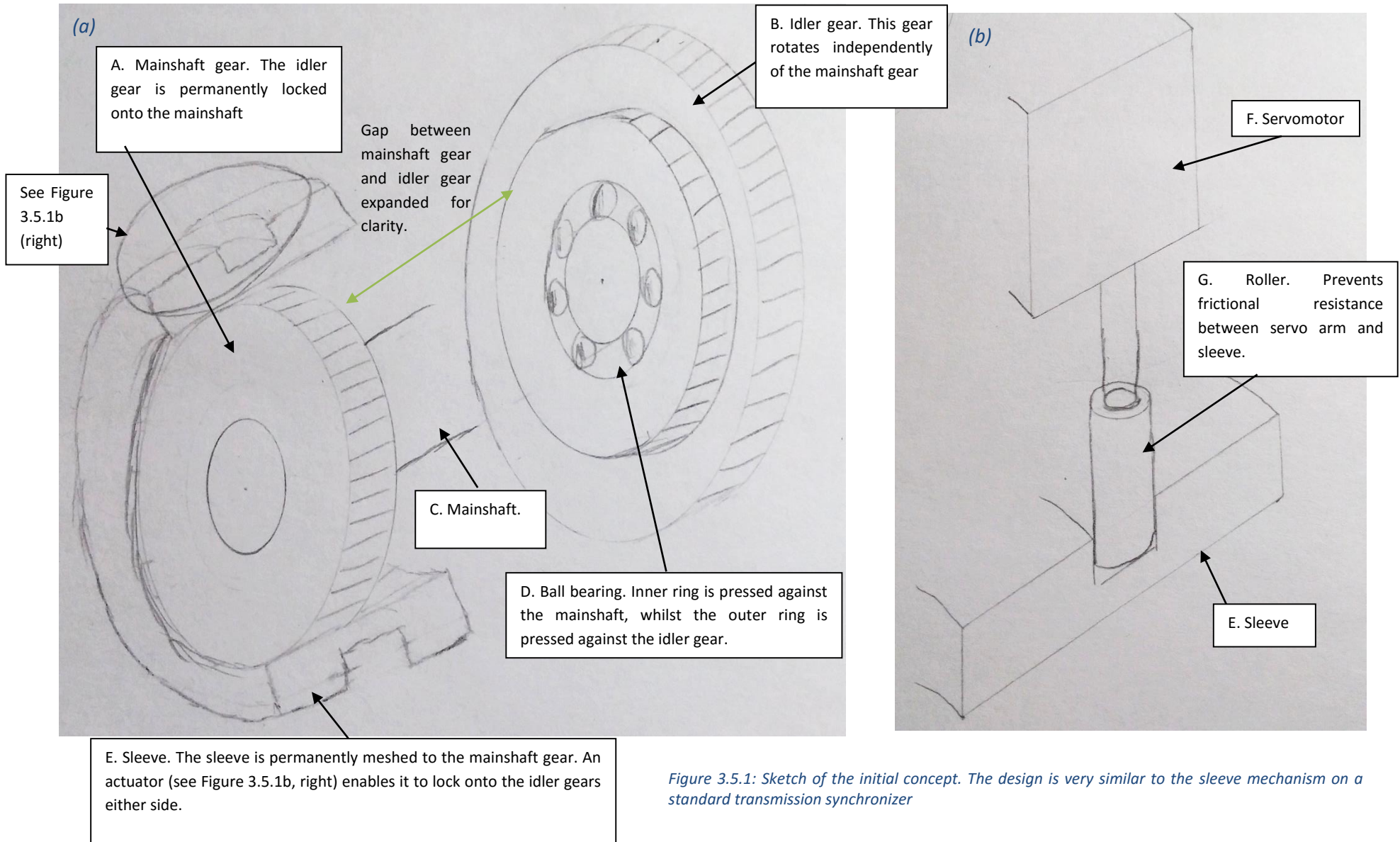
So that the sleeve can rotate freely and without friction from the servomotor's arm, a roller is used (G), having a lubricated inner surface. The roller's outer diameter should be small enough to prevent it from being able to touch both sides of the inner groove of the sleeve at the same time, as this would cause obvious unwanted frictional effects.

There are a few advantages to this design:

- It allows more than just two gear ratios to be used on the same mainshaft, although more than one sleeve would be needed for this.
- Can be put into neutral.

However, on the whole, this design has quite a number of disadvantages:

- Actuating the sleeve at the top only creates an imbalance of forces, potentially causing moments on the sleeve.
- A servo can only move in a circular fashion, and not linearly, meaning a possible new mechanism needs to be developed to achieve linear motion only.
- Due to imbalanced force transfer, locking the sleeve may take longer than required.
- Having a roller (component G) may require lubrication in order to operate effectively.
- To keep the sleeve locked, the servo would have to keep constant pressure on the sleeve. This force, and the sleeve rotating, may cause serious wear on the roller.



3.5.2 Chosen design

After some further considerations and minor changes, a final design was selected, as shown in Figure 3.5.2.

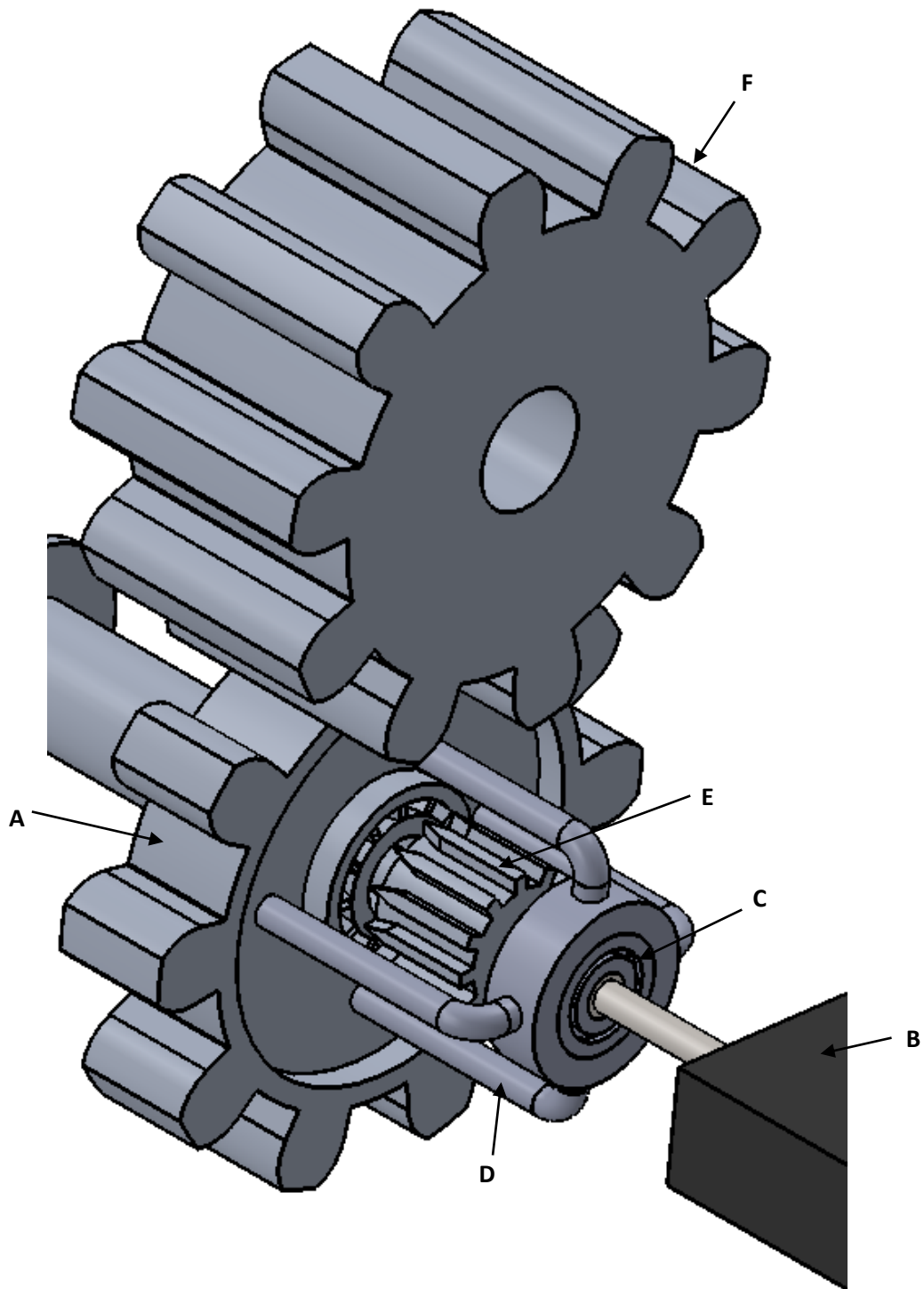


Figure 3.5.2: Gear shift mechanism chosen design

The sleeve (A) is actuated by an electric linear actuator (B). A miniature bearing (C) is positioned on the linear actuator's shaft so that frictionless rotation is allowed between the sleeve (A) and linear actuator shaft. Four connectors (D) provide symmetric force to the sleeve. The sleeve can slide

between the two gearbox output shafts (E), with teeth in order to mesh the sleeve to each shaft. The sleeve is in constant mesh with the output gear (F).

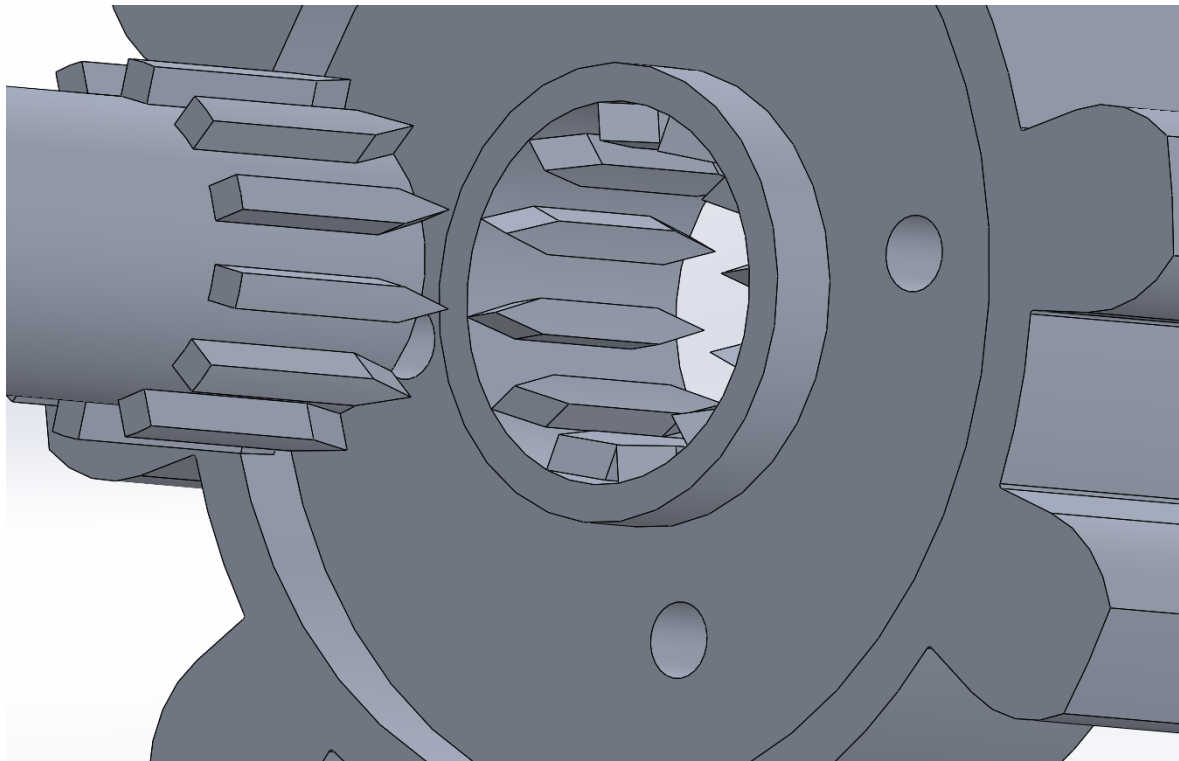


Figure 3.5.3: Close up of the inner section of the sleeve, and the torque output shaft (see Figure 3.4.1b). Notice the angled ends of the teeth, to prevent clashing or locking of the teeth during meshing.

For meshing the sleeve to each output shaft, teeth are placed on the inner section of the sleeve, and the outer sections of the output shafts. These teeth are designed to have angled geometries at the ends, otherwise termed the ‘roof angle’, in order that the teeth don’t clash when meshing occurs. The roof angle used in this design is 15°. The larger the roof angle, the larger the horizontal force acting to rotate the sleeve when the teeth meet, and the lower the vertical component acting in the direction of the travelling sleeve [27].

The outer teeth of the sleeve are in constant mesh with the output gear, through a ratio of 1, so that there is no speed or torque change. This output gear is then directly connected to the robotic gripper.

This design still utilises the sleeve meshing principle from standard transmissions and the initial concept, but it has a number of advantages over the initial concept:

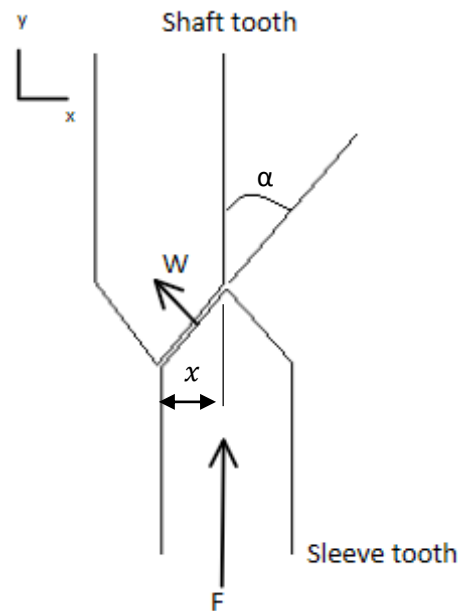
- The actuating forces are balanced across the sleeve
- The use of a linear actuator prevents the problems encountered with the servomotor’s circular motion
- A sturdier component – a ball bearing – is used, rather than a small roller, for the frictionless movement between sleeve and actuator shaft (linear motor shaft)
- Bearings are not needed for the two gears to be meshed, due to the concentricity of the two output shafts

Linear Actuator Selection

The linear actuator must provide some force, F , that is sufficient to rotate the inertia of the sleeve, output gear and gripper, and slide fully into locking position within a time of 0.6s (taken from the PDS).

Figure 3.5.4 displays the forces involved during full contact between a sleeve tooth and shaft tooth. It can be shown that the x-component of force W in Figure 3.5.4 is,

$$W_x = W \cos\left(\frac{\pi}{2} - \alpha\right) = F \cos \alpha \cos\left(\frac{\pi}{2} - \alpha\right)$$



Now, rotational acceleration needed is given as,

Figure 3.5.4: Free Body Diagram for sleeve and shaft teeth

$$\frac{d^2\theta}{dt^2} = \frac{T}{J} \quad (3.5.1)$$

Double integrating, and assuming zero initial conditions (i.e. zero angular velocity and position at $t = 0$ s) gives,

$$\theta = \frac{1}{2} \frac{T}{J} t^2 \quad (3.5.2)$$

θ is then the required rotational displacement of the sleeve needed to be displaced in order for the sleeve tooth to pass the shaft tooth. But torque, T , and sleeve angular position, θ , can be found in terms of linear force, F , and sleeve diameter, D ,

$$T = F \cos \theta \cos\left(\frac{\pi}{2} - \alpha\right) \frac{D}{2} \quad (3.5.3)$$

$$\theta = \frac{2x}{D} \quad (3.5.4)$$

Therefore, substituting Eqtns 3.5.4 and 3.5.3 into 3.5.2, and rearranging for F gives,

$$F = \frac{8xJ}{D^2} \frac{1}{\cos \alpha \cos\left(\frac{\pi}{2} - \alpha\right) t^2} \quad (3.5.2)$$

Letting $t = 0.2$ s (total gear change needs to be less than 0.6s in the PDS), $D = 0.01$ m, $x = 0.475 \times 10^{-3}$ m, $J = 0.069 \times 10^{-3}$ kg.m² (see Appendix A3) and roof angle, α , is $\pi/12$. Then from Eqtn 3.5.2, F is 0.13N.

Since the mass of the gears is so small, and the distance through which the gear must travel is small, the force required is small. Based on this, a linear actuator providing faster speed rather than larger loads is needed. A number of linear actuators on the market have been investigated, but a product sold by Active Robots (2016) shows to be most feasible, having a stroke length of 50mm and a no load speed of 12mm/s [28]. Travel distance for gear engagement is 8mm, so time taken for engagement is approx. 0.67s. Max load is 25N. This would fit the speed requirements of the machine.

3.6 Machine Assembly

The completed, fully assembled 3D model for the whole machine is shown in Figure 3.6.1. Note that small components such as bolts, screws etc. are not included in the model. However, the assembly displays an accurate visual for the machine layout.

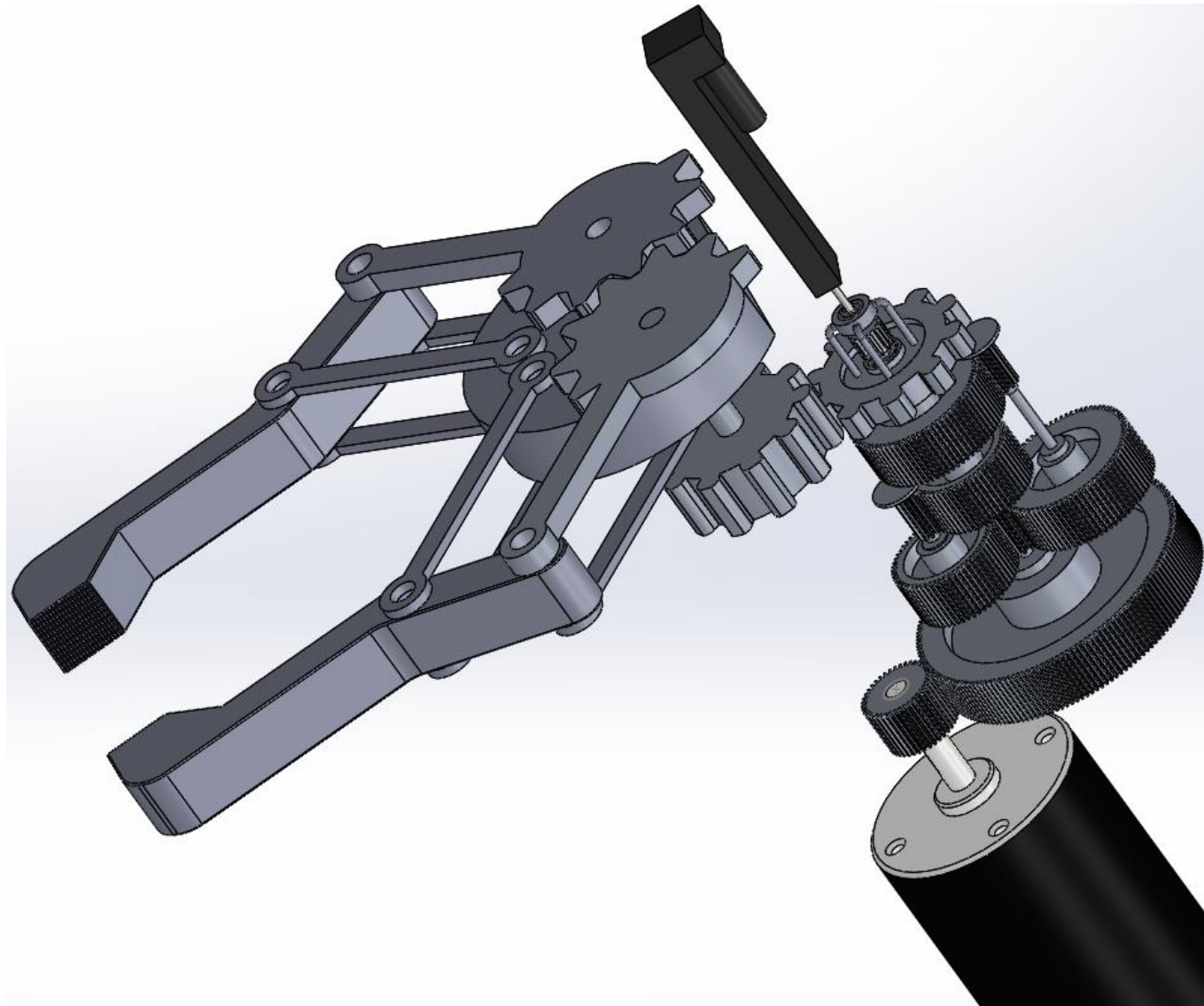


Figure 3.6.1: Complete assembly for the machine.

3.7 Electronic Circuitry

In order to alter the direction of the motor, a H-Bridge arrangement, using NPN and PNP transistors is used [29]. The schematic can be seen in Figure 3.6.1.

The logic for controlling the motor is given in Table 3.6.1.

Table 3.6.1: Logic for controlling the direction of rotation of the DC motor

Pin 5	Pin 6	Q1	Q2	Q3	Q4	Motor Direction
LOW	LOW	OFF	OFF	OFF	OFF	Stopped
HIGH	LOW	OFF	ON	ON	OFF	ACW
LOW	HIGH	ON	OFF	OFF	ON	CW
HIGH	HIGH	ON	ON	ON	ON	Not Allowed

Having Pin 5 and Pin 6 both HIGH simultaneously will cause a short-circuiting of the bridge, and hence this condition cannot be permitted [30]. The Arduino has therefore been programmed to ensure this does not happen if both switches, S1 and S2, are activated simultaneously. See section 3.8 for the software development.

For the control interface an Arduino Uno is implemented, which is based on the ATmega328P microcontroller [31].

By activating the mechanical switch, S1, the microcontroller is programmed to send a PWM signal from Pin 6, therefore causing the motor to rotate in a clockwise direction at the speed determined by the PWM duty cycle. S2 has the same effect for rotating the motor in an anti-clockwise direction.

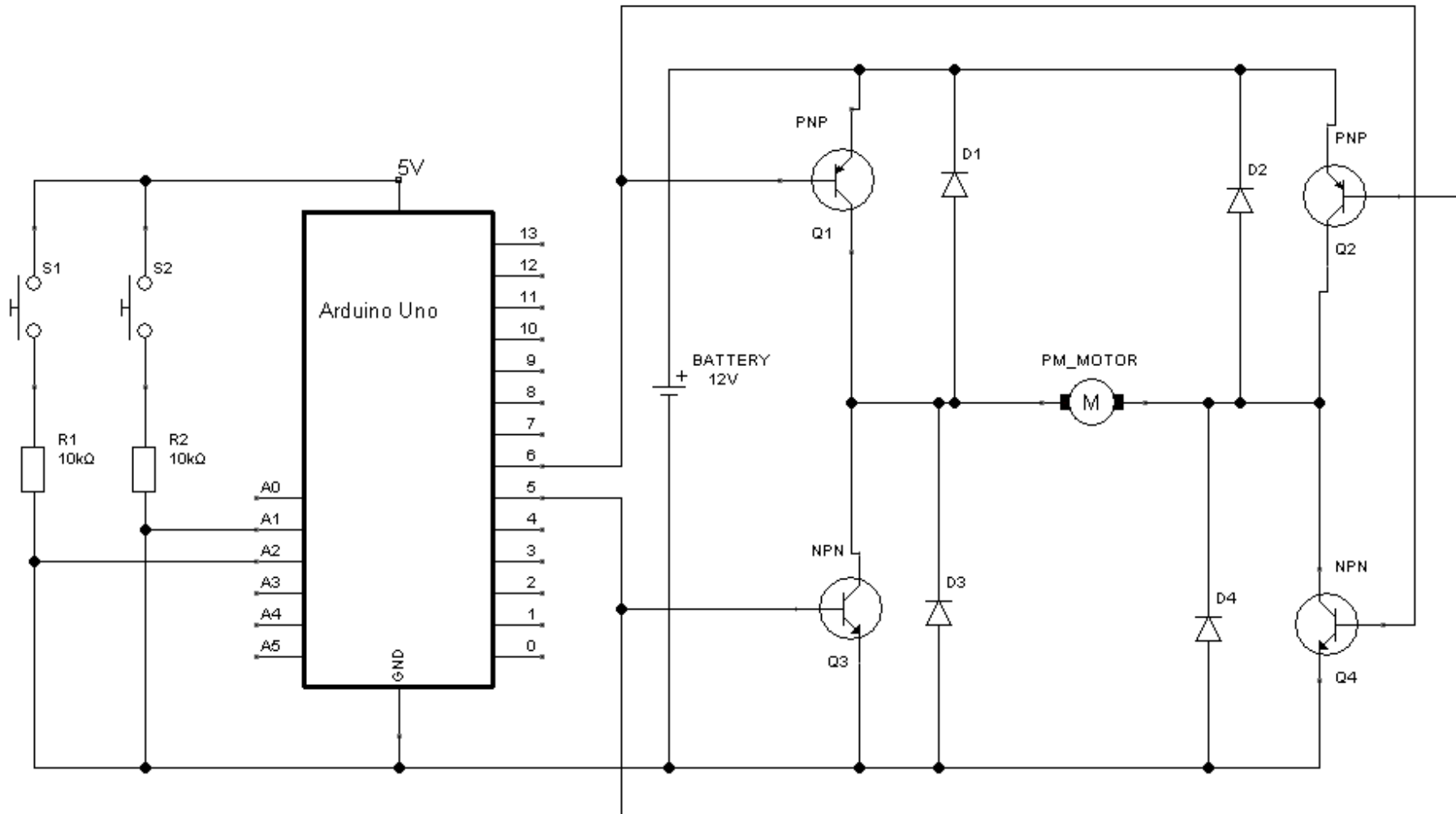


Figure 3.6.1: Schematic of the circuit used for controlling the DC motor. Pins 5 and 6 can output PWM signals, allowing the control of the speed of the DC motor, as well as its direction.

3.8 Software Development

Figure 3.8.1 displays the logic of the programme written for the Arduino for controlling the direction and speed of the DC motor. See Appendix A4 for the full code.

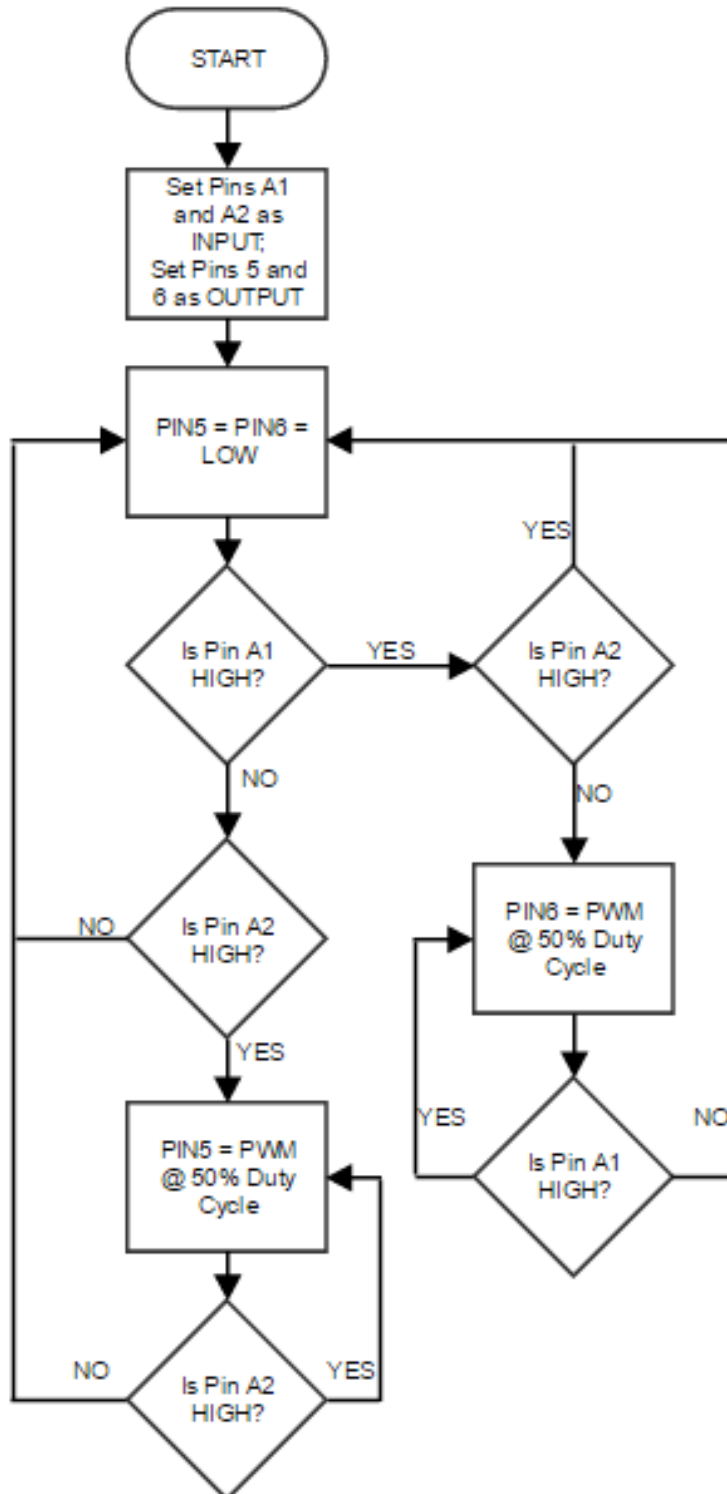


Figure 3.8.1: Flowchart displaying the logic used for controlling the DC Motor

4 Simulation and Analysis

4.1 Assumptions

In the development of the mathematical model, and for running the simulations, the following assumptions have been made:

- There is no frictional resistance in the gearbox
- There are no torsional spring elements in the gearbox
- Efficiency of the gearbox is 100%
- Inertia reflected to the DC Motor is perfect, i.e. $\eta = 1$ in Eqtn 2.1.6
- DC Motor torque and armature current have a linear relationship without an additional constant – i.e. plot in Figure 3.3.1 intercepts the y-axis (current) at OA.

4.2 Development of the Gearbox Mathematical Model

In order to analyse the gearbox performance, the mathematical model was developed, with the intention of finding the relationship between motor source voltage, and angular displacement of the gripper. The development of the model is discussed in this section.

The motor used in this machine is a DC permanent magnet motor. The schematic is shown in Figure 4.2.1 [32]. The permanent magnet is represented as a fixed field, with an armature circuit through which the current, $i_a(t)$, passes.

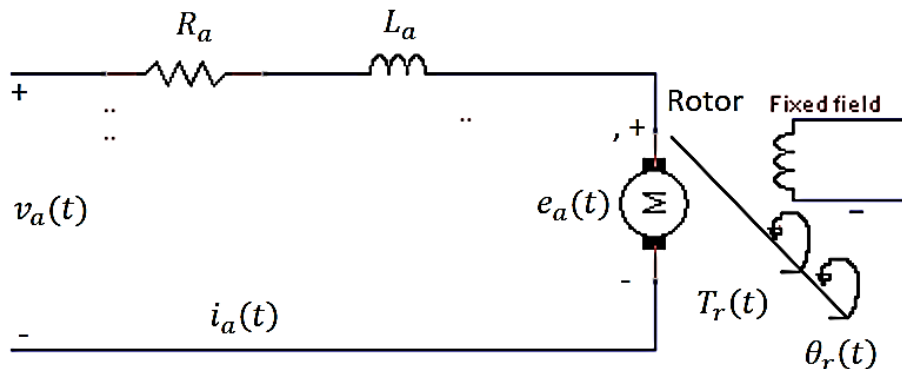


Figure 4.2.1: Schematic of the DC permanent magnet armature circuit

From Kirchhoff's voltage law, the governing equation for the armature circuit is [33],

$$R_a i_a(t) + L_a \frac{di_a(t)}{dt} + e_a(t) = v_a(t) \quad (4.2.1)$$

It can be shown from Faraday's law that the armature back e.m.f. is given as [33],

$$e_a(t) = k_b \frac{d\theta_r}{dt} \quad (4.2.2)$$

And the motor stall torque is a function of armature current (Eqtn 2.1.11) [34],

$$T_r(t) = k_t i_a(t) \quad (4.2.3)$$

Where k_b and k_t are constants for the motor.

Taking Laplace transforms of Eqtns 4.2.1-3 assuming zero initial conditions, and substituting Eqtns 4.2.2 and 4.2.3 into 4.2.1 yields,

$$\frac{(R_a + L_a s) T_r(s)}{K_t} + K_b s \theta_r(s) = V_a(s) \quad (4.2.4)$$

Now, for a rotational, mechanical, non-electric system, as shown in Figure 4.2.2, having a rotational inertia, J , and rotational damping, B , then the governing equation is given as [35],

$$T(t) = J \frac{d^2 \theta(t)}{dt^2} + B \frac{d\theta(t)}{dt} \quad (4.2.5)$$

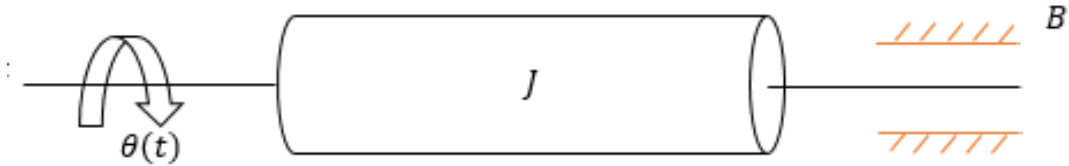


Figure 4.2.2: Schematic of a rotational, mechanical system

To complete the model, Eqtn 4.2.5 is Laplace transformed and substituted into Eqtn 4.2.4 with some rearrangement,

$$\frac{\theta_r(s)}{V_a(s)} = \frac{\frac{K_t}{R_a J_{re}}}{s + \frac{1}{J_{re}}(B_{re} + \frac{K_t K_b}{R_a})} \quad (4.2.6)$$

The armature inductance, L_a , has been assumed to be zero, as armature inductance is very small compared to armature resistance [36], and hence has been removed from the above Eqtn.

J_{re} and B_{re} are the inertia and damping reflected to the motor, respectively, and can be found using the principles discussed in Section 2.1.1. The relationship between angular displacement of the gripper, θ_g , and angular displacement of the motor, θ_r , is given by the gear ratios for each. I.e., $\theta_r = N_S \theta_g$ for the speed ratio and $\theta_r = N_T \theta_g$ for the torque ratio. These can be substituted accordingly into Eqtn 4.2.6.

4.2.1 Finding the Motor Constants

K_b can be found from Eqtn 4.2.2 and the no load speed from Figure 3.3.2 at 12V,

$$K_b = \frac{v_a}{\omega_{no-load}} = 0.0215 \quad (4.2.7)$$

K_t can be found from Eqtn 4.2.3 and the rotor stall torque and current from Figure 3.3.1,

$$K_t = \frac{T_{stall}}{i_a} = 0.0182 \quad (4.2.8)$$

4.2.2 System Transfer Function

Armature resistance is found from the stall situation of Eqtn 3.3.4 at 12V,

$$R_a = \frac{v_a}{i_a} = 90.23 \text{ m}\Omega \quad (4.2.9)$$

The gearbox inertia reflected to the DC motor is 8625 g.mm² (see Appendix A3)

It assumed there is no frictional resistance, and so $B_{re} = 0$. Therefore, the transfer function for this machine, from Eqtn 4.2.6, is,

$$\frac{\theta_r(s)}{V_a(s)} = \frac{\frac{0.0182}{0.09023 \times 0.000008625}}{s + \frac{0.0182 \times 0.0215}{0.000008625 \times 0.09023}} = \frac{23,386.29}{s[s + 502.79]} \quad (4.2.10)$$

Initial observations indicate the system is unstable, having one pole at zero in the s-plane. But this is desirable, since a constant rise in angular displacement is expected and required. The system also has a small time constant of $1/502.79 = 1.99\text{ms}$ for the first order term having the gain of 502.79. Therefore, the system should respond very quickly.

4.3 Gearbox Performance Simulations

Since the gearbox in torque mode would be static, and therefore have no moving parts, only the speed setting was analysed for optimum gripper closing and opening times.

Since $\theta_r = N_S \theta_g = 140 \theta_g$, Eqtn 4.2.10 can be re-written as,

$$\frac{\theta_g(s)}{V_a(s)} = \frac{167.04}{s[s + 502.79]} \quad (4.3.1)$$

The equivalent TF for Eqtn 4.3.1 in closed-loop, unity-negative feedback [37] is,

$$\frac{\theta_g(s)}{R(s)} = \frac{167.04}{s^2 + 502.79s + 167.04} \quad (4.3.2)$$

Where $R(s)$ is a reference input into the system, in order that the desired outcome is $R(s) = \theta_g(s)$.

Initial observations show that the closed-loop system is stable, having two poles at -0.33 and -502.46 in the s-plane. It is also overdamped, having a damping ratio of 19.46.

The range of angular displacement for the gripper is from 4° at fully open to 90° at fully closed, or from 0.07 – 1.57 rad, giving a net range of 1.5 rad.

4.3.1 Method

The following steps have been taken to simulate and analyse the performance of the gearbox:

1. Using Simulink, the open-loop model was created using the above TF.
2. A continuous input of 2V up to 12V was applied, in steps of 2V.
3. The time taken for the gripper to rotate from fully open to closed was recorded for each voltage input.
4. Steps 2 and 3 were repeated using a pulse modulator input to represent PWM, having a period of 2ms and a peak amplitude of 12V. 6V was then represented by having a 50% duty cycle, 2V by a 16.67% duty cycle etc.
5. The closed-loop model was then generated with the same system TF.
6. A continuous input of 6V, passing through a digital gain to give the desired gripper position was inputted, and the response simulated.
7. Settling time was recorded for unity gain.
8. A proportional-only controller was implemented to improve the settling time. Its gain was increased steadily from 1 up to a value giving the required output response and a sensible control signal.
9. Phase and Gain margins were determined for the system to ensure good safety margins for stability.
10. A Simscape physical model was setup, and the response to varying continuous inputs recorded, to compare against the open-loop Simulink simulation.

4.3.2 Open-Loop Simulation

Continuous Input

The open-loop model is shown in Figure 4.3.1.

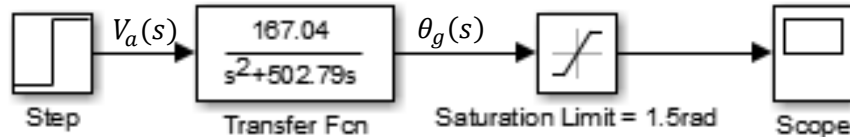


Figure 4.3.1: Open-loop model representing the machine

Saturation was applied to represent closure of the gripper. Results from the simulation for continuous voltage inputs, and times taken to achieve full closure of the gripper are shown in Table 4.3.1.

Table 4.3.1: Time taken in open-loop for gripper to close fully for a range of continuous input voltages.

Input (V)	Time (s)
2	2.259
4	1.131
6	0.754
8	0.566
10	0.453
12	0.378

Figure 4.3.2 plots the voltage input against time taken for the gripper to completely close.

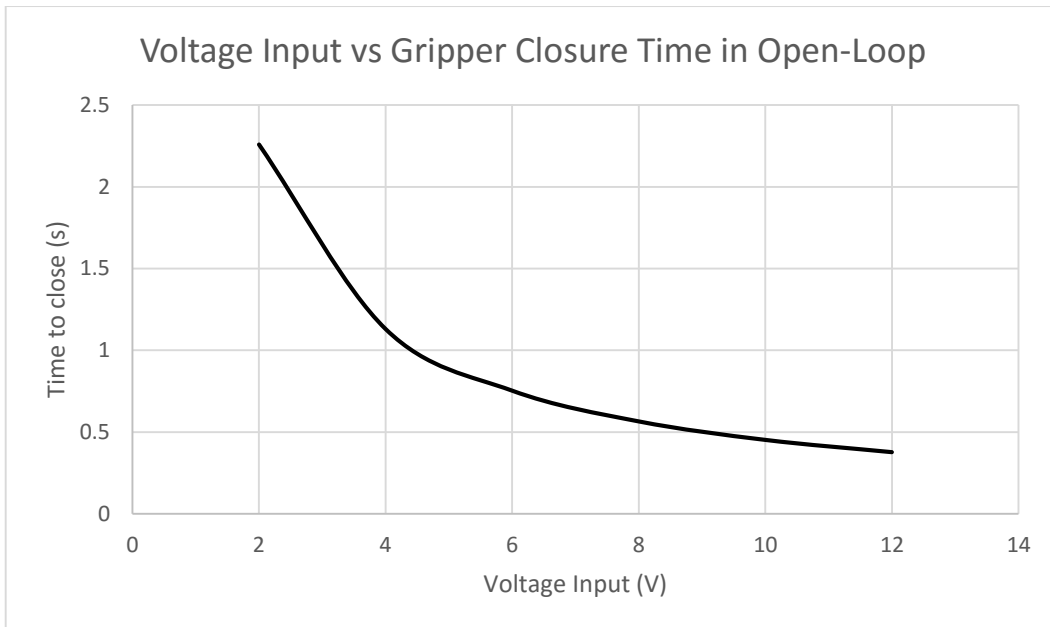


Figure 4.3.2: Plot of continuous voltage input vs time taken for full closure of gripper.

Pulse Modulated Input

The model for open-loop pulse generated input is shown in Figure 4.3.3.

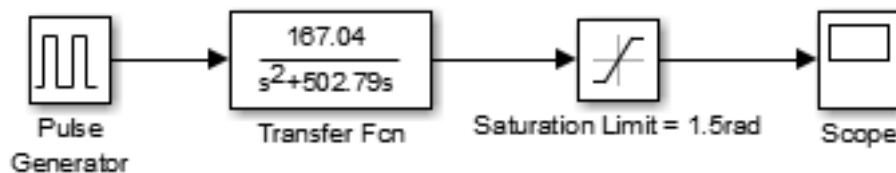


Figure 4.3.3: Open-loop model with pulse generated input.

The pulse generator was set at a period of 2ms, as that is the period of PWM the Arduino offers [38]. Duty cycle was varied for a peak voltage amplitude of 12V to give a range of average voltage levels. Table 4.3.2 shows the simulation results for PWM inputs.

Table 4.3.2: Time taken in open-loop for gripper to close fully for a range of PWM duty cycles. Peak amplitude was 12V.

Duty Cycle (%)	Input Average (V)	Time (s)
16.67%	2	2.258
33.33%	4	1.130
50%	6	0.754
66.67%	8	0.566
83.33%	10	0.453
100%	12	0.378

There is negligible difference in gripper closing time between continuous input and PWM input.

Figure 4.3.4 shows the response for a continuous input of 6V, and a pulse generated input of 50% duty cycle and peak amplitude of 12V to give an average of 6V. It is initially not obvious there is a difference

in response values between the two inputs in Figure 4.3.4a. However, Figure 4.3.4b shows a small difference of around 0.001 rad.

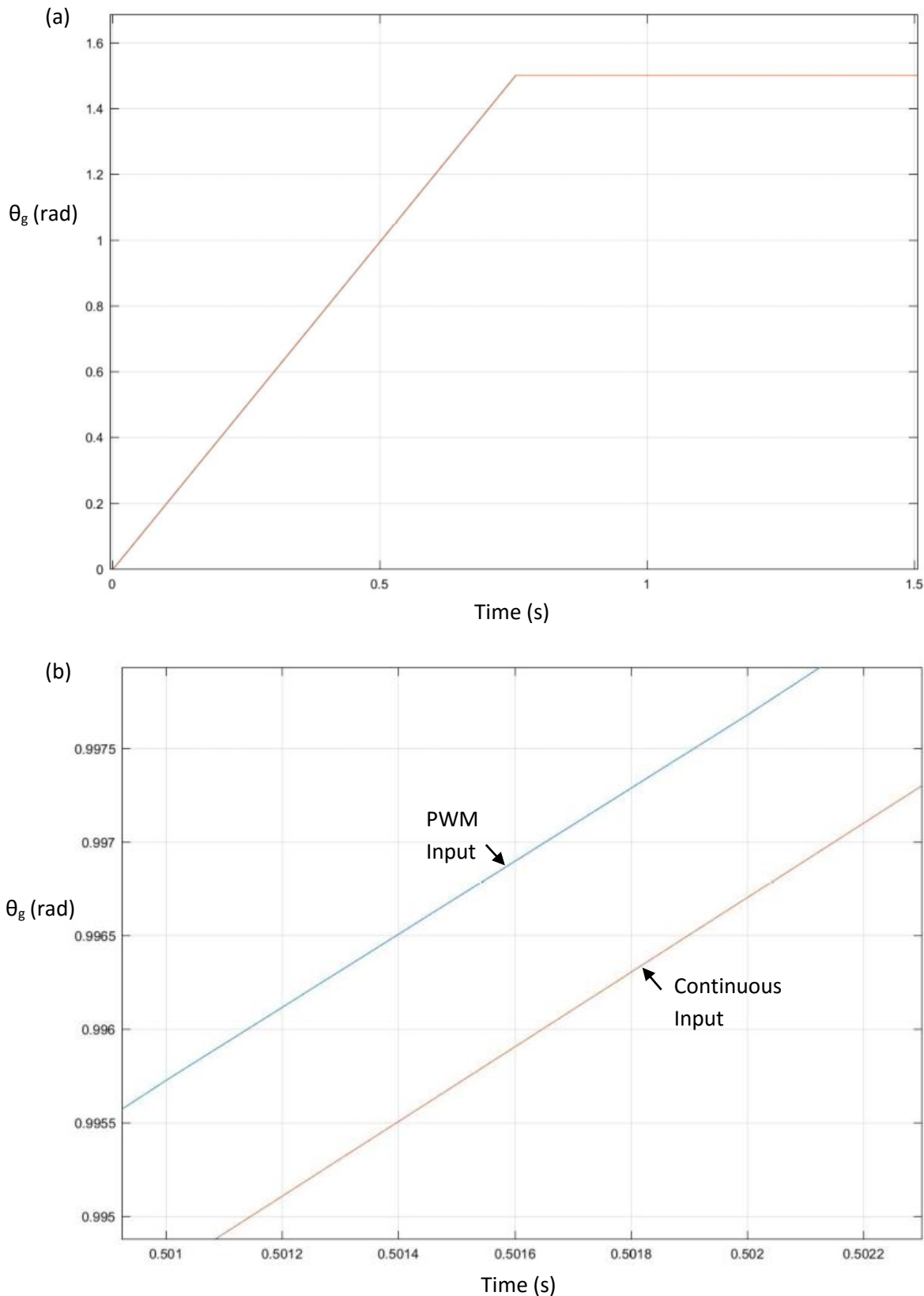


Figure 4.3.4: Example output responses for open-loop. (a) showing the output response for 6V continuous input vs 6V averaged PWM input. (b) reduced time scale showing the discrepancy between continuous input and PWM input.

4.3.3 Closed-Loop Simulation

The closed-loop model for the continuous input is shown in Figure 4.3.4.

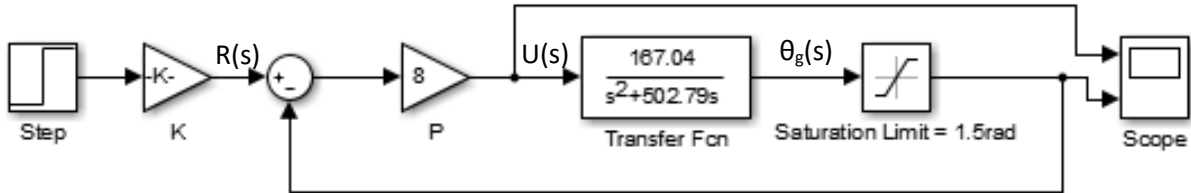


Figure 4.3.4: Closed-loop model having a continuous input of 6V.

The step input is a constant input of 6V. The angular displacement of the gripper is determined by the size of the input gain, K. A gain of $K = 0.25$ gives a reference input of 1.5, which would be the complete closing of the gripper from a fully open position. If it was desired that the gripper should displace by 0.25 rad, then gain $K = 0.25/6 = 0.0417$.

Settling time is considered to be the time at which the output value falls within 5% of the steady state value. Simulation was initially run setting $P = 1$. The settling time at this gain was 9.01s – far too slow, and therefore the proportional controller needed increasing. The proportional controller, P, was steadily increased from the gain value of 1, until the controller signal reached a maximum of 12, since the circuit will not be able to output more than 12V. The value for P was found at $P = 8$ for a displacement of 1.5 rad. Settling times for unity gain and gain of 8 are shown in Table 4.3.3 for two different gripper displacement amounts.

Table 4.3.3: Settling time in closed-loop for proportional gains of 1 (unity) and 8.

Total Gripper Displacement (rad)	Settling Time (s) for P=1	Settling Time (s) for P=8
0.25	8.97	1.12
1.5	9.01	1.12

Table 4.3.4 shows the values of proportional gains that are required to give an initial maximum control signal of 12 for varying displacements, and their associated settling times.

Table 4.3.4: Values for gains to achieve fastest settling times for varying displacements in closed-loop.

Total Gripper Displacement (rad)	Gain, K	Gain, P	Settling Time (s)
0.25	0.0417	48	0.18
0.5	0.0833	24	0.37
0.75	0.125	16	0.56
1	0.1667	12	0.75
1.25	0.2083	9.6	0.94
1.5	0.25	8	1.12

The response and control signal can be seen plotted in Figure 4.3.5 for a gripper displacement of 1.5 rad (i.e. fully open to full closure of the gripper).

Notice the control signal starts at 12V, but exponentially decreases, reaching a final value of 0 once the gripper has reached the desired position. Gains K and P are set to 0.25 and 8 respectively.

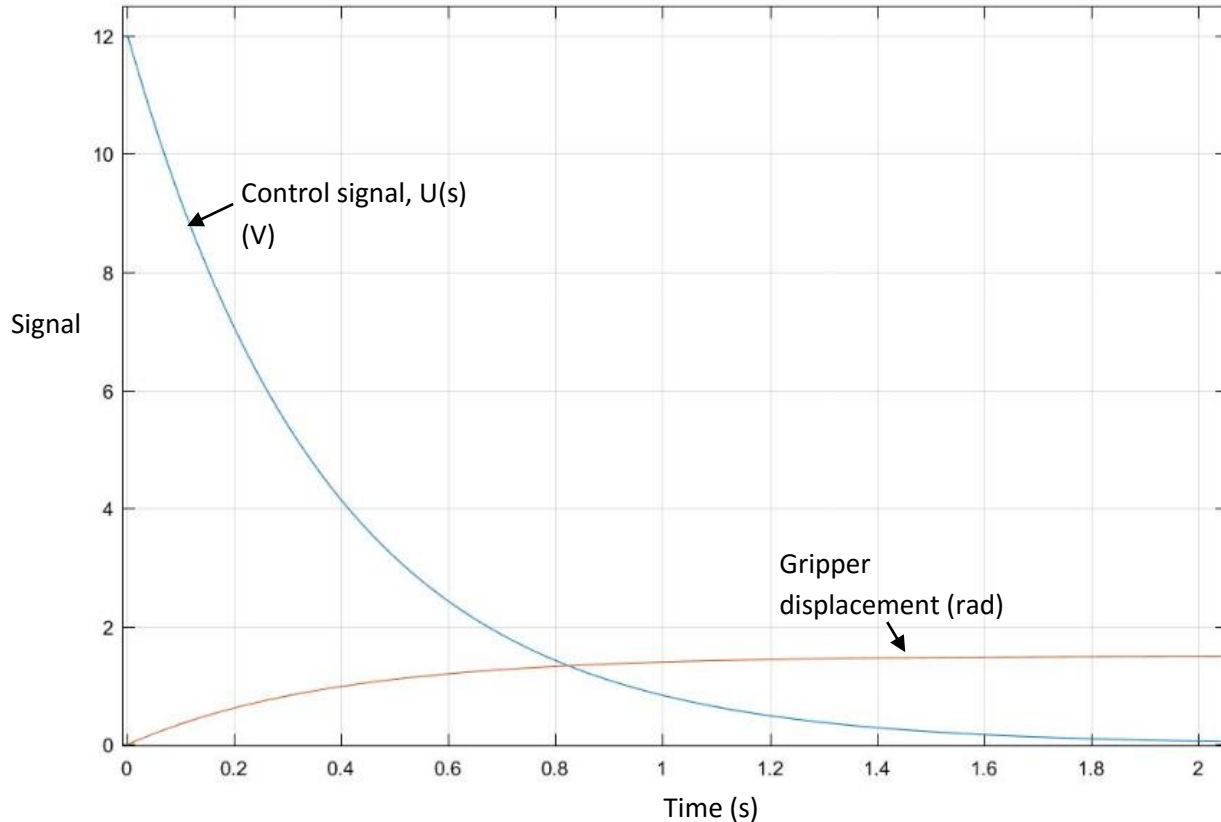


Figure 4.3.5: Gripper response for a displacement of 1.5 rad in the closed-loop system.

4.3.4 Stability

To ensure that the system would be stable in cases where the system's parameters change, or may not be fully known, the gain and phase margins for the system in Figure 4.3.1 are calculated from the system's Bode plots. The plots show an appropriate Phase margin of 90°, and an infinite gain margin. See Appendix A6 for the Bode plots.

4.3.5 Physical Modelling in Simscape

To confirm the responses from the mathematical model developed above, a physical model was generated in Simscape. The blocks used in the model were:

- Voltage source
- Resistor ($90.23\text{m}\Omega$)
- Current sensor
- DC Motor
- Two simple gear ratios, with ratios 4 and 35 (to give total ratio of 140)
- Inertia ($126,859\text{g.mm}^2$)
- Ideal Rotational Motion Sensor
- Saturation Limiter, limiting rotation to 1.5rad

The model is shown in Figure 4.3.7.

The results of running the simulation at varying voltage sources, and comparing to Table 4.3.1 are shown in Table 4.3.5.

Table 4.3.5: Times taken for gripper to displace from fully open to closed for Simscape model and derived mathematical model.

Input (V)	Derived Mathematical Model, Time (s)	Simscape Physical Model, Time (s)	Percentage Difference (%)
2	2.259	2.265	0.27
4	1.131	1.136	0.44
6	0.754	0.760	0.80
8	0.566	0.571	0.88
10	0.453	0.459	1.32
12	0.378	0.383	1.32

Figure 4.3.6 displays the plot for the output response of the OL system vs the Simscape model response. As shown, the responses are almost exactly the same. There is however a noticeable difference in the speed of response at in the initial stages of output, as seen in Figure 4.3.6(b).

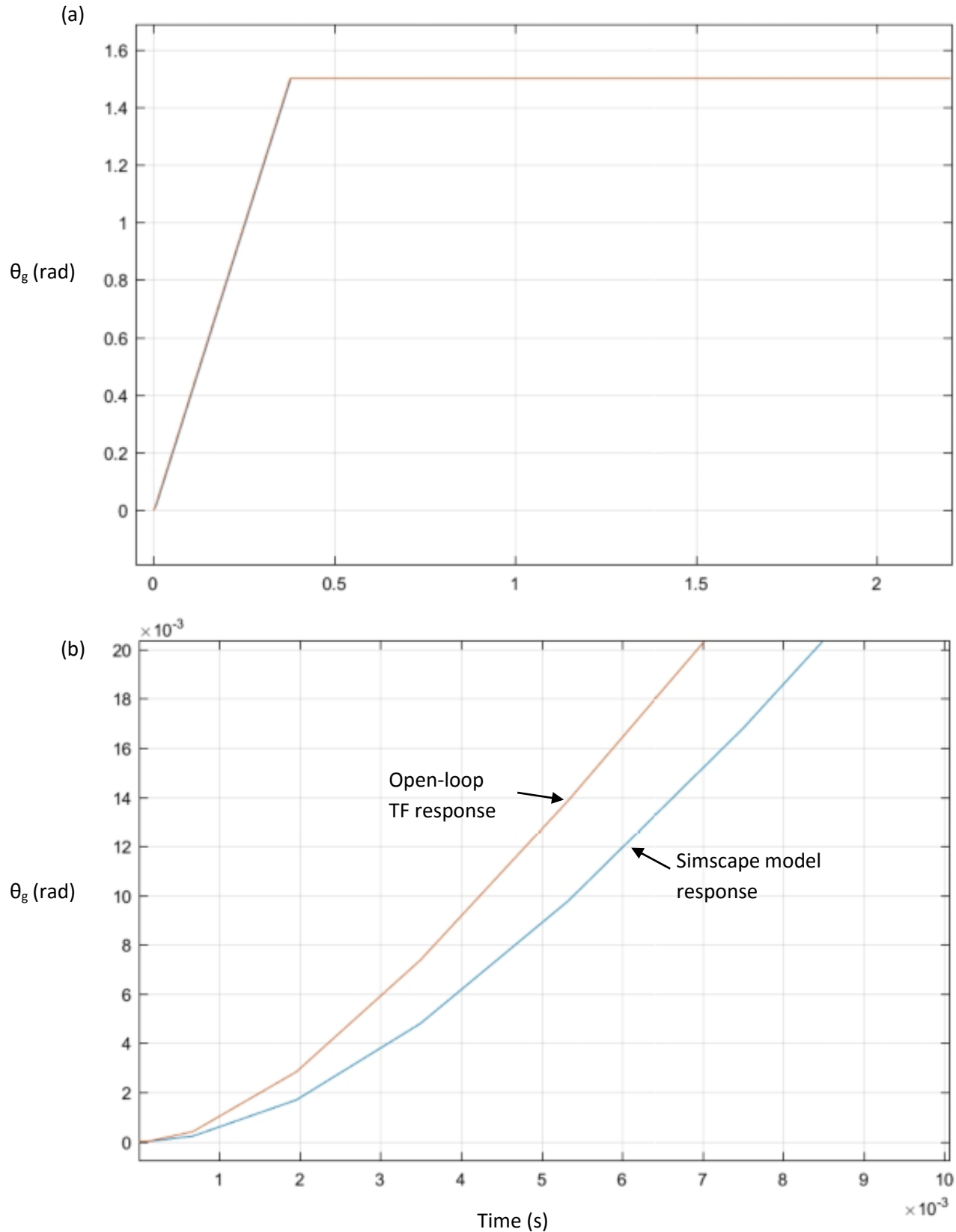


Figure 4.3.6: Output response for OL TF vs the Simscape model. Input is 12V continuous. Notice the small time scales (10^{-3}) in Figure (b).

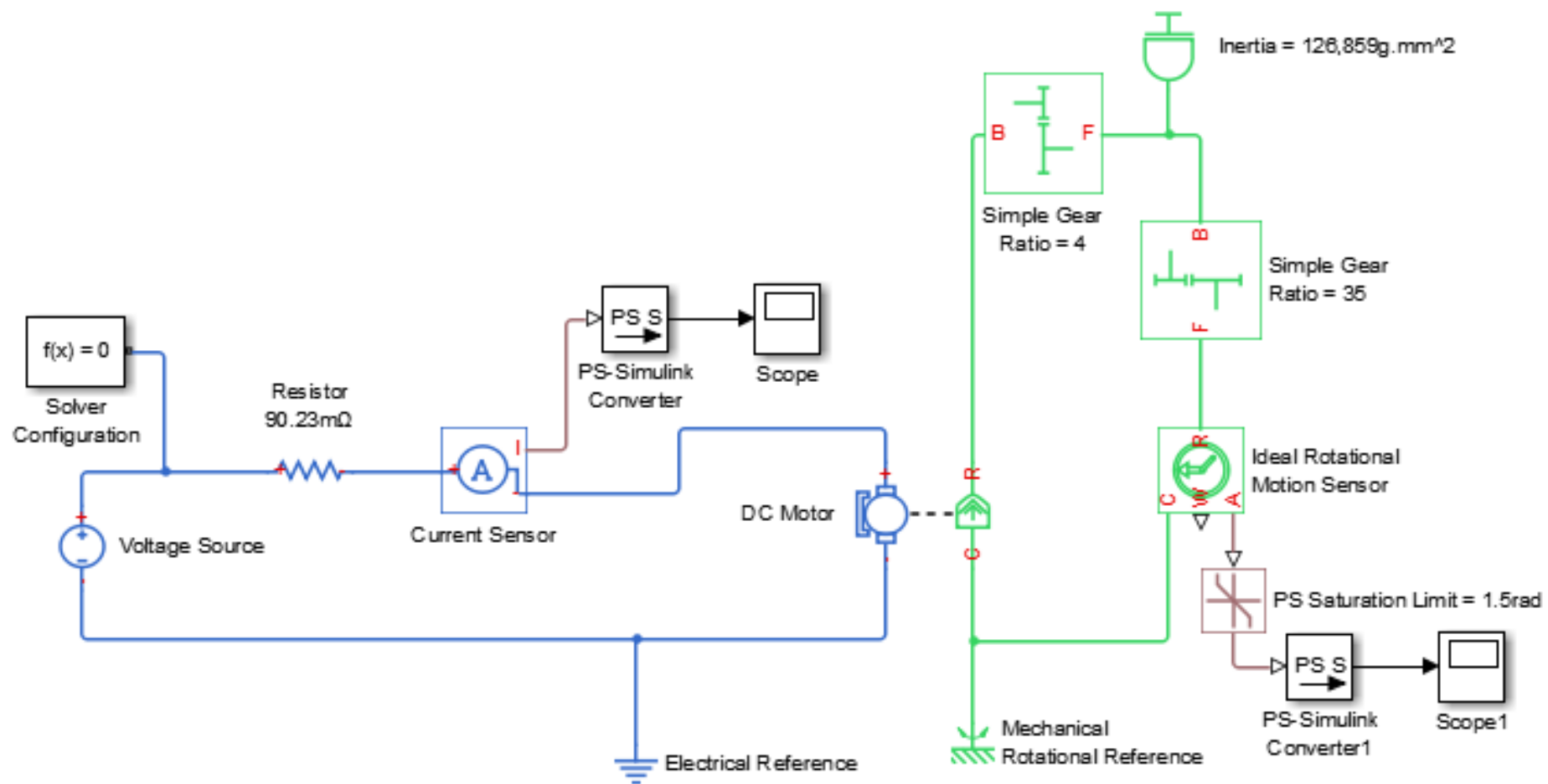


Figure 4.3.7: Simscape physical model representing the whole machine. In this image, the speed gear set is represented here as the second simple gear ratio having a value of 35. A value of 60.75 would represent engagement of the torque gear set.

5 Discussion

5.1 Gearbox Performance

Three methods were used in the design and analysis of the machine, and all three proved to agree well with each other. To determine the ratios required in the gearbox, a simple calculation taking the average angular velocity of the gripper link was computed for a gripper closure time of 0.45s (Section 3.2). The simulations gave a time of 0.38s gripper closure time. This is a 15.6% decrease vs the original time. But the initial calculation to obtain the time of 0.45s was computed for a gripper travel distance of 1.57 rad. Considering the actual distance is 1.5 rad, as was used in the simulations, it is expected that the real time should be slightly less than 0.45s, though not quite 0.07s less. It must also be taken into consideration that the DC motor characteristics used in the design process using the 0.45s was taken from the actual data, where there is some resistance within the motor such that the motor requires an initial amount of torque and current to start the motor accelerating (see Figures 3.3.1-3). In the simulations, it is assumed the motor starts accelerating immediately once current is applied, and therefore no time is wasted in the initial stages of powering the motor. Additionally, the design calculation was done using the most efficient motor speed, at 4640rpm. But as shown in the simulation response plot (Figure 4.3.4), the motor reaches no-load speed almost instantaneously. Using the time of 0.378s to close 1.5 rad at 12V (Table 4.3.1), gives a gripper rotational speed of 3.97 rad/s. The design speed was taken at 3.49 rad/s at the most efficient motor speed. This gives an increase of 13.8% for simulation speed vs the design speed. Then, including the travel distance difference already mentioned, the time discrepancy between simulation and design are expected and reasonable.

Furthermore, the results found from the open-loop mathematical models are consistent with the results gained from the physical model, with a maximum discrepancy in gripper closure times of only 0.006s. This difference can be considered negligible, and could easily arise from rounding errors obtained in the development of the mathematical model. It is noticeable from Figure 4.3.6 that the responses are almost the same. The no-load speed for each is equal, but the only difference is the acceleration of the gripper at $t = 0s$. The Simscape model outputs slightly slower acceleration in comparison to the OL TF model. Since both the models assume zero damping, this effect could only occur due to differences in the inertia calculations or torque constant. The torque constant in Eqtn 4.2.8 is calculated to 4 d.p. giving a possible percentage error of 0.5%. However, the stall torque inputted into Simscape is to 2 d.p. suggesting a possible error of 0.7%. Then the total acceptable error is 1.2% given the tolerances of the torque constants. Including the additional uncertainties of rounding errors in inertia calculations, the results from the Simscape and TF can be said to agree well with each other.

If the gearbox was to be analysed experimentally, then the results would most likely show that closure times are slightly slower than that found in the simulations. This is due to frictional forces that were neglected in the models. Bernd-Robert Höhn et al (2009) were able to demonstrate the efficiencies in various types of gearboxes [39], and an upper end estimate can be taken as approx. 4% power loss in many gearboxes. When it is considered that it is mostly torque that is effected by efficiencies, then the speed should have little to no differences between theory and experiment (from the simulations, the inclusion of the gearbox inertia only decreased the motor no load speed by approx. 30rpm compared to the test data, or a total percentage decrease of only 0.56%). But initial acceleration would

be affected. However, the motor is able to accelerate to full velocity within 0.003s anyway, so although overall time experimentally would likely be slower, the differences are likely to be negligible.

5.1.1 Open-Loop

It is obvious from Figure 4.3.4 that there is negligible difference in the gripper output response between a continuous input and a PWM input at 500Hz. There are significant reasons as to why a PWM input would be ideal over a continuous input, with the most significant reason being the energy consumption. A PWM input would only require the voltage source to be on for a limited amount of time, whereas a continuous input would require the voltage source to be on for the whole time. Take for example a desired input of 6V. In PWM, the voltage source need only be on for 50% of the time. For the continuous input however, the voltage source must be on for the whole time, at 12V, but a secondary component, such as a resistor or transistor must be employed. Here, half the power input would be wasted across this secondary component. It can therefore be said that in open-loop, a PWM input is the ideal solution for varying input voltage. This would have a significant effect on consumers, who would benefit from the extra battery life provided by PWM input.

The closure times obtained for varying input voltages were all acceptable, with the exception of the 2V input, when compared to the project design specification. All inputs from 4V upwards satisfy the required closure time of 1.5s, whilst inputs of 10V and 12V satisfy the optimum closing time of less than 0.5s.

5.1.2 Closed-Loop

The output responses between the open-loop system and the closed-loop are very different, both in terms of gripper closure time, gripper acceleration/deceleration and positioning of the gripper. For example, in open-loop, at an input voltage of 6V, the overall time for the gripper to travel from fully open to closed took 0.75s compared to 1.12s it took the closed-loop system having a similar input. But this is an unfair comparison, as the 6V input in the closed-loop was paired with a proportional gain to add only a reference signal. The actual signal entering the machine was the control signal, which from Figure 4.3.5 shows to decrease from 12V down to 0V rather than stay at a steady value of 6V as is the case with open-loop.

The CL model response time can be increased further through increasing the gain of the proportional controller. The control signal is limited to 12V, and so the high initial control signal would be a constant 12V value, before decaying to 0 as the gripper reaches its intended position. This would of course increase energy consumption, probably above the energy consumption of the OL model, but faster response times in CL vs OL are achievable if the user demands it. See Appendix A8 for the faster response plots in CL.

The closed-loop model has a number of advantages over the open-loop model. The additional reference signal does suggest the closed-loop model has higher energy consumption in comparison with the open-loop model. However, calculations on energy consumption show that the closed-loop system is slightly more energy efficient, as the control signal decays exponentially rather than staying constant as it does in open-loop. A full quantification of energy consumption for each system is discussed in Section 5.2.

The closed-loop model is also usable with a gripper position sensor. If the gripper was to be incorporated into a more complex robot system, such as an automated object grasper, a number of

senses would be in use to measure object size, shape etc. A gripper position sensor could be used to determine the displacement required from the gripper to open/close sufficiently enough to grab the object. Through the manipulation of gains K and P in the closed-loop system (Figure 4.3.4), exact gripper displacements can be calculated, and hence more accurate positioning of the gripper is achievable in closed-loop.

It should also be noted that the signal inputted into the motor is safer for the closed-loop system. In open-loop, the user has direct control of the control signal inputted into the motor, and therefore circumstances can arise where the user continues to input a voltage into the motor even when the gripper is fully closed, causing a stall condition. Over time, this could cause wear on the motor. The closed-loop mitigates this problem, as the voltage drops immediately to zero once the desired position has been reached.

The stability of the system, as analysed using the Bode plots of the open-loop system, shows that there is a large phase margin of 90° . This is sufficient phase margin to ensure stability here. The phase plot however comes very close to -180° at around 10,000 rad/s. The frequency of the PWM output from the Arduino ranges from 490Hz, or 3,078.8 rad/s on most pins, up to 980Hz, or 6,157.5 rad/s on pins 5 and 6 [38]. Therefore, since the PWM cannot output frequencies outside of the 3,079-6,158 rad/s range, the system will be well within the stability regions.

5.2 Evaluation of Energy Consumption

For evaluating the energy consumption of each system, the total energy used to displace the gripper by 1.5 rad (fully open to closed, or vice versa), with an input of 6V, shall be calculated for open-loop and closed-loop.

5.2.1 Open-Loop

It is assumed that the motor accelerates to full speed instantly, and thus current is close to zero. Then in open-loop power consumption is small if frictional forces are neglected. In fact, from the motor data (Appendix A2.2) power input at no-load speed is 32.4W. Considering it takes only 0.75s for the gripper to close fully, this equates to a total amount of,

$$\text{Energy} = \frac{32.4 \times 0.75}{2} = 12.15J$$

The half is due to the PWM input, in which the duty cycle is at 50% (on half the time, off the other half).

5.2.2 Closed-Loop

In closed-loop, the input signal to the motor continually decreases, from a value of 12V down to 0V (see Figure 4.3.5). But for the sake of analysis, it is assumed that the motor is close to but not exactly at no-load speed. Therefore, as performed in open-loop, a constant current is assumed, and is taken as the same current level for no load-speed at 12V. If the total voltage is calculated over the total time of the gripper closing, then, energy can be found from [40],

$$\text{Energy} = \int_0^t P dt = I \int_0^t V(t) dt \quad (5.2.1)$$

Where $P = VI$, and I is constant.

The control signal in Figure 4.3.5 can be estimated from the following function (See Appendix A5),

$$U(t) = V(t) = 1.25t^4 - 8.88t^3 + 23.10t^2 - 26.47t + 11.71 \quad (5.2.2)$$

Then the integral in Eqtn 5.2.1, ignoring the I term, can be solved by integrating Eqtn 5.2.2, from $t = 0$ to $t = 1.12s$, where 1.12s is the time taken to fully close the gripper,

$$U_{total} = \int_0^{1.12} (1.25t^4 - 8.88t^3 + 23.10t^2 - 26.47t + 11.71) dt = 4.27V.s \quad (5.2.3)$$

Then from Eqtns 5.2.1 and 5.2.3, and taking current as 2.7A at no-load (see Appendix A2.2),

$$Energy = 2.7 \times 4.27 = 11.53J \quad (5.2.4)$$

But the addition of the reference signal, R , is additional energy consumption. For using with an Arduino, the analogue input pins have a rated resistance of $100M\Omega$ [41], and recommends an output impedance of $10k\Omega$ or less [42]. Power is then given as [43],

$$P = \frac{V^2}{R} = \frac{6^2}{(100 \times 10^6 + 10 \times 10^3)} = 0.360 \times 10^{-6} W$$

And therefore, as total time to close the gripper is 1.12s, the energy used is $0.36 \times 10^{-6} \times 1.12 = 0.40 \times 10^{-6}$ J. This is clearly negligible. It can be concluded therefore that the open-loop system uses only 5% more energy than closed-loop.

5.3 Further Applications

The gearbox here is mechanically connected to the gripper section of the robotic arm. However, it could be possible to use the gearbox with other parts of a robotic arm, such as the arm joints. In deciding upon a suitable robotic arm for use in manufacturing, both the payload and the speed become a major consideration [44]. If the gear change mechanism were to operate quick enough, then in many applications it may be more beneficial to use a robot arm made of a light weight material having good strength, perhaps a fibre-reinforced composite, which can be actuated at fast speeds for when the gripper is moving between objects. For picking and manipulating objects, the gear change can offer the higher torque ratio to enable the object to be lifted effectively.

Industrial robotic arms also widely incorporate press brakes. Within industry there has been a reluctance to use automated press brakes due to reasons of substantial programming efforts, expenses and limited resource [45]. However, using the closed-loop control system proposed in this project, the use of brakes can be avoided altogether. Although brakes may allow faster travel of the arm, the complexities of incorporating the additional brake system and the costs of doing so may not be advantageous.

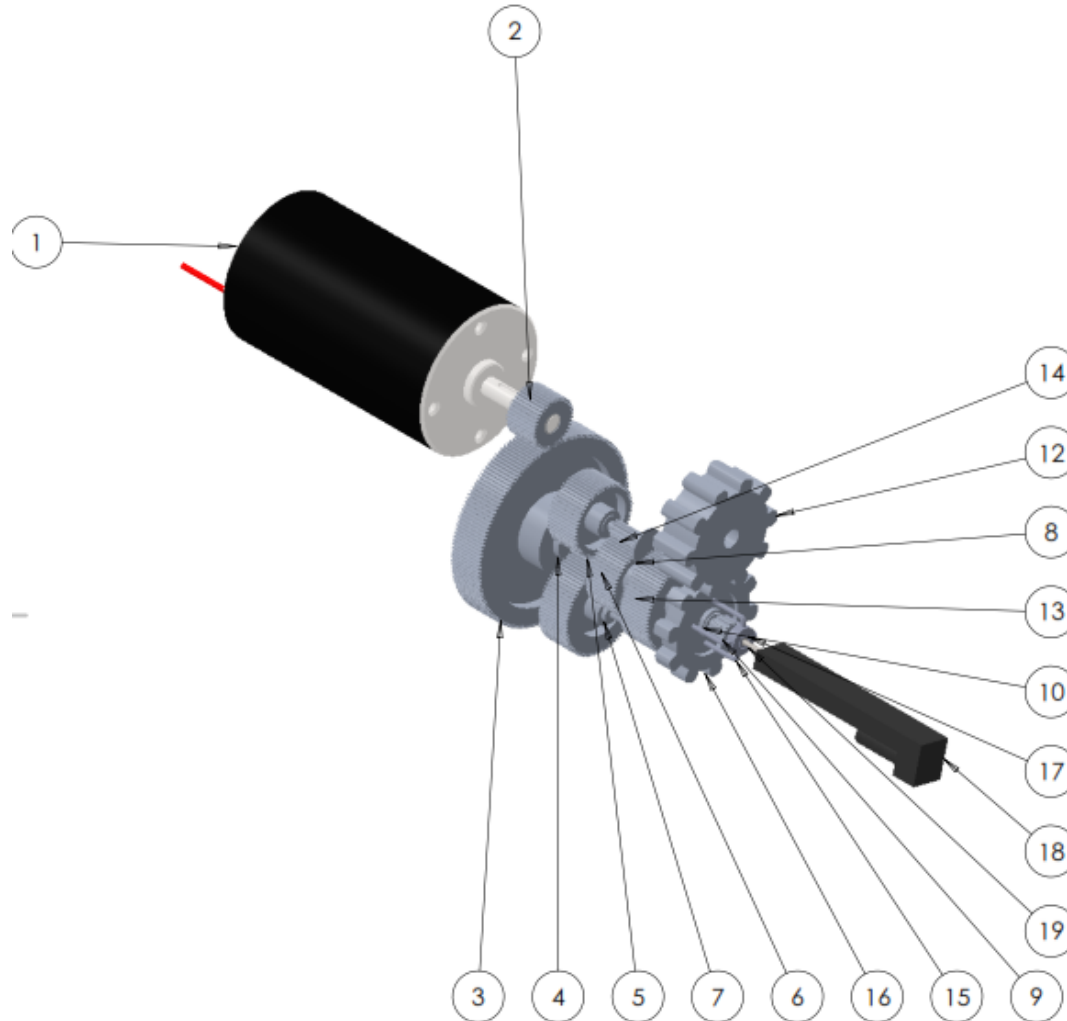
Finally, as mentioned previously, the closed-loop model would allow for a complex robotic gripper setup, having cameras to sense object size, shape, surface texture etc. The closed-loop system, with a position sensor on the gripper, would allow for the object geometry to be compared to the gripper positioning. Algorithms could be developed that would accurately grip objects at optimal speed (i.e. algorithms that would determine the reference signal in Figure 4.3.4).

6 Manufacturing and Costing

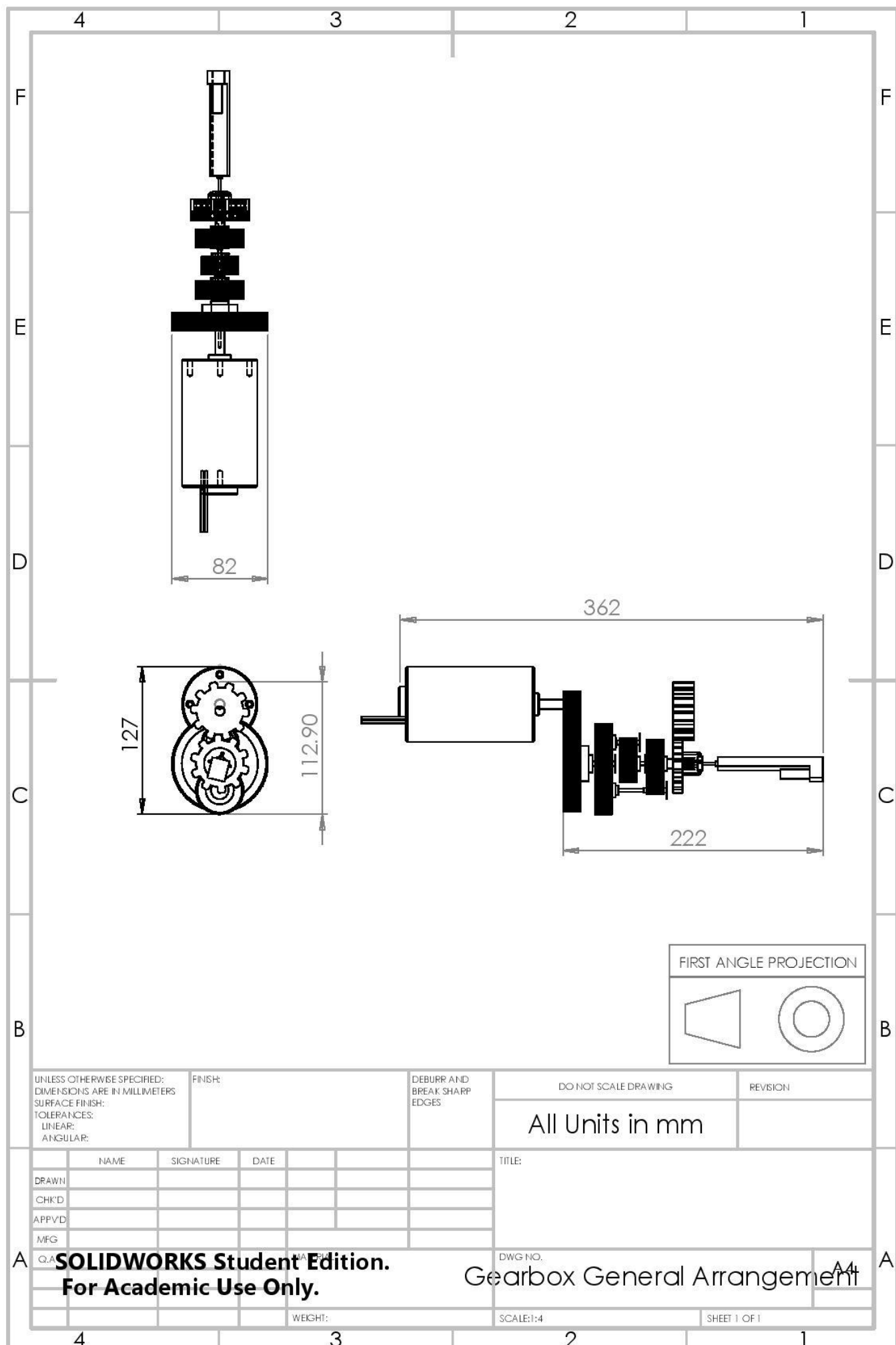
Engineering drawings are presented for those components that require manufacturing, namely gears, shafts and gripper components. All drawings can be found in the Appendix (A7). Presented here are important general arrangement and cross-sectional drawings.

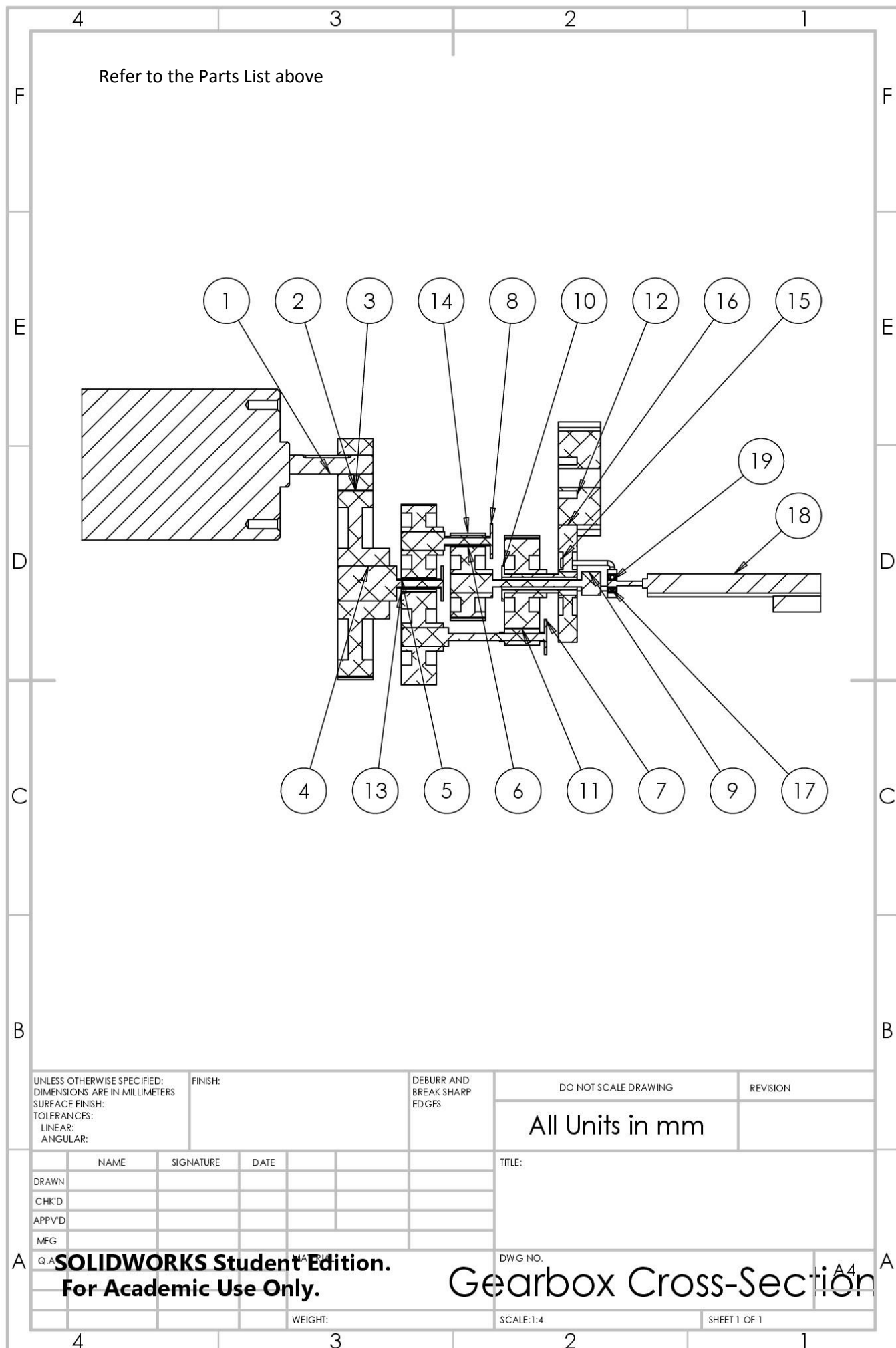
6.1 Gearbox Engineering Drawings

6.1.1 3D Model, Parts List, General Arrangement and Cross-section

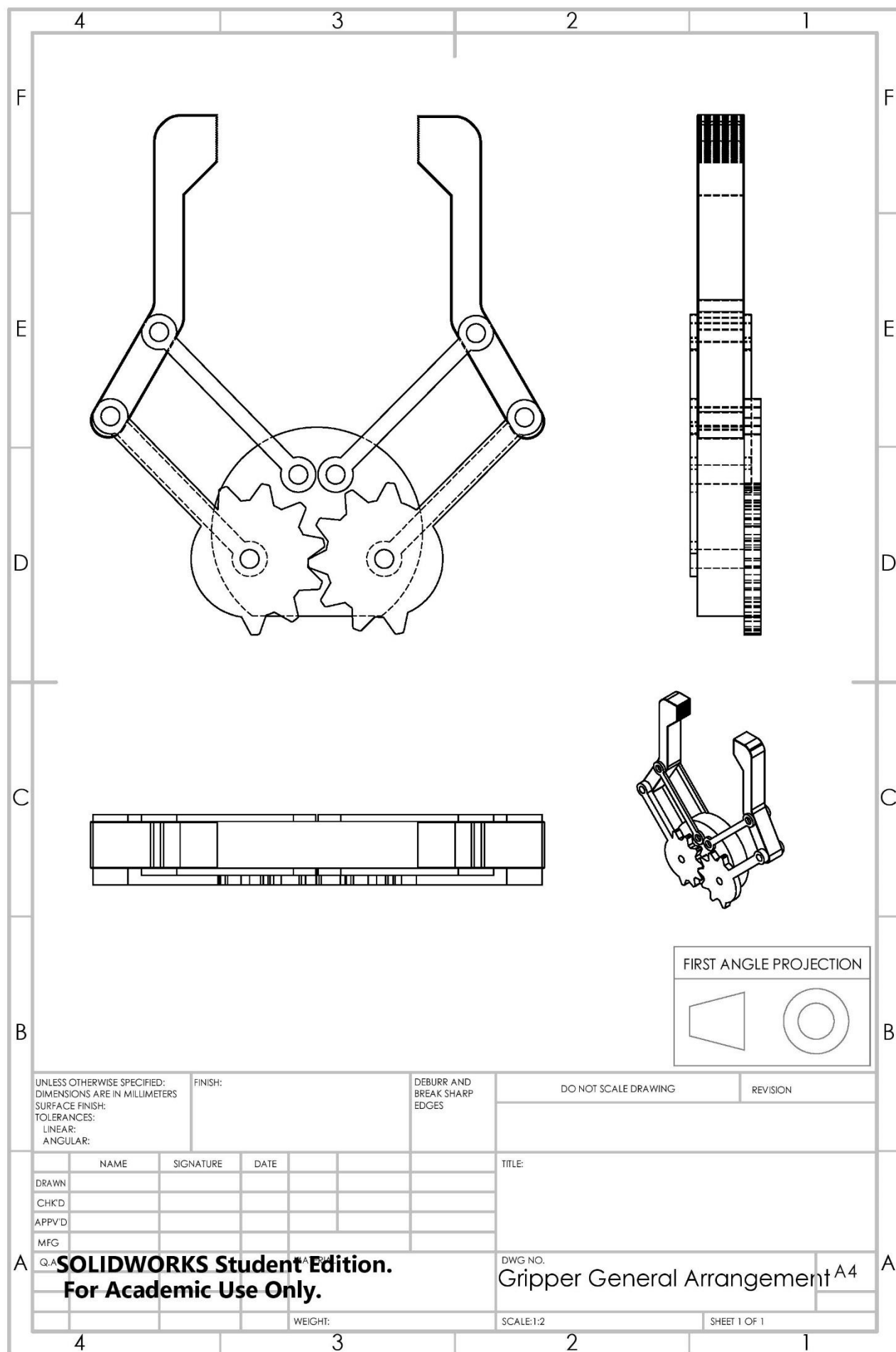


ITEM NO.	PART NUMBER	DESCRIPTION	QTY.
1	CIM MOTOR AndyMark FR801-001	DC Motor	1
2	40 Teeth	DC Motor Gear	1
3	160 Teeth	Head Gear	1
4	15mm Shaft	Head Gear Shaft	1
5	10 Teeth	Splitter Gear	1
6	59 Teeth	Speed Gear	2
7	8mm Shaft Stepped	Torque Gear Shaft	1
8	8mm Shaft Stepped Short	Speed Gear Shaft	1
9	8mm Shaft Stepped Geared	Speed Output Shaft	1
10	8mm Shaft Hollowed	Torque Output Shaft	1
11	10 Teeth (1)		1
12	Output Gear	Connects Directly to the Gripper	1
13	78 Teeth	Torque Gear	2
14	10 Teeth (2)		1
15	Bearing attachment	Connects Linear Actuator to Sleeve	1
16	Sleeve	Mashes the Output Shafts to the Output Gear	1
17	Ball Bearing		1
18	Linear Actuator Body		1
19	Linear Actuator Shaft		1





6.2 Gripper General Arrangement



6.3 Estimated Cost to Manufacture

The costs to manufacture the machine are based on a one-off manufacturing, using conventional manufacturing techniques (mainly lathe and mill machining). The material used for the majority of the components is Aluminium Alloy. The costs for manufacturing the gearbox and gripper components are obtained from estimations using the online “Cost Estimator” software designed by Custompart [46]. For manufacturing the gearbox and gripper components using conventional machining techniques and with a typical Aluminium alloy, the estimated cost is approx. £200. Then, including the cost of the DC Motor (£30.73) [47], the Arduino (£16.16) [48], and linear motor (£51.34) [28] the total estimated cost is,

$$\text{Estimated Cost} = \text{£200} + \text{£30.73} + \text{£16.16} + \text{£51.34} = \text{£295.23}$$

7 Conclusions

Current progress in the development of robotic grippers within literature has shown to be a developing, progressive area to work in, with lots of room for innovation. Of particular interest is in the intelligent control of grippers and the manipulation of gripper dynamics to achieve effective automated gripping of objects.

Two machines have been presented and designed in this report: a two-finger robotic gripper, and an automatic gearbox.

The two-finger gripper design can achieve an opening distance of 136.84mm at its widest. It has been designed to include a contact area of 19mmx19mm on each finger, with a jolted surface to increase frictional force.

The automatic gearbox has been designed to have two gear ratios: 140 and 243. A selected DC motor is used, giving a max output speed of 5330rpm at 12V, and a max stall torque of 2.36Nm at 12V. The ratio of 140 has been designed specifically to optimize the speed of the gripper – the gripper can close from fully open to closed in its shortest time at 0.378s when 12V input is used. The ratio of 243 has been designed for achieving high torque. To avoid possible damage to the motor, the motor is limited to 6V input when in high torque. The highest possible torque achievable at the gripper therefore shows to be 292Nm. The gripper should comfortably grip objects of up to 10kg without any slip.

An original design idea for an automatic gear shift mechanism has been proposed. The new design has a number of advantages over conventional gear locking mechanisms used in synchronizers, including balanced forces across the sliding sleeve and the elimination of fragile components – ball bearings – from the mainshaft gears due to the concentric design of the output shafts.

The mathematical model in differential form for the whole machine has been developed, and the Laplace transfer function has been determined from the differential for displaying the relationship between DC voltage input and the gripper position.

Simulations using Simulink on OL and CL setups of the transfer function have been performed to determine gripper response times based on varying input voltages. In OL, the gripper can achieve closing times of 1.2s or less if 4V or greater is inputted.

The CL system is constructed as a negative feedback loop with a proportional controller. The reference signal can be altered from 0 to 1.5V, 1.5V representing full closure of the gripper (1.5 rad). A proportional only controller is used, offering satisfactory response times. To achieve full gripper closure in CL takes 1.12s. Whilst slower than the OL system, the controllability of gripper position makes the CL superior to the OL system.

The CL system uses slightly less energy than the OL system, due to the controlled decay of the input voltage – OL system uses approx. 12.15J for a full closure of the gripper, CL uses approx. 11.53J to achieve the same. It has been suggested that the energy consumption of the CL could be increased in order to achieve faster gripper closure times than the OL system, if the user desires it.

The gearbox and gripper designed in this project would allow for greater control of gripper speeds and forces, and could prove effective in many applications, such as manufacturing, where both speed of the robotic arm and gripping forces are essential to robust manufacturing having short lead times.

7.1 Comparison to the Project Design Specification

The key figures from the PDS are here compared to the actual figures obtained from the design.

Power: PDS: Minimum power requirement of 210W at the gripper. Design: Max gripper power achievable is 320W.

Force: PDS: Gripper force of 240N total. Design: Max gripper force achievable is 292Nm.

Speed: PDS: Full closure of gripper within 1.5s, or 0.5s for optimum. Design: Max achievable speed is in OL at 0.378s.

Timing: PDS: Full engagement of gear to be completed in less than 0.6s. Design: Calculations show an achievable time of 0.67s.

Dimensions: PDS: Gearbox net size no larger than 80x80x50mm. Design: Size is 82x112.9x222mm excluding the DC motor size.

PDS: Gripper widest distance of 130mm + 10mm. Design: Widest distance is 136.84mm.

Weight: PDS: Max weight of 200g for the gearbox. Design: Solidworks "Mass Properties" estimate of 400g.

Most of the specifications were met in the design. The dimensions of the gearbox however were much larger than in the specification, and this in turn had an effect on the weight. Reducing gear widths and diameters by altering teeth dimensions may reduce these values to the specified limits, and should be considered as further work.

The speed of gear engagement is 0.07s slower than the value in the PDS. Therefore, an option of sourcing a slightly quicker linear motor could be chosen, or if the travel distance for the sleeve were reduced from 8mm to, say, 7mm, the time could be reduced to 0.58s which would satisfy the PDS value.

7.2 Further work

There are three main areas of further work that would need to be completed in the physical design of the machine. The first is the casing or housing of the gearbox, as mentioned in the comments of the PDS. Included in this would be the securing of the gear shafts of the gearbox. The casing should cover the gears, shafts, DC motor and linear motor. It should be designed to add support points for the shafts to prevent any of the gears from un-meshing and reduce vibration.

Second, a locking mechanism would ideally need to be developed that would lock the gearbox in place during high torque stall situations. For example, when the gripper is to apply a large torque to pick a heavy object, the motor should apply a large initial torque. But the motor would be stationary, and would be in a stall situation. Having some mechanism, perhaps a third set of teeth in line with the two output shafts for speed and torque (see Figure 3.5.2) that are stationary, would relieve the torque output from the motor. Then the DC motor may apply high torque for a very short time period, after which the linear motor would engage the sleeve with the stationary, additional teeth. So long as these

teeth can withstand the reaction force from the gripper, the large gripping force could be retained without risking burnout of the motor.

Third, when the gripper is fully closed, the angle of the linkages in the current design is 78.55° (see Appendix A9). But it is found from Eqtn 3.2.2 that the force the gripper can apply is directly proportional to the sine of the angle of the linkages. Therefore, the gripper needs redesigning to increase the gripper closure angle to 90° . The base plate should be widened, and the linkage gear's diameters should be increased in order to achieve this.

In terms of additional simulations, then it is vital that the linear motor performance be simulated and analysed. Currently, only the linear motor speed and distance travelled has been used to select an appropriate linear motor. Therefore, as completed on the DC motor, simulations should be run to verify this design decision, and to check how it performs under different voltage levels to get the performance required using the least amount of energy.

Further software development should be completed for the gear shifting mechanism, and for incorporating the closed-loop system. This would include the reading of user inputs for the torque and speed setting, and actuating the linear motor as necessary to select the correct gear ratio. For the closed-loop motor control, the conversion of a reference signal and calculation to achieve the appropriate control signal (of PWM form) to attain the desired output response would need to be developed.

Noticing that CL control uses slightly less energy than the OL system, since the control signal can be controlled. It is therefore possible to improve energy consumption further, by using a more complex controller, whilst retaining the fast response times. Or, if energy consumption was more important than response time, the gain of the proportional controller can be reduced, giving slower response times but saving on energy consumption.

Finally, physical building and testing of the machine would be vital. Building the machine would require suitable selection of bolts to secure the gripper components. Testing should be completed on individual aspects, including:

- Testing of the DC motor H-Bridge controller
- Open-loop and closed-loop motor performance for speed of motor
- Testing of the gear changing mechanism, to check for meshing and timing
- Evaluation of the energy consumption for both open-loop and closed-loop DC motor control, and for the linear motor.

8 Reflection

The majority of this project has been in the application of the engineering principles and modules taught to me throughout my Bachelor's degree. It has helped not only to reinforce the engineering principles I have been taught, but has encouraged me to search for information from other disciplines, such as in software development, electrical engineering and embedded systems.

Perhaps one of the most useful tools used is the logbook. The logbook allowed me not only to document work I have completed, but gave me space in which I could write down ideas, equations, drawings etc. In conjunction with the timing plans I had set myself, it helped concentrate my efforts effectively on the individual tasks that were required, and to complete the project in good time for submission.

I spent the majority of time during first semester gathering a large amount of background theory, and completing a literature search. I realized how important this process was in ensuring that the work I would go on to complete was accurate, realistic and original.

To improve my efforts for future projects, I have realized that I should create a more focused effort when performing the literature search. The majority of the literature I surveyed was of little or no use to the project I was working on, and this was partly due to the fact that I limited my area of search to only the University's library gateway. Further investigations eventually led me to other resources, such as public libraries, online academic sites etc. that offered information that may not have been found in literature within the University. This is typically true of journals and other reports that may not be part of the subscription packages of the University.

9 References

- [1] RobotWorx, “Advantages of Automation,” 2015. [Online]. Available: www.robots.com/articles/viewing/advantages-of-automation.
- [2] B. Mashadi and D. A. Crolla, Vehicle Powertrain Systems, John Wiley & Sons Inc, 2011.
- [3] AREXX, “Robot Arm,” AREXX, 2010. [Online]. Available: http://www.arexx.com/robot_arm/html/en/index.htm. [Accessed 02 April 2016].
- [4] D. Jelaska, Gears and Gear Drives, Chichester: John Wiley & Sons Ltd, 2012.
- [5] S. P. Radzevich, “Tooth Ratio of a Gear Pair,” in *Theory of Gearing Kinematics, Geometry, and Synthesis*, Hoboken: Taylor and Francis, 2012, p. 32.
- [6] J. Bird and C. Ross, “Work, Energy and Power,” in *Mechanical Engineering Principles*, Abingdon, Routledge, 2012, p. 175.
- [7] L. Kren, “Getting A Handle on Inertia,” *Machine Design*, vol. 71, no. 15, p. 92, 1999.
- [8] S. P. Radzevich, “External Spur Gears,” in *Dudley's Handbook of Practical Gear Design and Manufacture, Second Edition*, Boca Raton, Hoboken: Taylor and Francis, 2012, p. 22.
- [9] A. Hughs and B. Drury, “Electric Motors - The Basics,” in *Electric Motors and Drives*, Oxford, Elsevier Ltd., 2013, pp. 20-21.
- [10] A. Hughs and B. Drury, “Specific Loadings,” in *Electric Motors and Drives*, Oxford, Elsevier Ltd., 2013, p. 20.
- [11] K. Taylor, *Electric Motors*, Sheffield: Sheffield Hallam University, 2014.
- [12] A. Hughs and B. Drury, “Electric Motors - The Basics,” in *Electric Motors and Drives*, Oxford, Elsevier Ltd., 2013, p. 22.
- [13] A. Hughs and B. Drury, “Voltage Control - DC Output from DC Supply,” in *Electric Motors and Drives*, Oxford, Elsevier Ltd., 2013, pp. 41-43.
- [14] D. Ashby, “Basic Theory,” in *Electrical Engineering 101*, London, Elsevier Inc., 2012, pp. 25-26.
- [15] H. Naunheimer, B. Bertsche, J. Ryborz and W. Novak, “Gearshift Mechanisms,” in *Automotive Transmissions: Fundamentals, Selection, Design and Application*, Berlin, Springer Berlin Heidelberg, 2011, pp. 316-318.
- [16] A. Yadav, G. Kaur and A. Sharma, “Microcontroller Based Open-loop Speed Control,” *International Journal of Research in Engineering & Applied Sciences, Volume 2, Issue 6*, 2012.

- [17] N. Venkataramana Naik and S. S. P, "Improved Torque and Flux Performance of Type-2 Fuzzy-based Direct Torque Control Induction Motor Using Space Vector Pulse-width Modulation," *Electric Power Components and Systems*, pp. 658-669, 2014.
- [18] L. Weize, W. Wenlong, T. Bingquan and M. Jianwei, "Research on Torque Control of Brushless DC Motor for Electric Vehicle," *Applied Mechanics and Materials*, Vols. 496-500, pp. 1260-1264, 2014.
- [19] F. Dimeas, D. V. Sako, V. C. Moulianitis and N. A. Aspragathos, "Design and fuzzy control of a robotic gripper for efficient strawberry harvesting," *Robotica*, pp. 1085-1098, 2015.
- [20] S.-J. Huang, W.-H. Chang, J.-Y. Su and Y.-C. Liu, "Distributed Control Intelligent Robotic Gripper," *Applied Mechanics and Materials* Vols. 479-480, pp. 742-746, 2014.
- [21] N. I. Glossas and N. A. Aspragathos, "Fuzzy logic grasp control using tactile sensors," *Mechatronics*, vol. 11, no. 7, pp. 899-920, 2001.
- [22] S. Krenich, "Optimal Design of Robot Gripper Mechanism using Force and Displacement Transmission Ratio," *Applied Mechanics and Materials*, vol. 613, pp. 117-125, 2014.
- [23] C. Lanni and M. Ceccarelli, "An Optimization Problem Algorithm for Kinematic Design of Mechanisms for Two-Finger Grippers," *The Open Mechanical Engineering Journal*, vol. 3, pp. 49-62, 2009.
- [24] Y. Zhang, S. Finger and S. Behrens, "Planar Linkages," Carnegie Mellon University, [Online]. Available: <https://www.cs.cmu.edu/~rapidproto/mechanisms/chpt5.html>. [Accessed 02 April 2016].
- [25] VEX Robotics, "VEX Robotics Motor Data - CIM Motor (217-2000)," VEX Robotics, 04 November 2015. [Online]. Available: <http://motors.vex.com/cim-motor>. [Accessed 02 April 2016].
- [26] A. Hughs and B. Drury, "Equivalent Circuit," in *Electric Motors and Drives*, Oxford, Elsevier Ltd., 2013, p. 28.
- [27] D. V. Neto, D. G. Florencio, P. Rodrigues and J. Fernandez, "Manual Transmission: Synchronization Main Aspects," Society of Automotive Engineers, 2006.
- [28] Active Robots, "L12 EV3 Linear Actuator 50mm," [Online]. Available: <http://www.active-robots.com/l12-ev3-linear-actuator-50mm>. [Accessed 02 April 2016].
- [29] D. Harres, "The Bipolar Transistor," in *MSP430-based Robot Applications*, Burlington, Elsevier Science, 2013, pp. 46-52.
- [30] C. Mitchell, Talking Electronics, [Online]. Available: <http://www.talkingelectronics.com/projects/SpotMistakes/SpotMistakesP1.html>. [Accessed 04 April 2016].

- [31] Arduino, “Technical Specs,” Arduino, 2016. [Online]. Available: <https://www.arduino.cc/en/Main/ArduinoBoardUno>. [Accessed 4 April 2016].
- [32] N. S. Nise, “Electromechanical System Transfer Functions,” in *Control Systems Engineering, Third Edition*, USA, John Wiley & Sons, Inc., 2000, pp. 87-91.
- [33] D. K. Anand and Z. R. B, “Modelling of Physical Systems,” in *Introduction to Control Systems*, Bodmin, Butterworth-Heinemann Ltd, 1995, p. 37.
- [34] E. H. Wernick, “Direct Current Motors,” in *Electric Motor Handbook*, Maidenhead, McGraw-Hill Book Company (UK) Limited, 1978, p. 51.
- [35] D. K. Anand and Z. R. B, “Modelling of Physical Systems,” in *Introduction to Control Systems*, Bodmin, Butterworth-Heinemann Ltd, 1995, pp. 21-23.
- [36] N. S. Nise, “Electromechanical System Transfer Functions,” in *Control Systems Engineering, Third Edition*, USA, John Wiley & Sons, Inc., 2000, p. 89.
- [37] K. Dutton, S. Thompson and B. Barraclough, “Block Diagrams,” in *The Art of Control Engineering*, Essex, Pearson Education Limited, 1997, p. 91.
- [38] Arduino, “analogWrite(),” 2016. [Online]. Available: <https://www.arduino.cc/en/Reference/AnalogWrite>. [Accessed 13 April 2016].
- [39] B.-R. Höhn, K. Michaelis and M. Hinterstoißer, “Optimization of Gearbox Efficiency,” *goriva i maziva*, vol. 4, no. 48, pp. 441-480, 2009.
- [40] RMIT University, “Electrical principles - Terminology,” RMIT University, 2009. [Online]. Available: <https://www.dlsweb.rmit.edu.au/toolbox/electrotech/toolbox1204/resources/01principles/03terminology/07power.htm>. [Accessed 4 April 2016].
- [41] Atmel, *ATMEL 8-BIT Microcontroller Datasheet*, San Jose: Atmel Corporation, 2015, p. 310.
- [42] Atmel, *ATMEL 8-BIT Microcontroller Datasheet*, San Jose: Atmel Corporation, 2015, p. 244.
- [43] W. H. Roadstrum and D. H. Wolaver, “Power and Energy,” in *Electrical Engineering for all Engineers*, USA, John Wiley & Sons, Inc., 1994, pp. 19-20.
- [44] M. Bélanger-Barrette, “How To Choose The Right Industrial Robot,” Robotiq, 22 April 2014. [Online]. Available: <http://blog.robotiq.com/bid/70408/How-to-Choose-the-Right-Industrial-Robot>. [Accessed 04 April 2016].
- [45] K. Miller, “Press Brakes and Robots,” Robotic Industries Association, 17 May 2011. [Online]. Available: http://www.robotics.org/content-detail.cfm/Industrial-Robotics-Industry-Insights/Press-Brakes-and-Robots/content_id/2779. [Accessed 04 April 2016].

- [46] CustomPartNet, "Cost Estimator," [Online]. Available: <http://www.custompartnet.com/estimate/machining/>. [Accessed 6 April 2016].
- [47] RobotShop, "12V 5310 RPM "CIM" Brushed DC Motor," 2016. [Online]. Available: <http://www.robotshop.com/uk/12v-5310-rpm-cim-brushed-dc-motor.html>. [Accessed 6 April 2016].
- [48] RS Components Ltd, "Arduino Uno SMD Rev3," 2016. [Online]. Available: <http://uk.rs-online.com/web/p/processor-microcontroller-development-kits/7697409/>. [Accessed 6 April 2016].
- [49] Boston University Physics, "Friction," 2012. [Online]. Available: <http://physics.bu.edu/~duffy/py105/Friction.html>. [Accessed 20 11 2012].
- [50] J. A. Fleming, "Electromagnetic Induction," in *Magnets and Electric Currents*, London, E. & F. N. Spon Ltd, 1902, pp. 173-174.
- [51] C. Maxfield, "An Introduction to Electric Circuits," in *Electrical Engineering*, Amsterdam, Newnes/Elsevier, 2008, pp. 12-13.

Appendices

A1. Gripper Vector Analysis

As the gripper must be able to pick up objects of various sizes, the gripper finger must always remain “fixed” in rotation. This means point C (from Figure 3.3.2) cannot rotate about points A or B, but can only move translationally in x and y. Example of notation: \vec{V}_{C-O_2} means the vector velocity of point C with respect to point O₂. The following is the vector derivation to determine angles θ_1 and θ_2 and AO_1 and BO_2 .

$$\vec{V}_{C-O_2} = \vec{V}_{C-B} + \vec{V}_{B-O_2} \quad \text{and} \quad \vec{V}_{C-O_1} = \vec{V}_{C-A} + \vec{V}_{A-O_1}$$

But,

$$\vec{V}_{C-B} = \vec{V}_{C-A} = 0$$

Therefore,

$$\vec{V}_{C-O_2} = \vec{V}_{B-O_2} \quad \text{and} \quad \vec{V}_{C-O_1} = \vec{V}_{A-O_1} \quad (1)$$

Similarly,

$$\vec{V}_{B-O_1} = \vec{V}_{B-A} + \vec{V}_{A-O_1} \quad \text{and} \quad \vec{V}_{A-O_2} = \vec{V}_{A-B} + \vec{V}_{B-O_2}$$

But,

$$\vec{V}_{B-A} = \vec{V}_{A-B} = 0$$

Therefore,

$$\vec{V}_{B-O_1} = \vec{V}_{A-O_1} \quad \text{and} \quad \vec{V}_{A-O_2} = \vec{V}_{B-O_2} \quad (2)$$

But,

$$\vec{V}_{A-O_1} = \vec{V}_{A-O_2} = \vec{V}_{B-O_2}$$

But from the definition of tangential velocity above becomes,

$$\vec{V}_{A-O_1} = \vec{V}_{B-O_2} \quad \Rightarrow \quad AO_1 \vec{\omega}_1 = BO_2 \vec{\omega}_2 \quad (3)$$

Splitting up into vertical and horizontal velocities,

$$[V_{A-O_1}]_H = AO_1 \vec{\omega}_1 \sin \theta_1 \quad [V_{B-O_2}]_H = BO_2 \vec{\omega}_2 \sin \theta_2$$

$$[V_{A-O_1}]_V = AO_1 \vec{\omega}_1 \cos \theta_1 \quad [V_{B-O_2}]_V = BO_2 \vec{\omega}_2 \cos \theta_2$$

Therefore,

$$AO_1 \vec{\omega}_1 \sin \theta_1 = BO_2 \vec{\omega}_2 \sin \theta_2 \quad (4)$$

$$AO_1 \vec{\omega}_1 \cos \theta_1 = BO_2 \vec{\omega}_2 \cos \theta_2 \quad (5)$$

Dividing (4) by (5),

$$\frac{\sin \theta_1}{\cos \theta_1} = \frac{\sin \theta_2}{\cos \theta_2} \quad \text{therefore} \quad \theta_1 = \theta_2 \quad \text{and} \quad AO_1 \vec{\omega}_1 = BO_2 \vec{\omega}_2$$

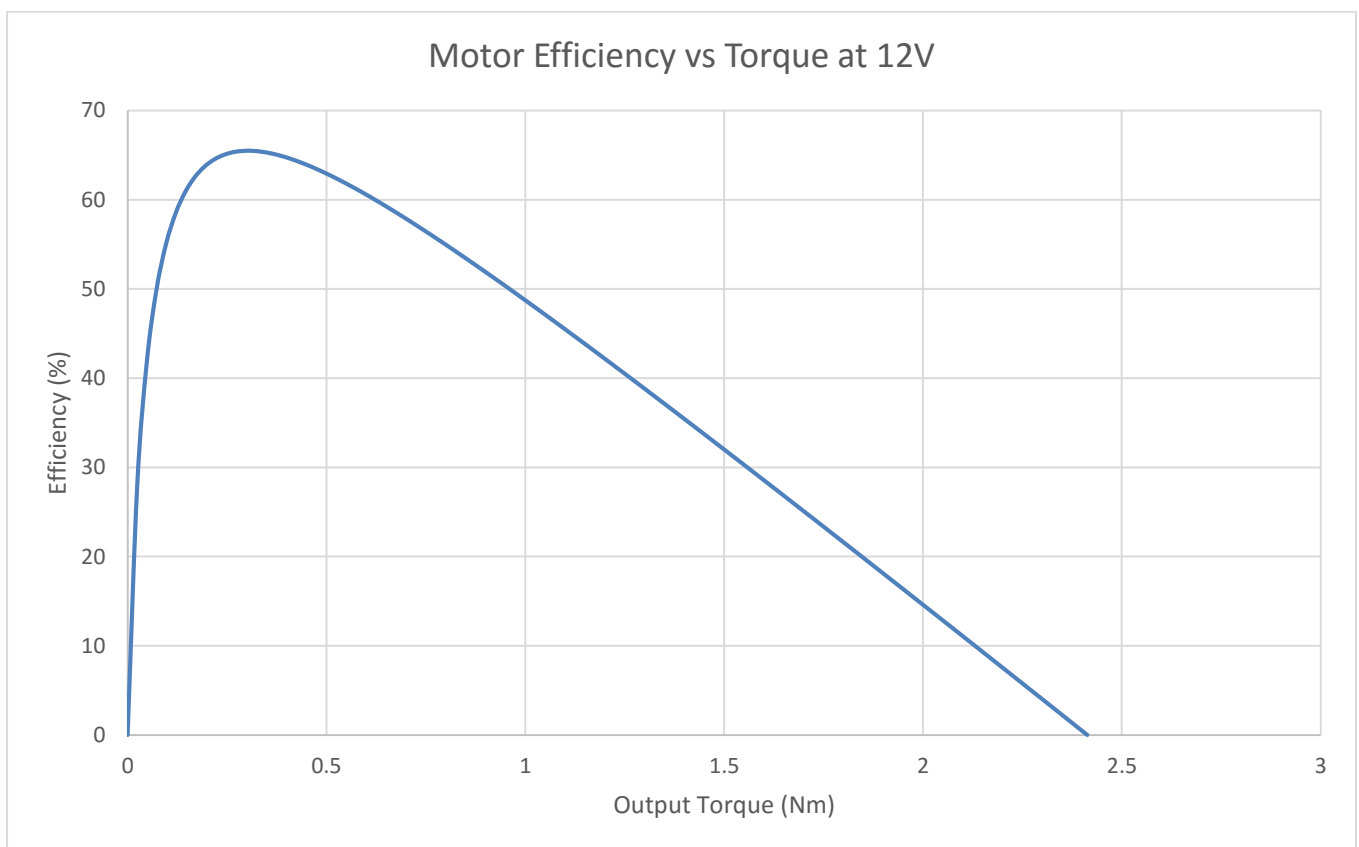
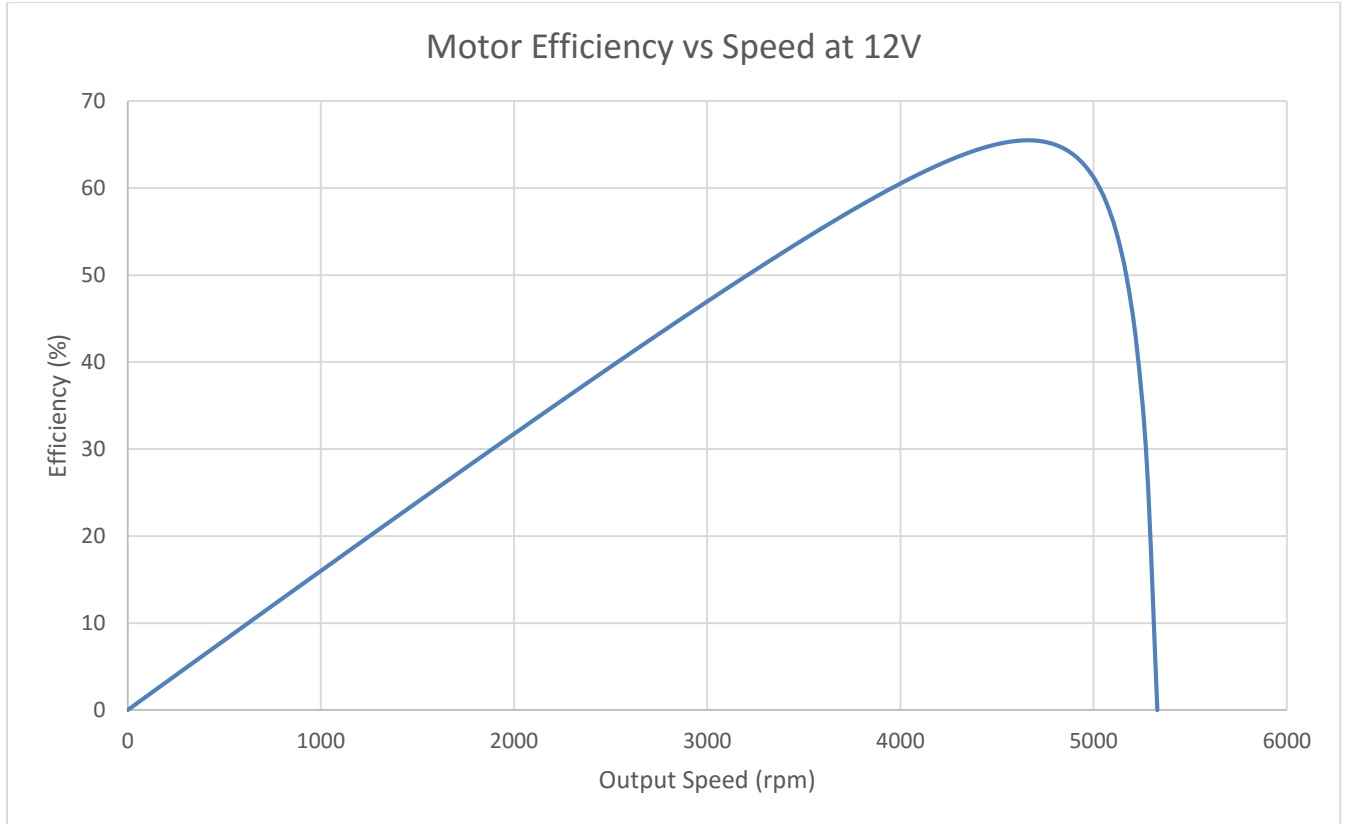
In order for $\theta_1 = \theta_2$ at all times, it must also hold that the change in angle must be equal after a given amount of time, i.e,

$$\frac{d\theta_1}{dt} = \frac{d\theta_2}{dt} = \vec{\omega}_1 = \vec{\omega}_2 \quad (6)$$

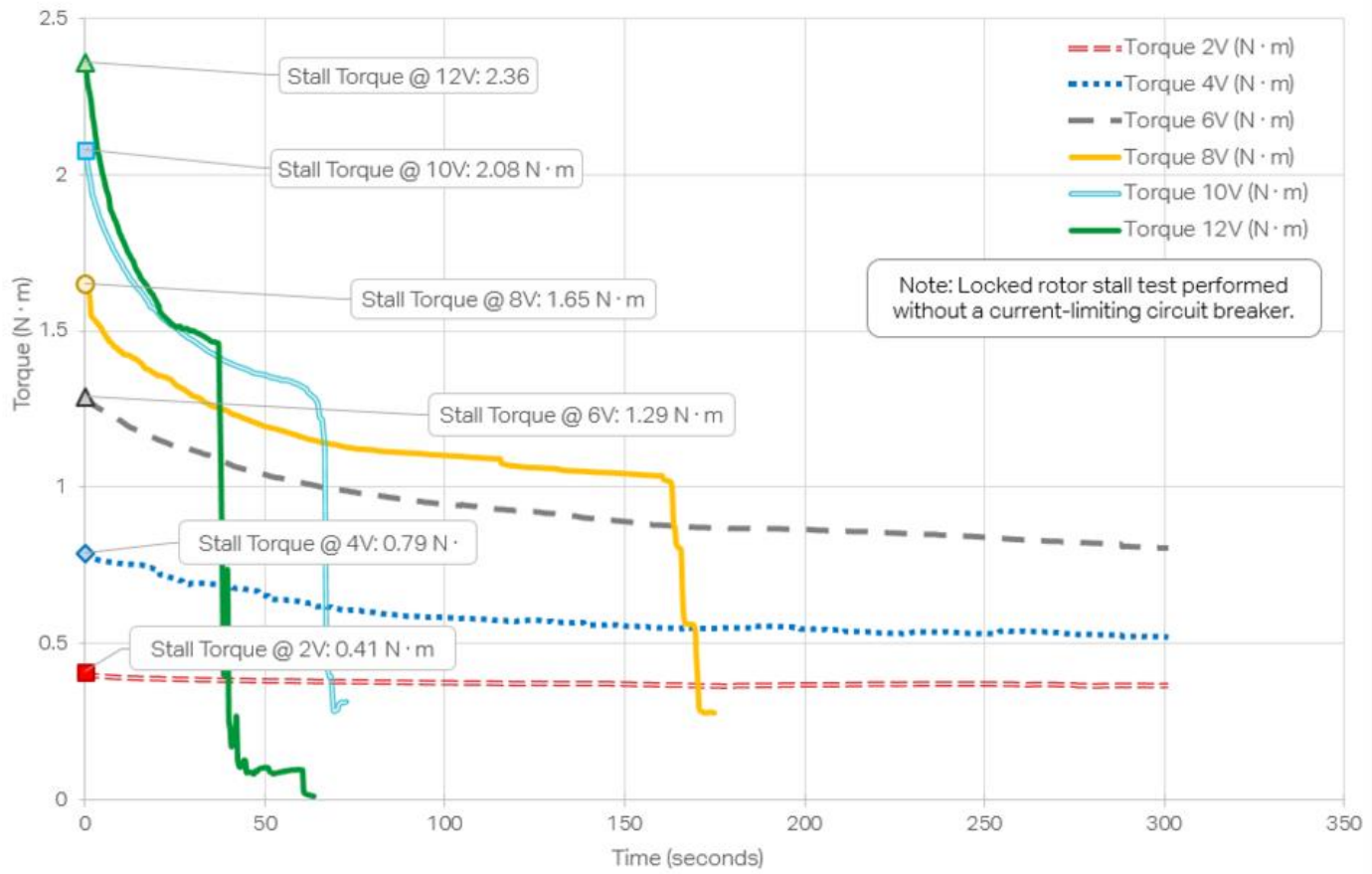
And therefore,

$$AO_1 = BO_2 \quad (7)$$

A2.1 CIM Motor Efficiency Data and Locked Motor Test



Locked Rotor Stall Test - CIM (217-2000)



A2.2 Full Motor Test Data

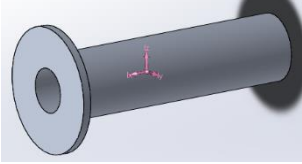
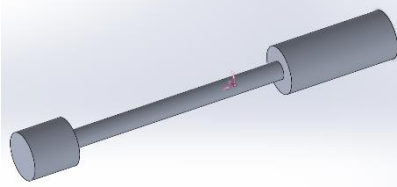
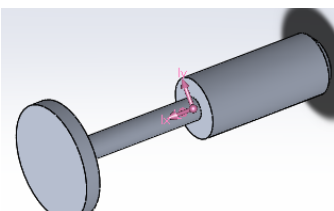
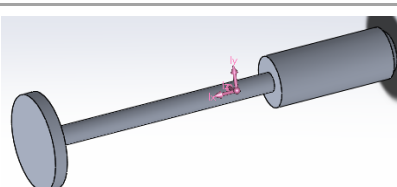
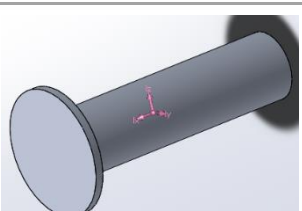
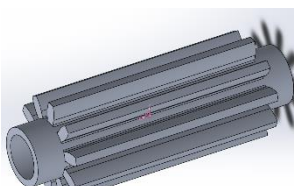
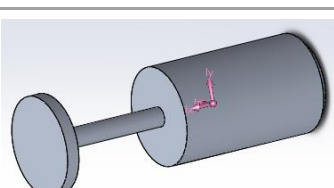
Speed (RPM)	Torque (N·m)	Current (A)	Supplied Power (W)	Output Power (W)	Efficiency (%)	Power Dissipation (W)
0	2.413	131.055	1572.66	0	0	1572.66
53.3	2.38887	129.771	1557.252	13.334	0.856	1543.918
106.6	2.36474	128.488	1541.856	26.398	1.712	1515.458
159.9	2.34061	127.204	1526.448	39.193	2.568	1487.255
213.2	2.31648	125.921	1511.052	51.718	3.423	1459.334
266.5	2.29235	124.637	1495.644	63.974	4.277	1431.67
319.8	2.26822	123.354	1480.248	75.961	5.132	1404.287
373.1	2.24409	122.07	1464.84	87.679	5.986	1377.161
426.4	2.21996	120.787	1449.444	99.127	6.839	1350.317
479.7	2.19583	119.503	1434.036	110.305	7.692	1323.731
533	2.1717	118.22	1418.64	121.215	8.544	1297.425
586.3	2.14757	116.936	1403.232	131.855	9.397	1271.377
639.6	2.12344	115.652	1387.824	142.225	10.248	1245.599
692.9	2.09931	114.369	1372.428	152.327	11.099	1220.101
746.2	2.07518	113.085	1357.02	162.158	11.95	1194.862
799.5	2.05105	111.802	1341.624	171.721	12.799	1169.903
852.8	2.02692	110.518	1326.216	181.014	13.649	1145.202
906.1	2.00279	109.235	1310.82	190.038	14.498	1120.782
959.4	1.97866	107.951	1295.412	198.792	15.346	1096.62
1012.7	1.95453	106.668	1280.016	207.277	16.193	1072.739
1066	1.9304	105.384	1264.608	215.493	17.04	1049.115
1119.3	1.90627	104.1	1249.2	223.439	17.887	1025.761
1172.6	1.88214	102.817	1233.804	231.116	18.732	1002.688
1225.9	1.85801	101.533	1218.396	238.524	19.577	979.872
1279.2	1.83388	100.25	1203	245.662	20.421	957.338
1332.5	1.80975	98.966	1187.592	252.531	21.264	935.061
1385.8	1.78562	97.683	1172.196	259.13	22.106	913.066
1439.1	1.76149	96.399	1156.788	265.46	22.948	891.328
1492.4	1.73736	95.116	1141.392	271.521	23.789	869.871
1545.7	1.71323	93.832	1125.984	277.313	24.629	848.671
1599	1.6891	92.549	1110.588	282.835	25.467	827.753
1652.3	1.66497	91.265	1095.18	288.087	26.305	807.093
1705.6	1.64084	89.981	1079.772	293.07	27.142	786.702
1758.9	1.61671	88.698	1064.376	297.784	27.977	766.592
1812.2	1.59258	87.414	1048.968	302.229	28.812	746.739
1865.5	1.56845	86.131	1033.572	306.404	29.645	727.168
1918.8	1.54432	84.847	1018.164	310.31	30.477	707.854
1972.1	1.52019	83.564	1002.768	313.946	31.308	688.822
2025.4	1.49606	82.28	987.36	317.313	32.138	670.047
2078.7	1.47193	80.997	971.964	320.411	32.965	651.553
2132	1.4478	79.713	956.556	323.239	33.792	633.317

2185.3	1.42367	78.429	941.148	325.798	34.617	615.35
2238.6	1.39954	77.146	925.752	328.088	35.44	597.664
2291.9	1.37541	75.862	910.344	330.108	36.262	580.236
2345.2	1.35128	74.579	894.948	331.859	37.081	563.089
2398.5	1.32715	73.295	879.54	333.341	37.899	546.199
2451.8	1.30302	72.012	864.144	334.553	38.715	529.591
2505.1	1.27889	70.728	848.736	335.496	39.529	513.24
2558.4	1.25476	69.445	833.34	336.169	40.34	497.171
2611.7	1.23063	68.161	817.932	336.573	41.149	481.359
2665	1.2065	66.878	802.536	336.708	41.956	465.828
2718.3	1.18237	65.594	787.128	336.573	42.76	450.555
2771.6	1.15824	64.31	771.72	336.169	43.561	435.551
2824.9	1.13411	63.027	756.324	335.496	44.359	420.828
2878.2	1.10998	61.743	740.916	334.553	45.154	406.363
2931.5	1.08585	60.46	725.52	333.341	45.945	392.179
2984.8	1.06172	59.176	710.112	331.859	46.733	378.253
3038.1	1.03759	57.893	694.716	330.108	47.517	364.608
3091.4	1.01346	56.609	679.308	328.088	48.297	351.22
3144.7	0.98933	55.326	663.912	325.798	49.072	338.114
3198	0.9652	54.042	648.504	323.239	49.844	325.265
3251.3	0.94107	52.758	633.096	320.411	50.61	312.685
3304.6	0.91694	51.475	617.7	317.313	51.37	300.387
3357.9	0.89281	50.191	602.292	313.946	52.125	288.346
3411.2	0.86868	48.908	586.896	310.31	52.873	276.586
3464.5	0.84455	47.624	571.488	306.404	53.615	265.084
3517.8	0.82042	46.341	556.092	302.229	54.349	253.863
3571.1	0.79629	45.057	540.684	297.784	55.075	242.9
3624.4	0.77216	43.774	525.288	293.07	55.792	232.218
3677.7	0.74803	42.49	509.88	288.087	56.501	221.793
3731	0.7239	41.207	494.484	282.835	57.198	211.649
3784.3	0.69977	39.923	479.076	277.313	57.885	201.763
3837.6	0.67564	38.639	463.668	271.521	58.559	192.147
3890.9	0.65151	37.356	448.272	265.46	59.219	182.812
3944.2	0.62738	36.072	432.864	259.13	59.864	173.734
3997.5	0.60325	34.789	417.468	252.531	60.491	164.937
4050.8	0.57912	33.505	402.06	245.662	61.101	156.398
4104.1	0.55499	32.222	386.664	238.524	61.688	148.14
4157.4	0.53086	30.938	371.256	231.116	62.252	140.14
4210.7	0.50673	29.655	355.86	223.439	62.788	132.421
4264	0.4826	28.371	340.452	215.493	63.296	124.959
4317.3	0.45847	27.087	325.044	207.277	63.769	117.767
4370.6	0.43434	25.804	309.648	198.792	64.199	110.856
4423.9	0.41021	24.52	294.24	190.038	64.586	104.202
4477.2	0.38608	23.237	278.844	181.014	64.916	97.83
4530.5	0.36195	21.953	263.436	171.721	65.185	91.715

4583.8	0.33782	20.67	248.04	162.158	65.376	85.882
4637.1	0.31369	19.386	232.632	152.327	65.48	80.305
4690.4	0.28956	18.103	217.236	142.225	65.47	75.011
4743.7	0.26543	16.819	201.828	131.855	65.33	69.973
4797	0.2413	15.536	186.432	121.215	65.018	65.217
4850.3	0.21717	14.252	171.024	110.305	64.497	60.719
4903.6	0.19304	12.968	155.616	99.127	63.7	56.489
4956.9	0.16891	11.685	140.22	87.679	62.53	52.541
5010.2	0.14478	10.401	124.812	75.961	60.86	48.851
5063.5	0.12065	9.118	109.416	63.974	58.469	45.442
5116.8	0.09652	7.834	94.008	51.718	55.014	42.29
5170.1	0.07239	6.551	78.612	39.193	49.856	39.419
5223.4	0.04826	5.267	63.204	26.398	41.766	36.806
5276.7	0.02413	3.984	47.808	13.334	27.891	34.474
5330	0	2.7	32.4	0	0	32.4

A3. Gearbox and Gripper Component Inertias

All inertias are calculated using Solidwork's "Mass Analysis" tool. The inertias for the gearbox components are:

Component name	Component image	Material	Density (g/mm ³)	Moment of inertia (g.mm ²)
8mm Shaft Hollowed		Aluminium 3003 Alloy	0.0027	40.38
8mm Shaft Stepped Geared		Aluminium 3003 Alloy	0.0027	30.13
8mm Shaft Stepped Short		Aluminium 3003 Alloy	0.0027	46.92
8mm Shaft Stepped		Aluminium 3003 Alloy	0.0027	48.95
8mm Shaft		Aluminium 3003 Alloy	0.0027	45.99
10 Teeth Gear		Aluminium 3003 Alloy	0.0027	4.38
15mm Shaft		Aluminium 3003 Alloy	0.0027	359.60

40 Teeth Gear		Aluminium 3003 Alloy	0.0027	682.60
78 Teeth Gear		Aluminium 3003 Alloy	0.0027	8847.36
59 Teeth Gear		Aluminium 3003 Alloy	0.0027	2446.96
160 Teeth Gear		Aluminium 3003 Alloy	0.0027	126494.59

Reflecting the speed gears first to shaft 3:

$$J_{3,S} = \frac{J_{5,e}}{N_S^2} = \left(J_5 + \frac{J_6}{N_S^2} \right) \frac{1}{N_S^2}$$

Where,

$$\frac{N_4}{N_3} = \frac{N_6}{N_5} = N_S$$

Doing the same for the torque gears:

$$J_{3,T} = \frac{J_{8,e}}{N_T^2} = \left(J_8 + \frac{J_9}{N_T^2} \right) \frac{1}{N_T^2}$$

Where,

$$\frac{N_7}{N_3} = \frac{N_9}{N_8} = N_T$$

Therefore, the total effective inertia at shaft 3 is:

$$J_{3,e} = J_3 + \left(J_5 + \frac{J_6}{N_S^2} \right) \frac{1}{N_S^2} + \left(J_8 + \frac{J_9}{N_T^2} \right) \frac{1}{N_T^2}$$

So, the total reflected inertia to the motor is:

$$J_{M,e} = J_M + \frac{J_{3,e}}{N_H^2} = J_M + \left[J_3 + \left(J_5 + \frac{J_6}{N_S^2} \right) \frac{1}{N_S^2} + \left(J_8 + \frac{J_9}{N_T^2} \right) \frac{1}{N_T^2} \right] \frac{1}{N_H^2}$$

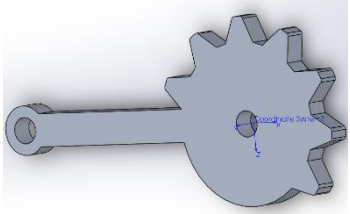
$$J_{M,e} = 682.6 + \left[126,858.57 + \left(2,498.26 + \frac{2,477.09}{5.9^2} \right) \frac{1}{5.9^2} + \left(8,900.69 + \frac{8,893.35}{7.8^2} \right) \frac{1}{7.8^2} \right] \frac{1}{4^2}$$

$$= 8,625.17 \text{ g.mm}^2$$

Notice that the majority of the reflected inertia comes from the 160 toothed gear and the motor inertia ($126,858.57 * (1/4^2) + 682.6 = 8,611.26$).

Inertias for the gripper assembly components are given as follows:

Component name	Component image	Material	Density (g/mm ³)	Moment of inertia (g.mm ²)
Sleeve		Aluminium 3003 Alloy	0.0027	825.1
Output Gear		Aluminium 3003 Alloy	0.0027	1,736.5
8mm Output Shaft		Aluminium 3003 Alloy	0.0027	2,901.5

Link Geared		Aluminium 3003 Alloy	0.0027	63,553.7
-------------	---	----------------------	--------	----------

A4. Arduino Code for DC Motor Control

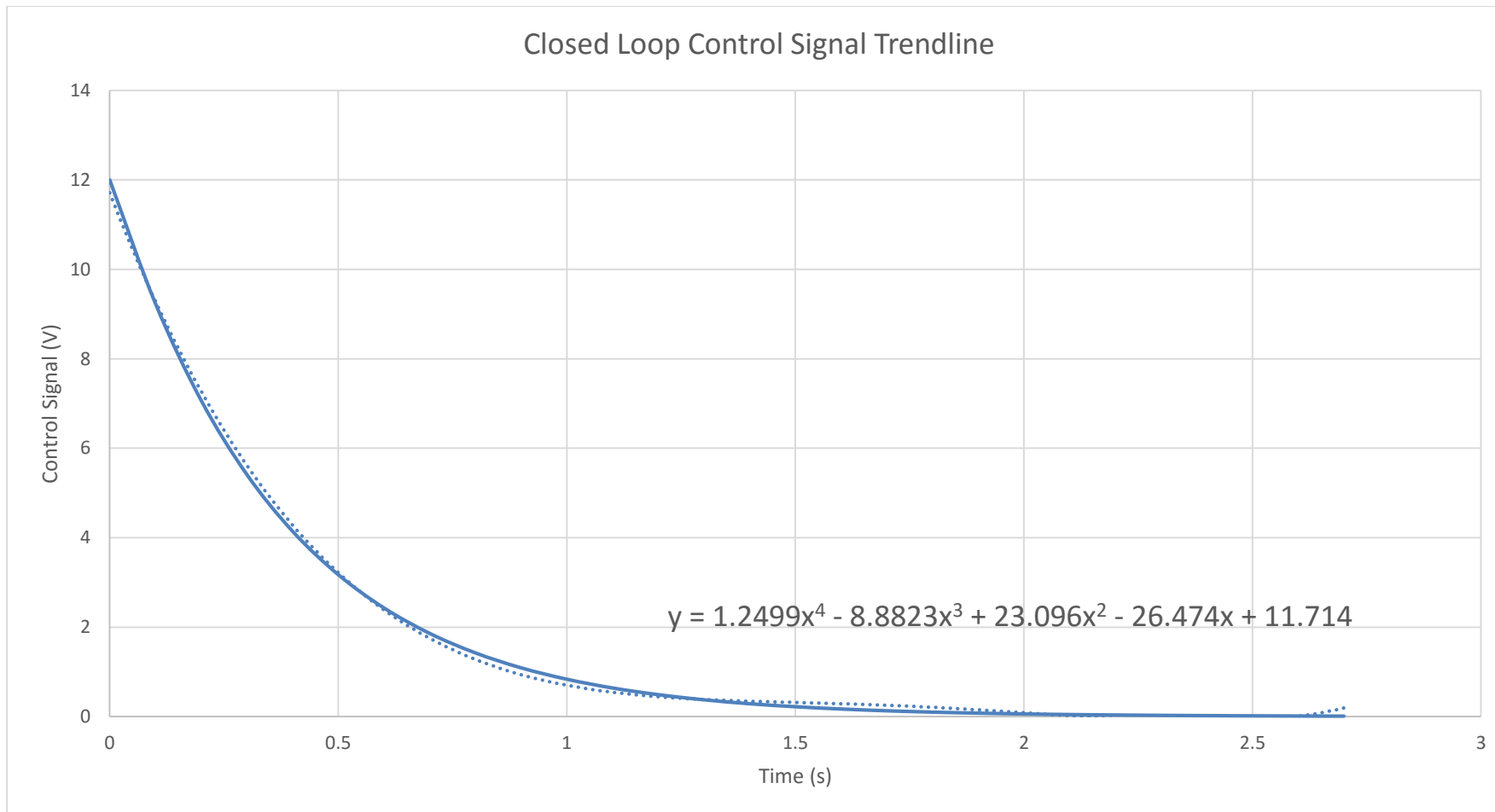
```
//setting constants for the input and output pins
const int SwitchCW = A1;
const int SwitchACW = A2;
const int PinCW = 6;
const int PinACW = 5;

//setting variables for measuring motor speed and direction
int motorSpeed = 0;
int CWSwitchState = 0;
int ACWSwitchState = 0;

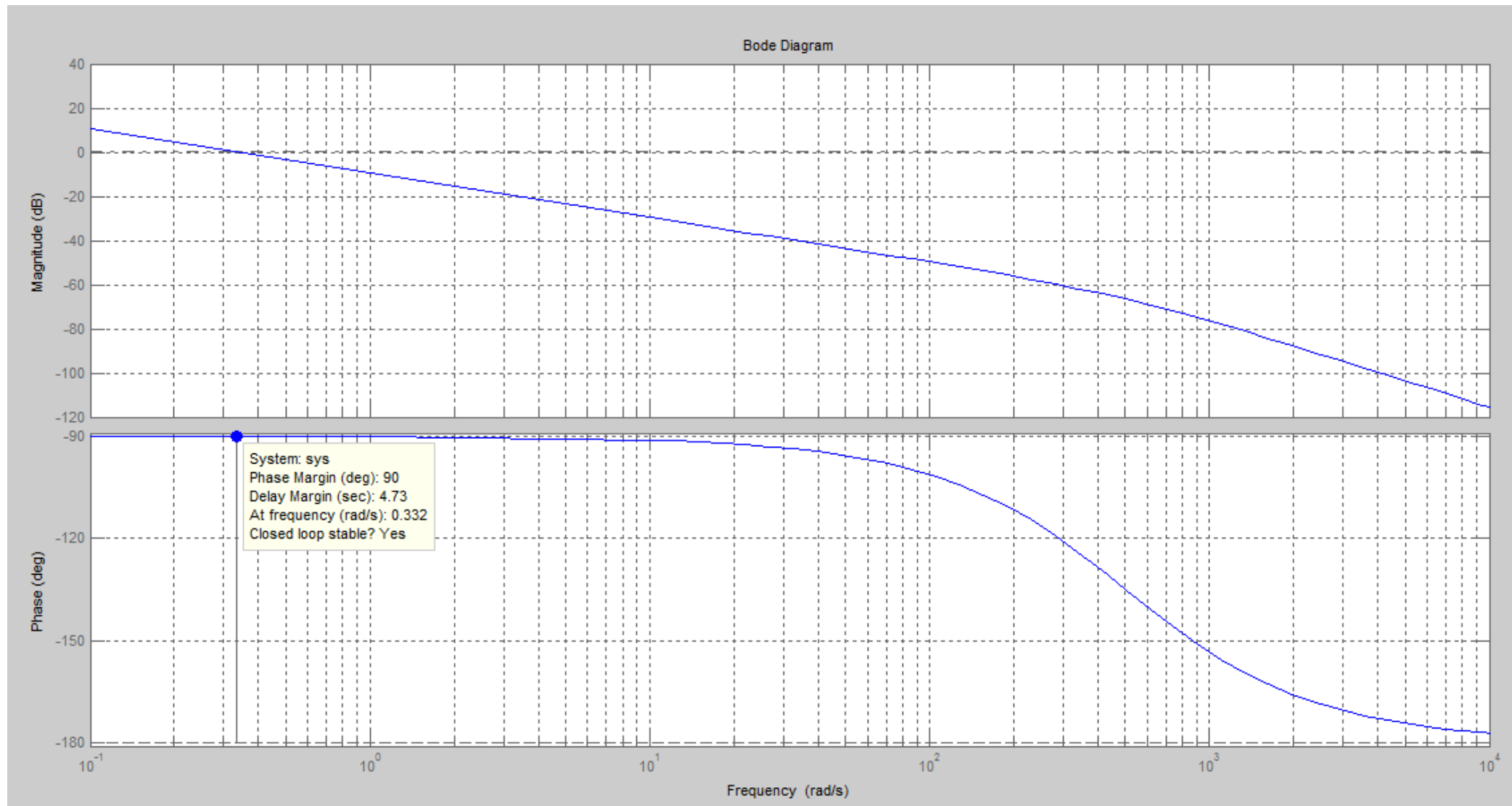
void setup() {
  pinMode(SwitchCW, INPUT);
  pinMode(SwitchACW, INPUT);
  pinMode(PinCW, OUTPUT);
  pinMode(PinACW, OUTPUT);
}

void loop() {
  CWSwitchState = digitalRead(SwitchCW);
  ACWSwitchState = digitalRead(SwitchACW); //this line and the one above reads the voltage levels of the two input switches
  motorSpeed = 256 * 0.5; //here the motor speed is fixed at half. an analog input would need to be implemented for the user to control motor speed

  if (CWSwitchState == 1) {
    if (ACWSwitchState == 0) {
      digitalWrite(PinCW, motorSpeed); //if CW switch is HIGH and ACW is LOW, the motor is driven in a CW direction at the set motor speed
    }
  }
  else if (ACWSwitchState == 1) {
    digitalWrite(PinACW, motorSpeed); //if ACW switch is HIGH and CW is LOW, the motor is driven in an ACW direction
  }
  else {
    digitalWrite(PinCW, 0);
    digitalWrite(PinACW, 0); //if both switches are HIGH or both are LOW, the motor is set to stationary
  }
}
```

A5. Closed Loop Control Signal Trendline Fitting Using Excel's "Trendline" Tool

A6. Bode Plots for the TF of the System



A7. Engineering Drawings

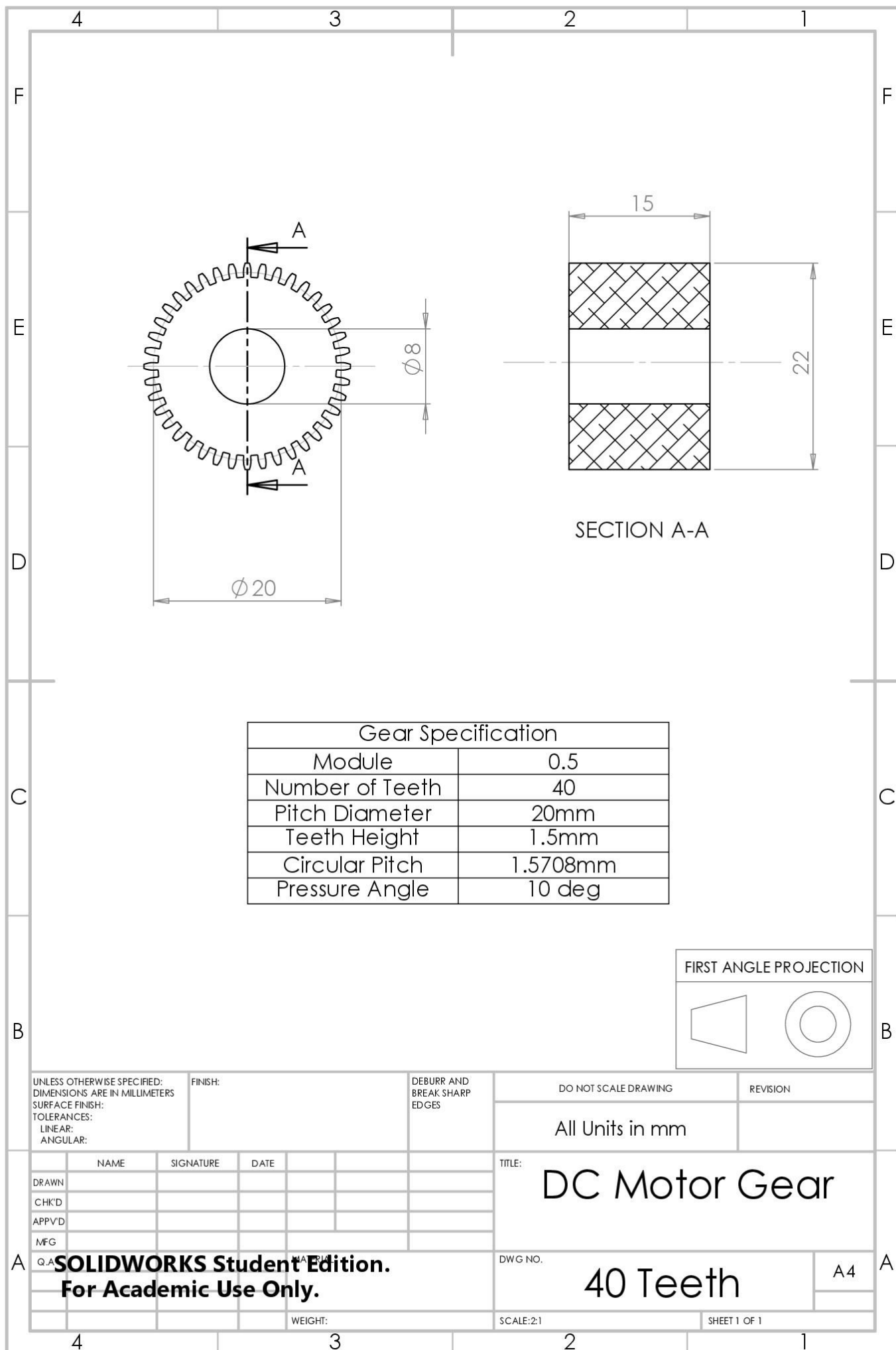
	4	3	2
F			F
E			E
D			D
C			C
B			B
A			A

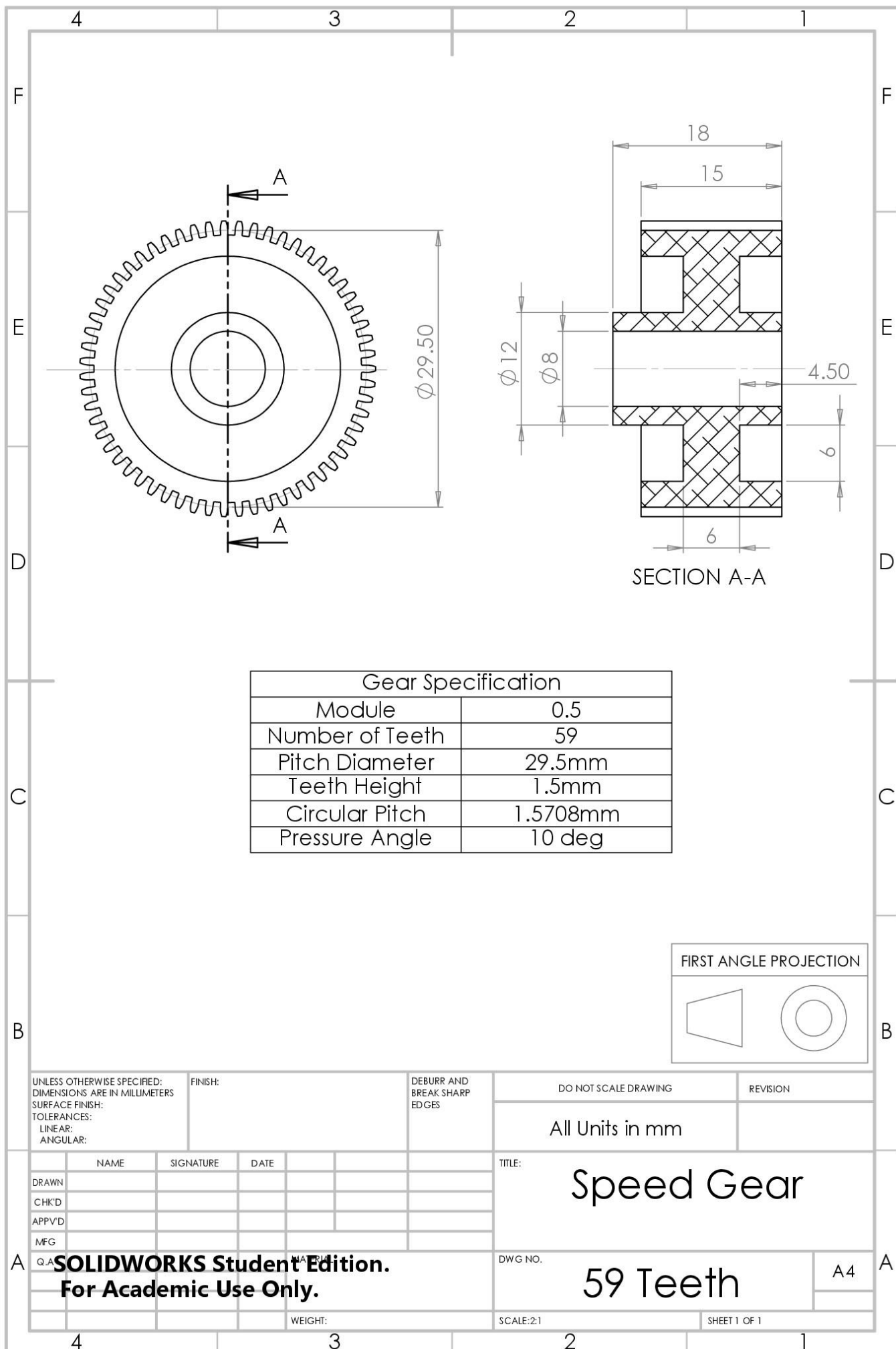
SECTION A-A

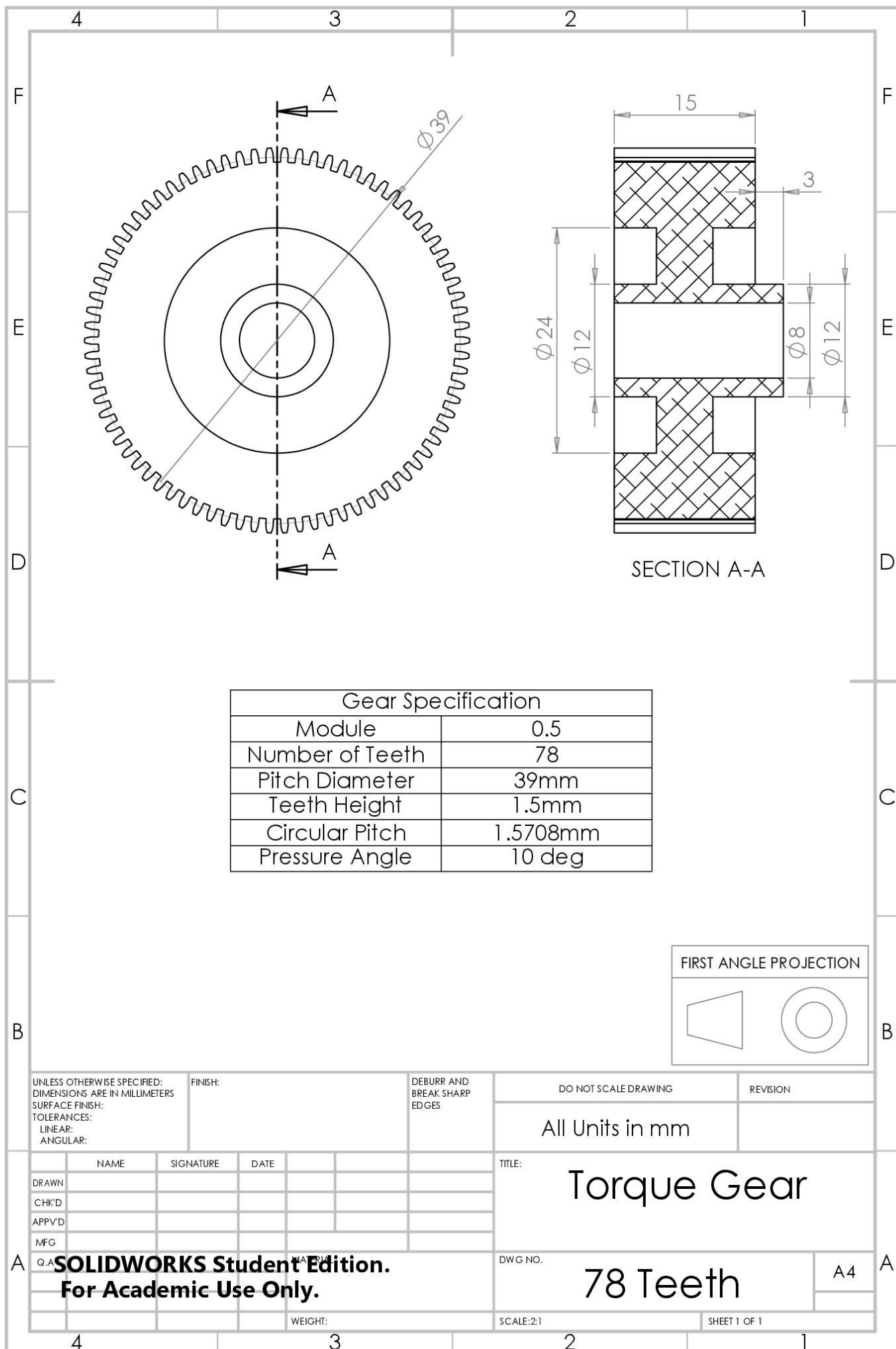
Gear Specification	
Module	0.5
Number of Teeth	10
Pitch Diameter	5mm
Teeth Height	1.5mm
Circular Pitch	1.5708mm
Pressure Angle	10 deg

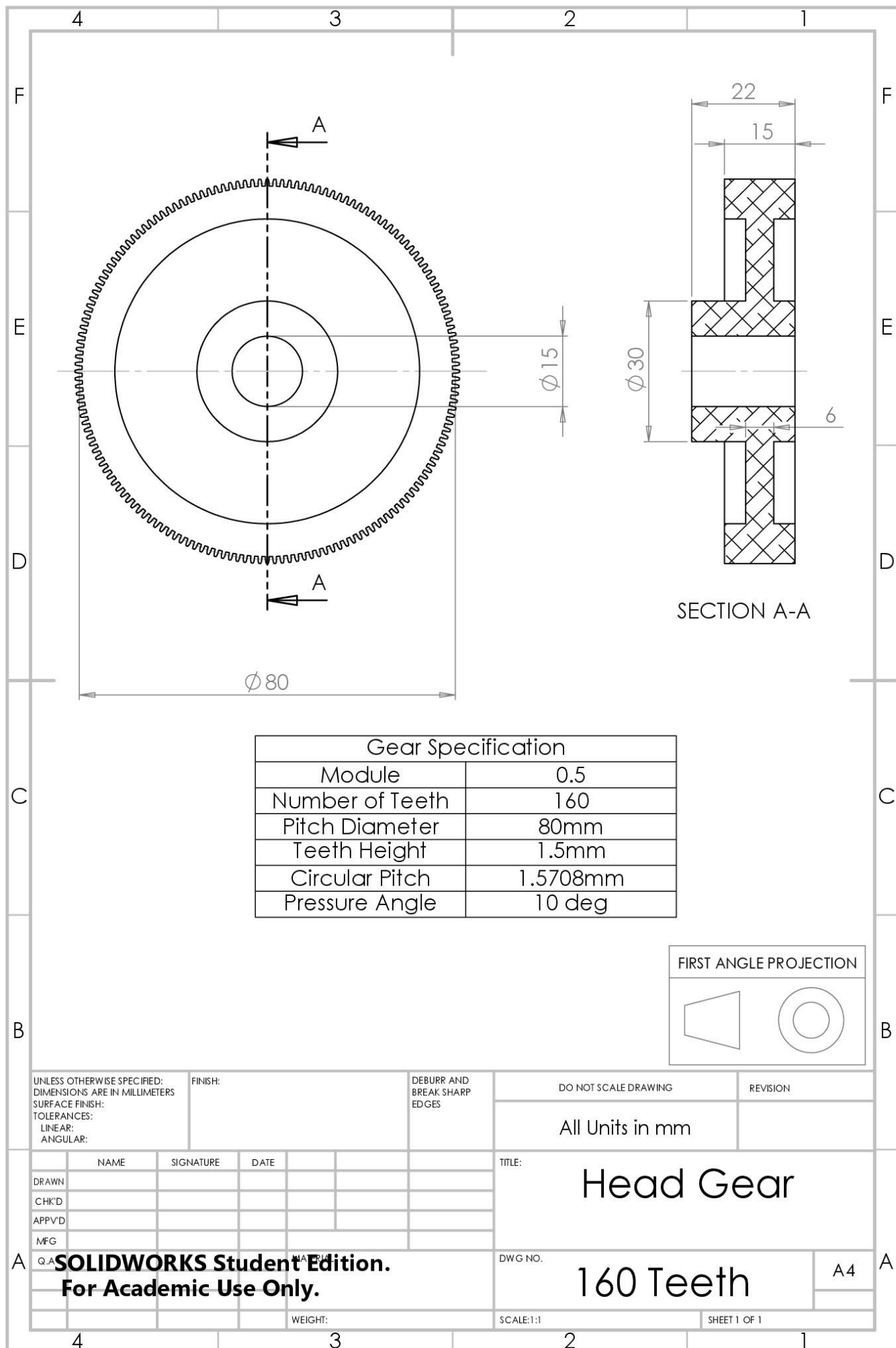
FIRST ANGLE PROJECTION	

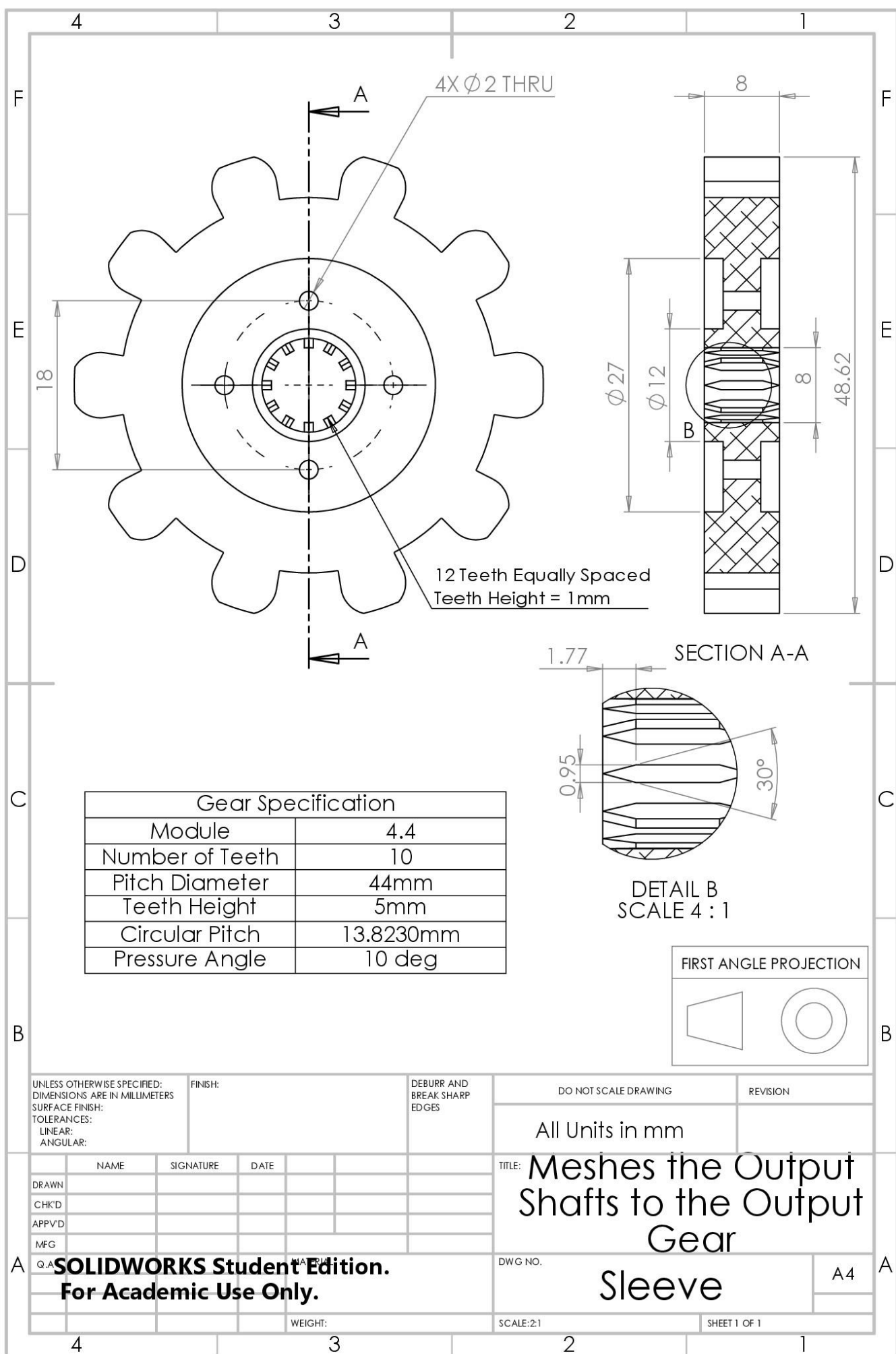
UNLESS OTHERWISE SPECIFIED: DIMENSIONS ARE IN MILLIMETERS SURFACE FINISH: TOLERANCES: LINEAR: ANGULAR:		FINISH:	DEBURR AND BREAK SHARP EDGES	DO NOT SCALE DRAWING	REVISION
All Units in mm					
DRAWN	NAME	SIGNATURE	DATE	TITLE: Splitter Gear	
CHK'D					
APP'D					
MFG					
A Q.A SOLIDWORKS Student Edition. For Academic Use Only.				DWG NO. 10 Teeth	A4
				SCALE: 5:1	SHEET 1 OF 1
				4	3
				2	1

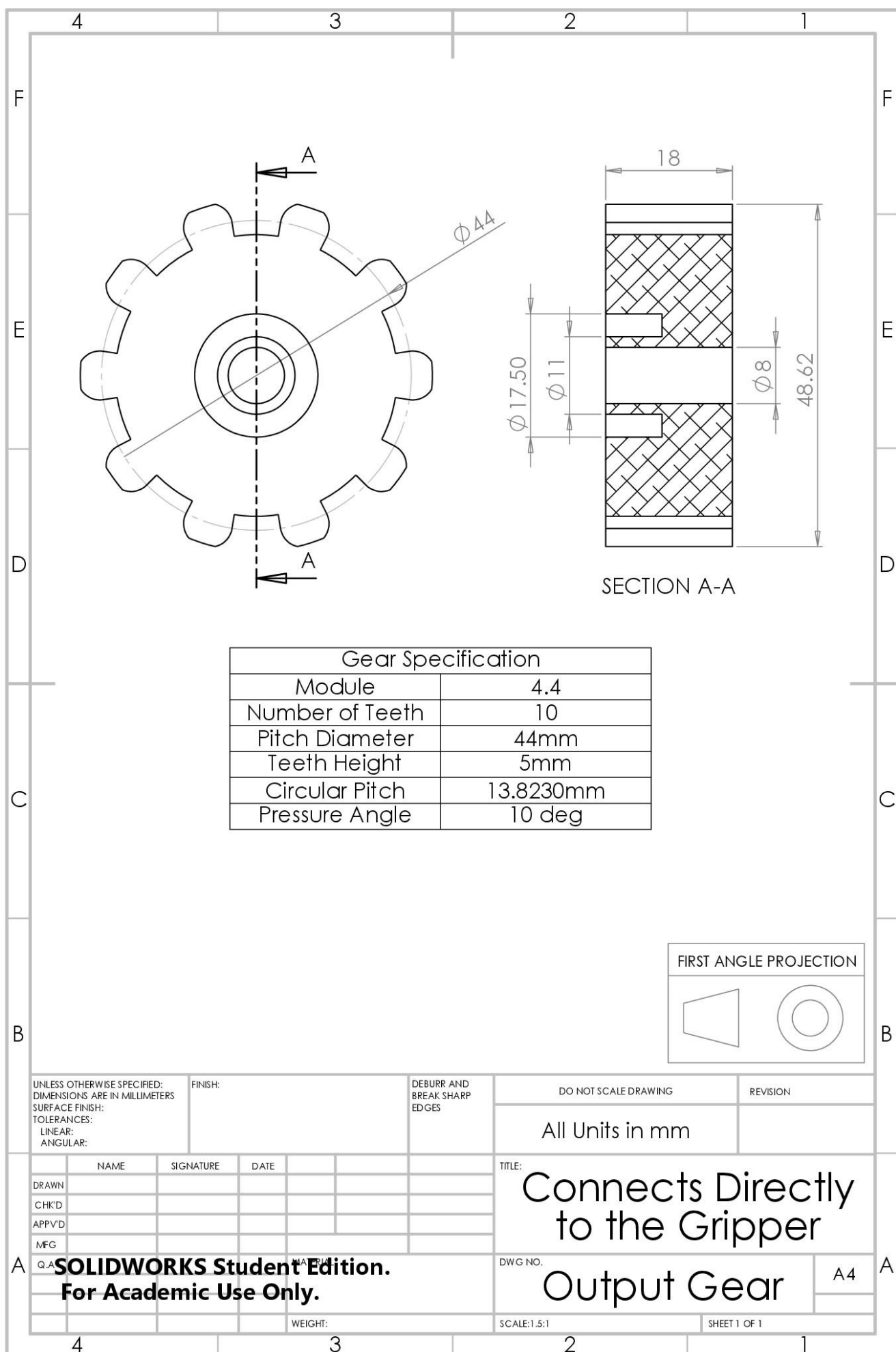


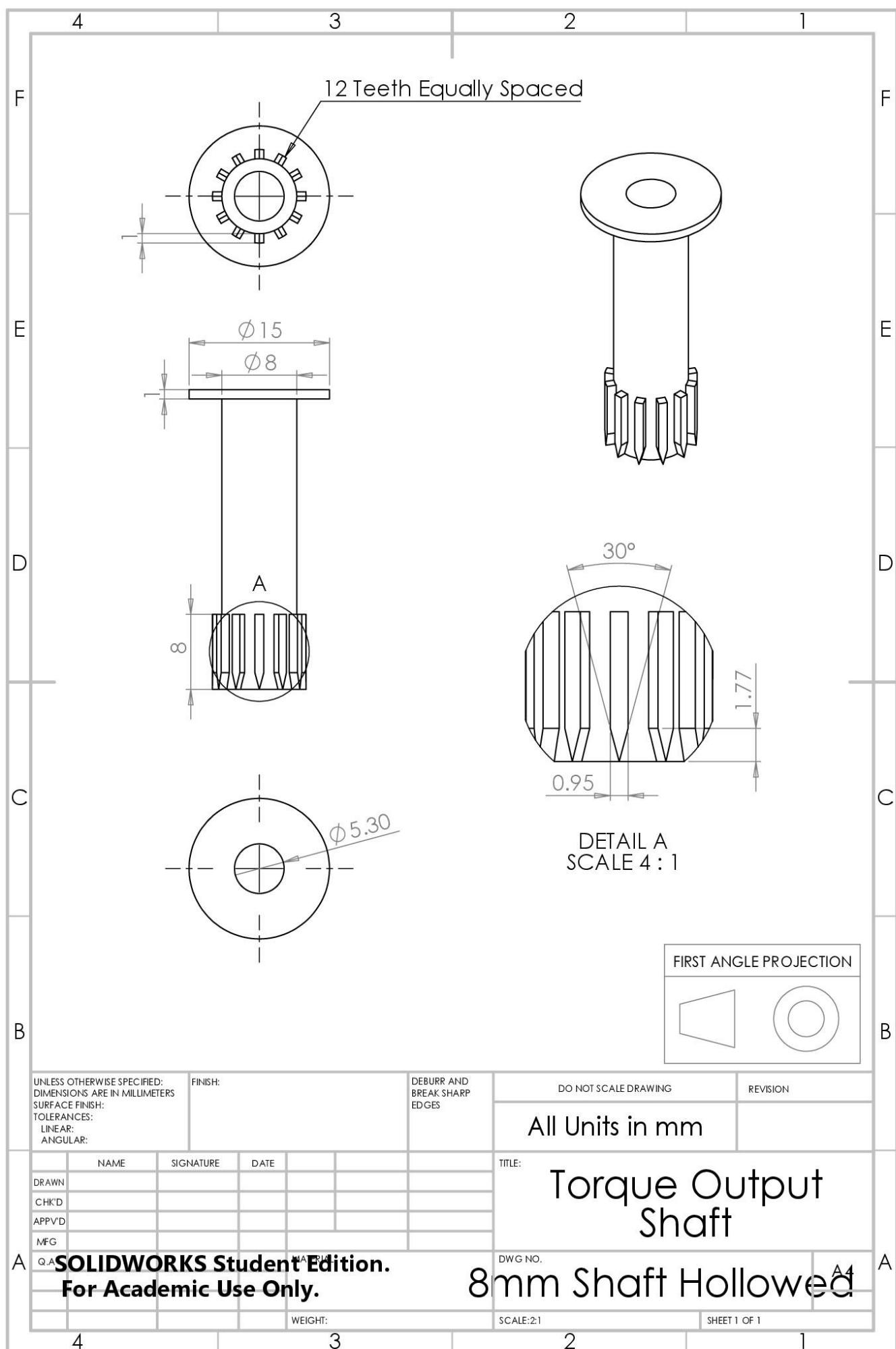


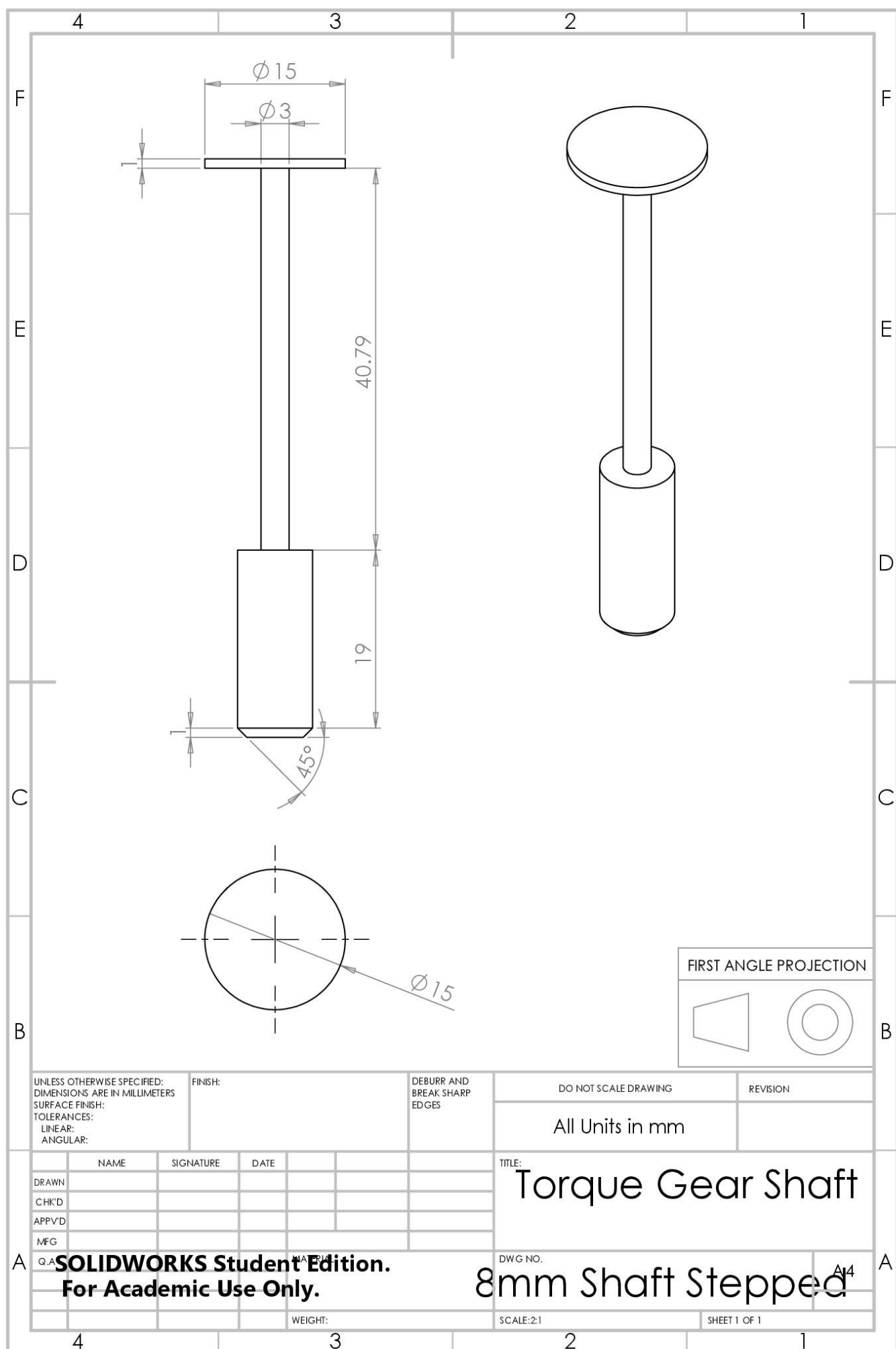


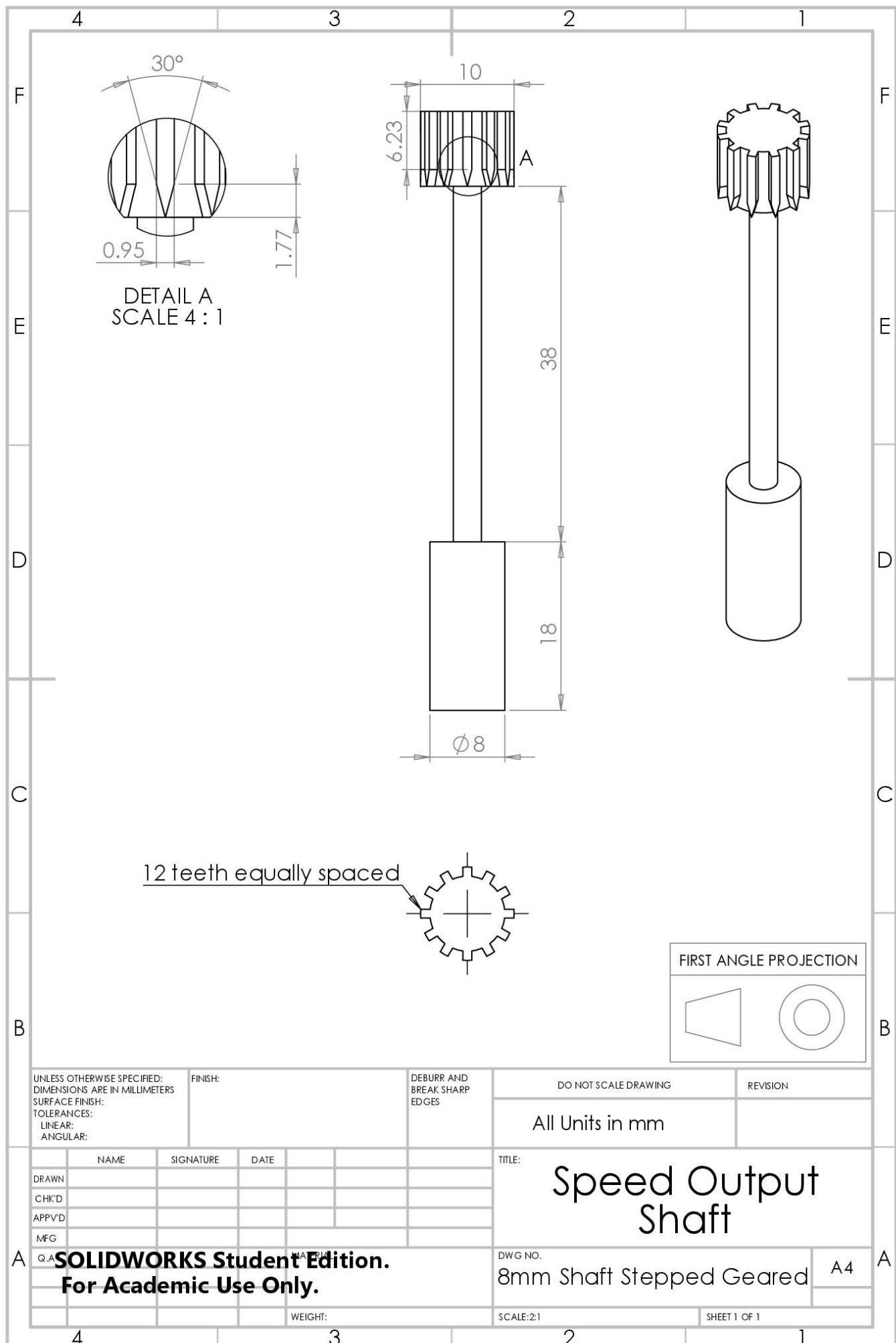


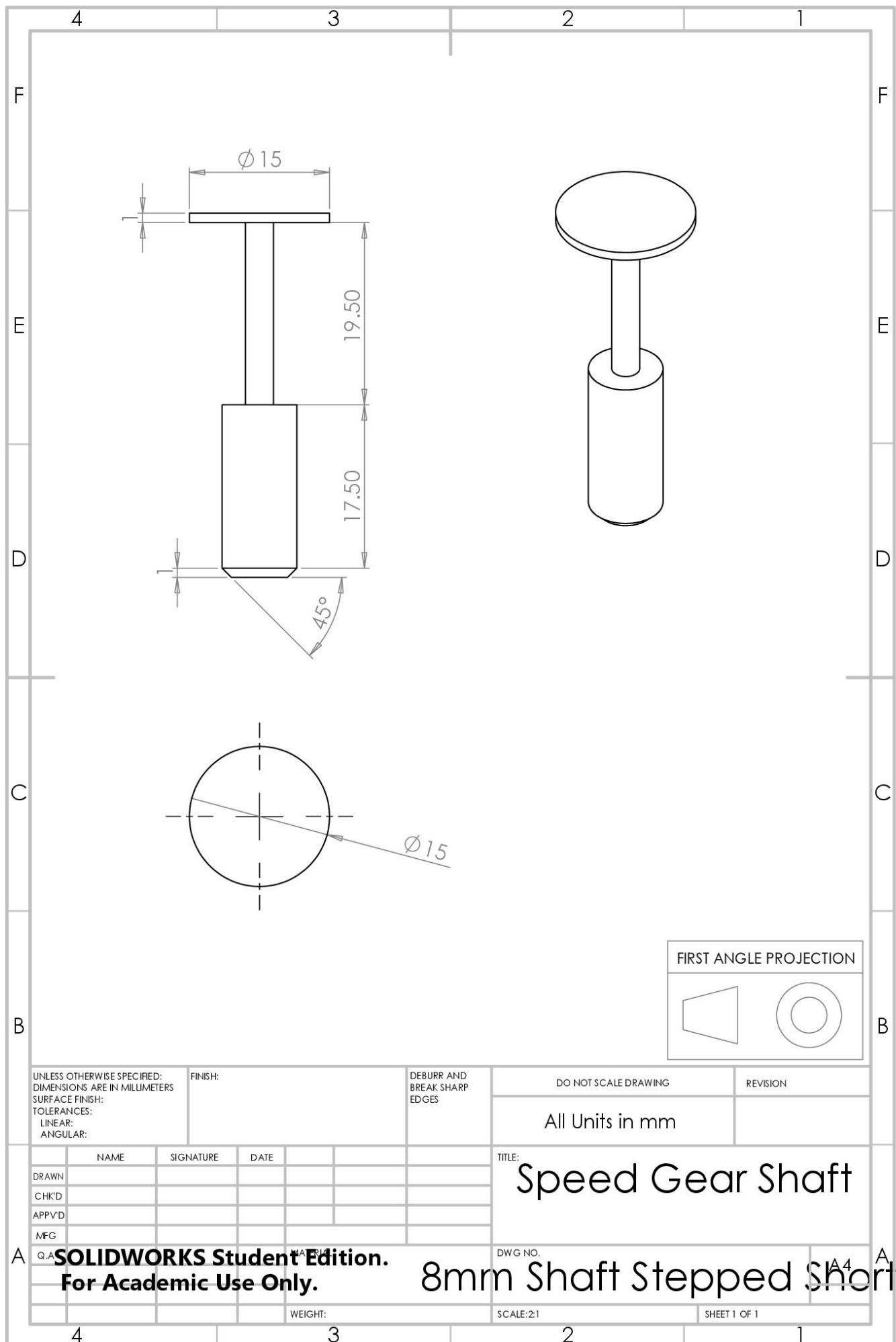


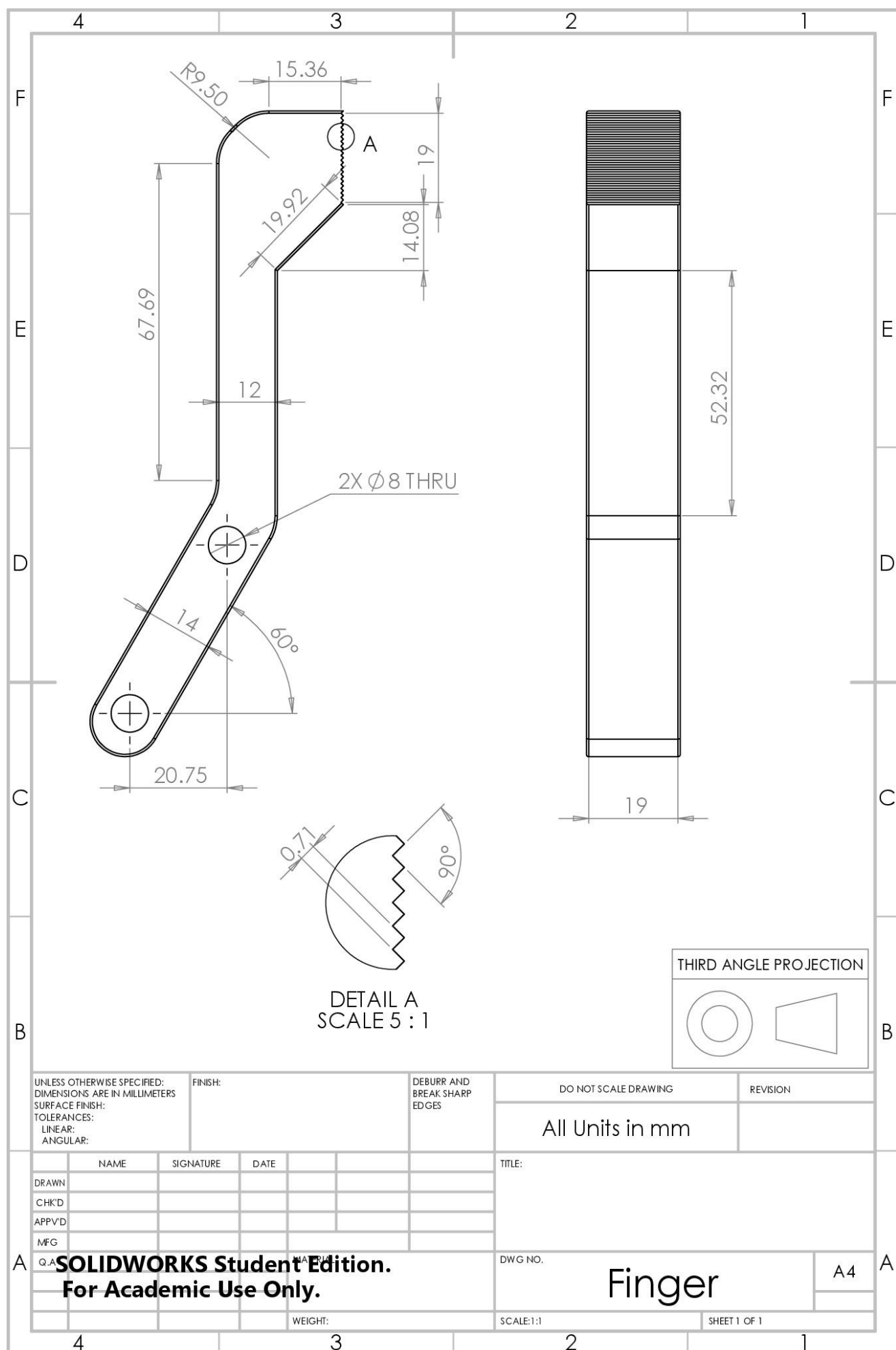


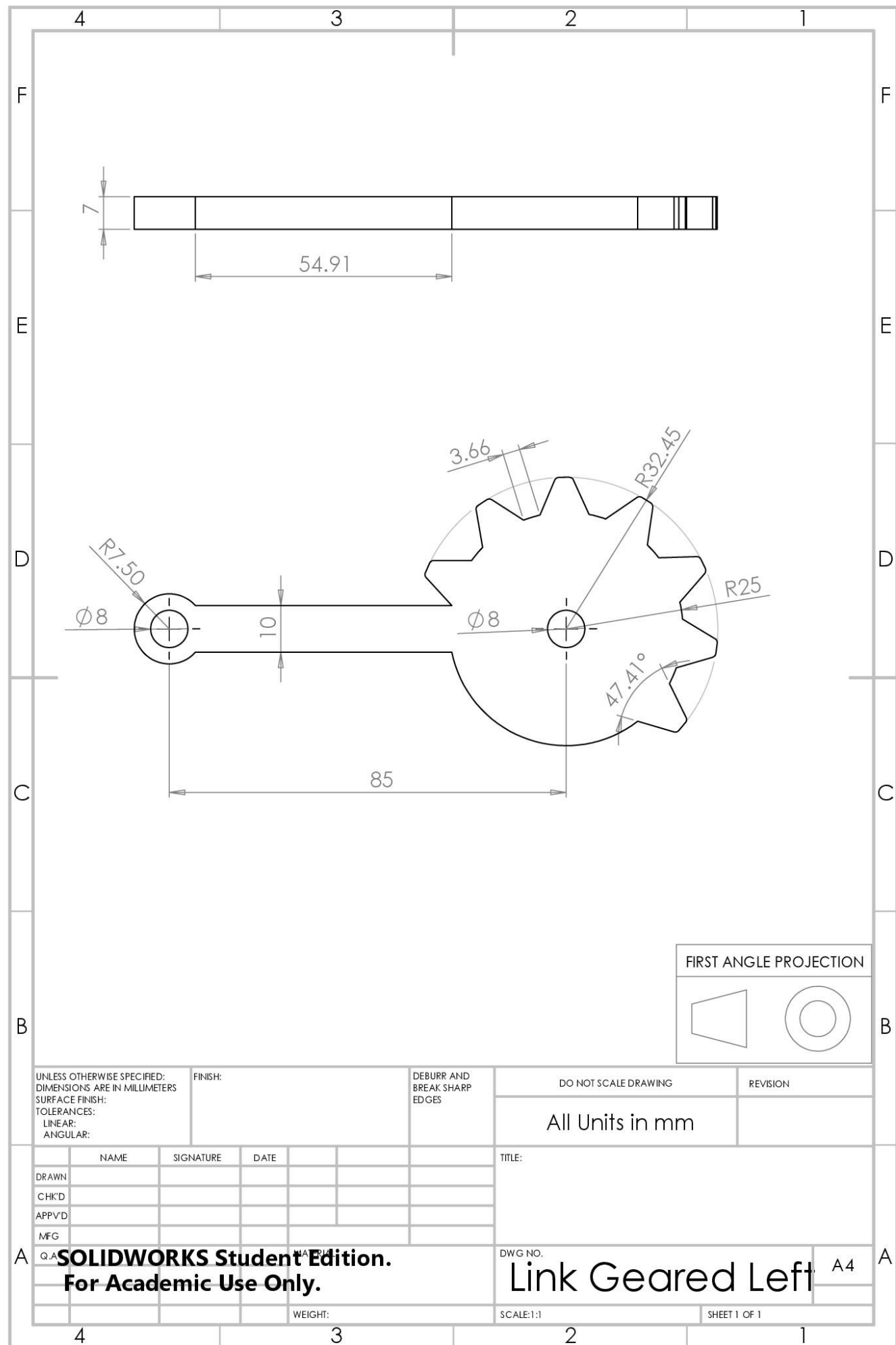


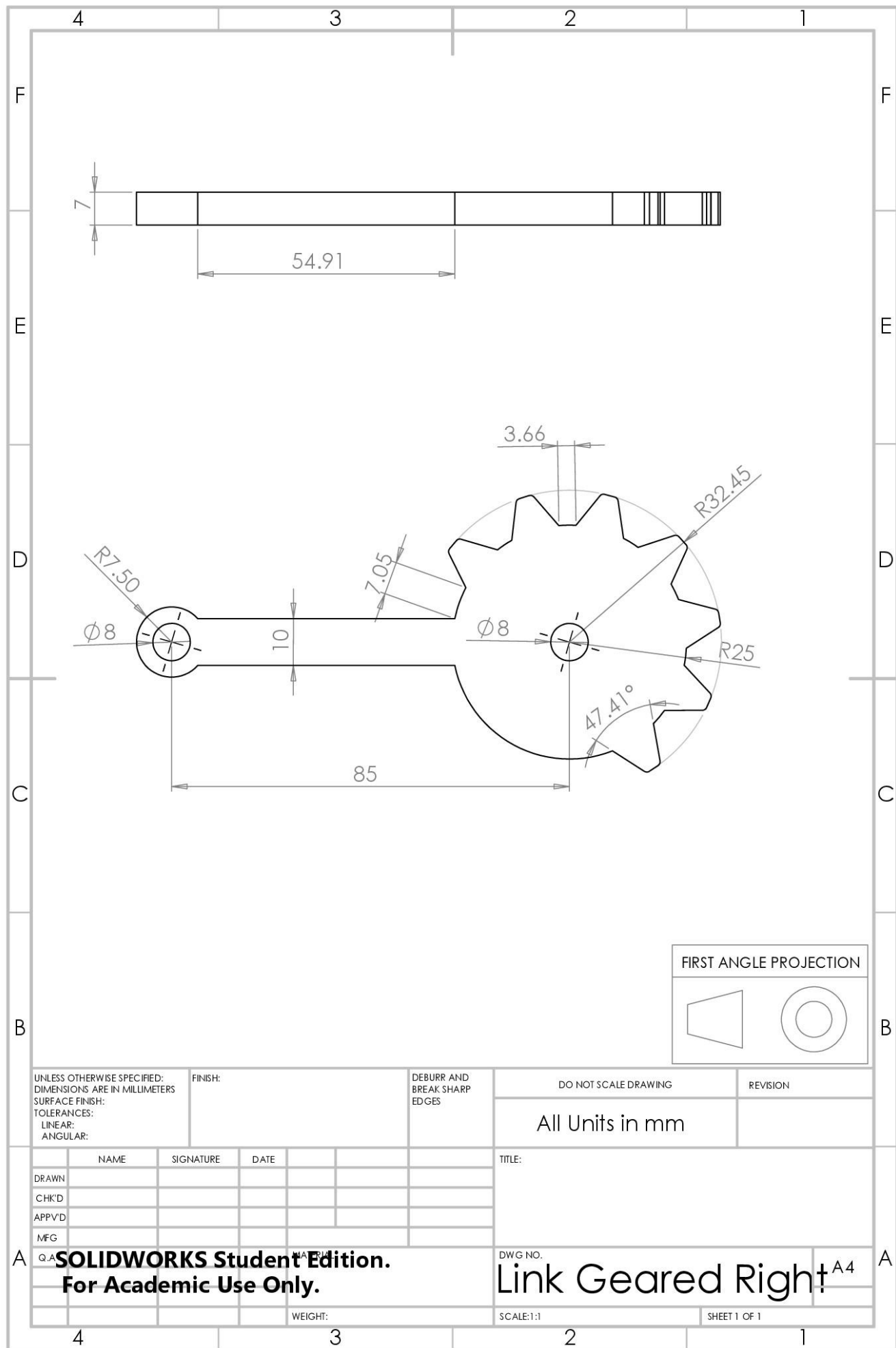


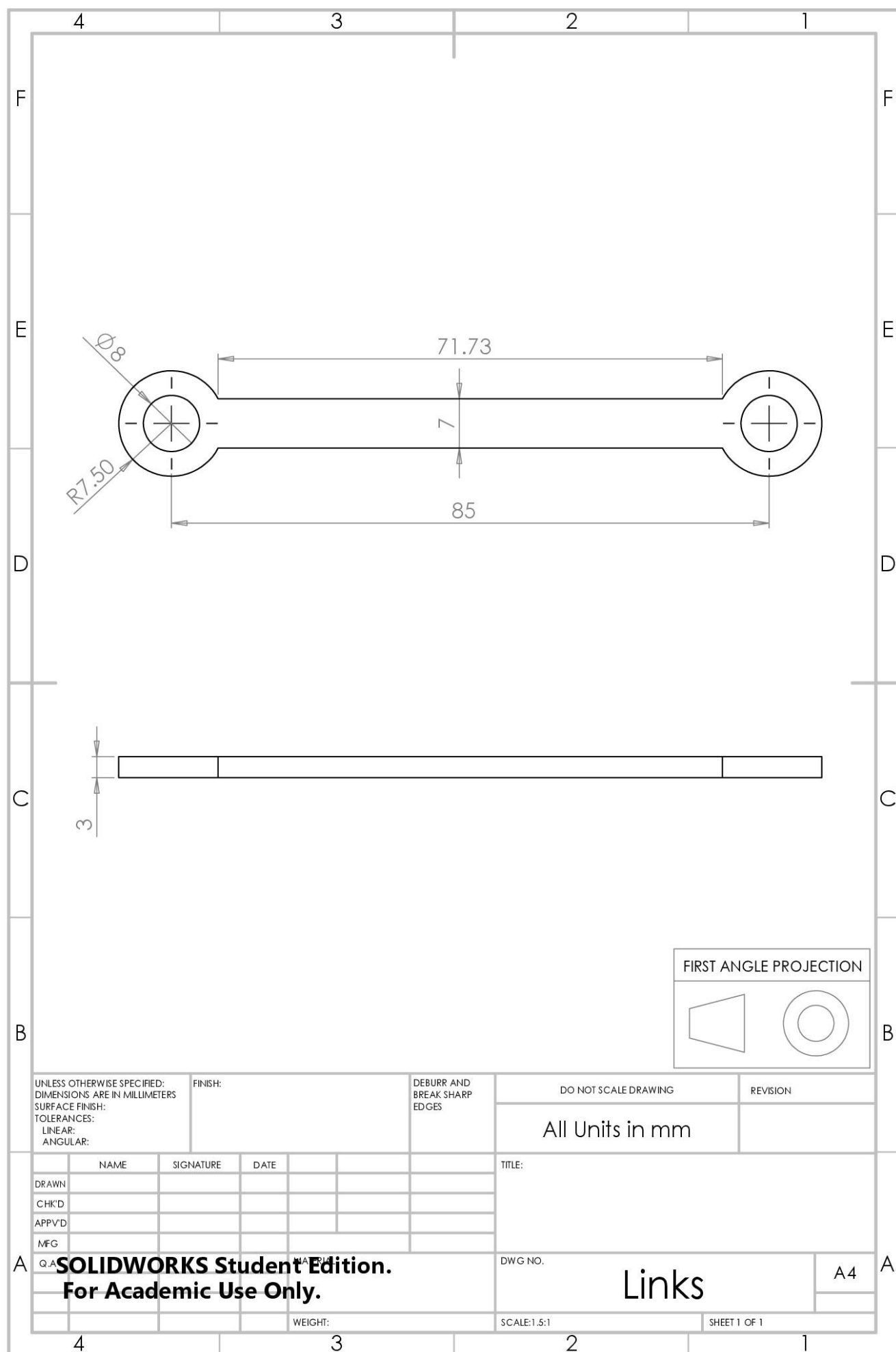


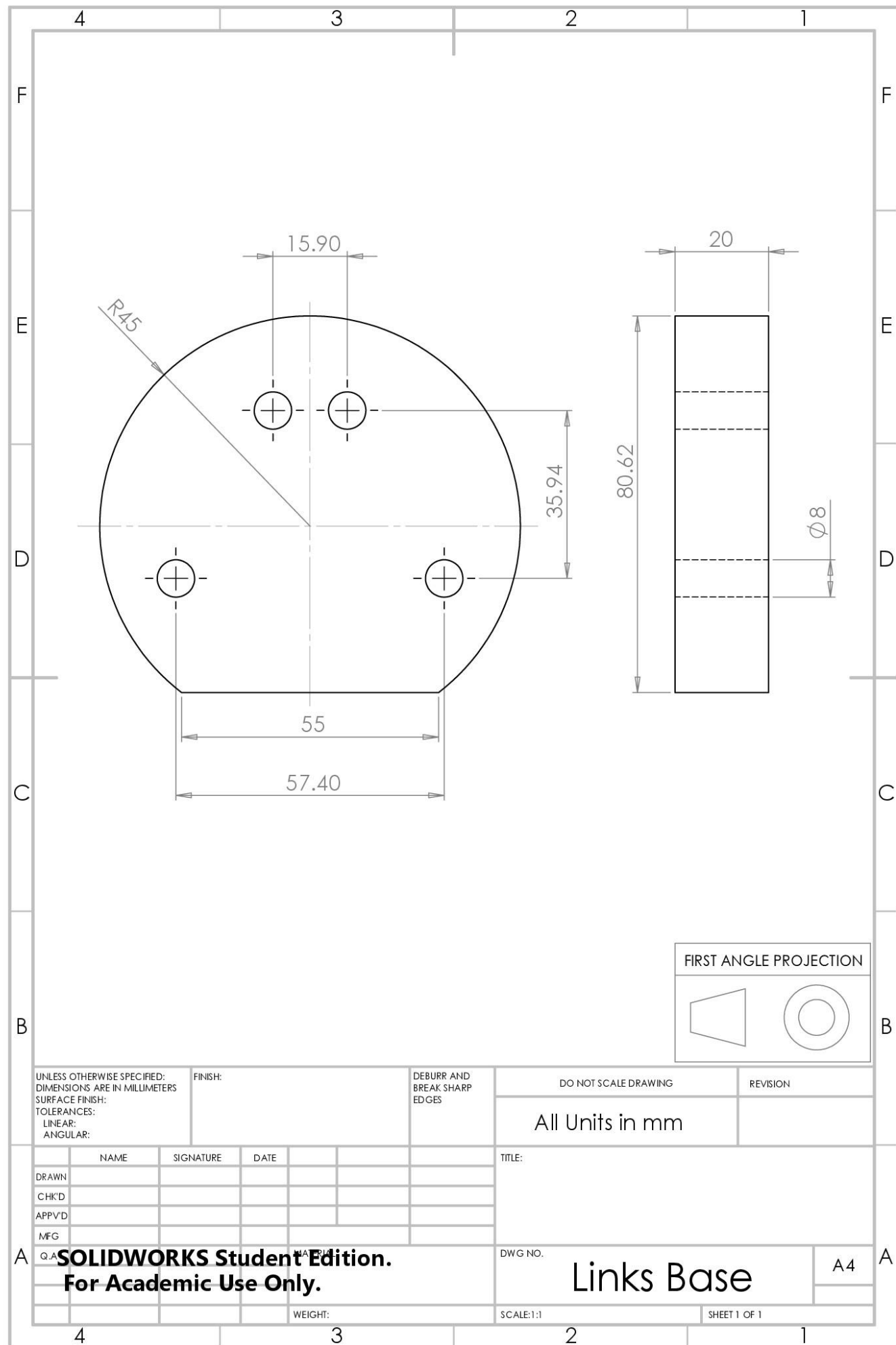






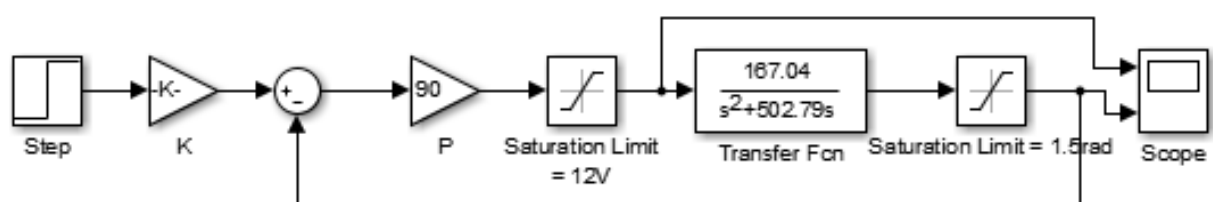
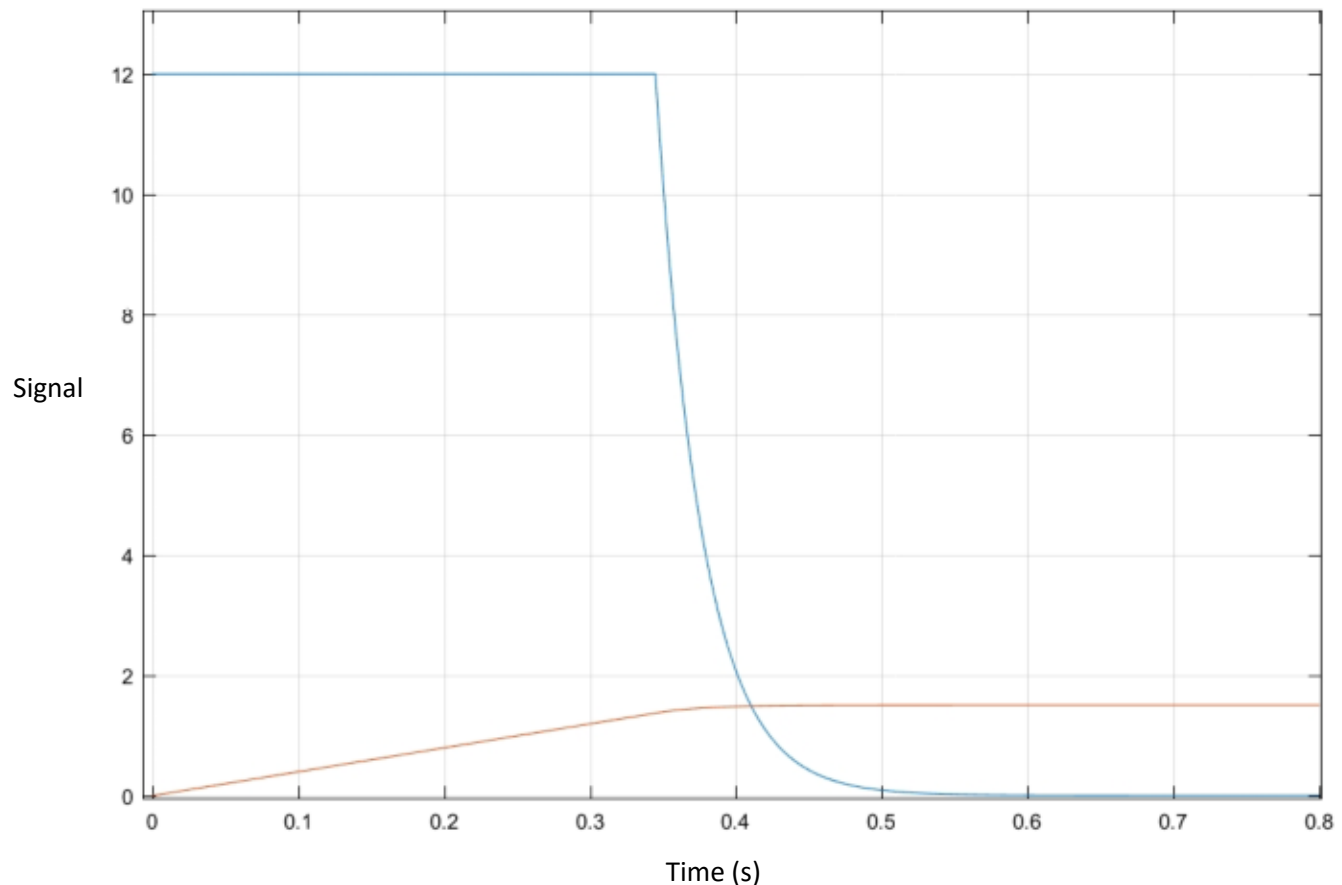






A8. CL Response Plots for Increased Proportional Gain

The response here is for a proportional gain value of 90. The gripper is able to reach 95% of full closure within a time of 0.36s, close to the OL closure time. Notice the limiting of the control signal at 12V, before decaying at around 0.345s as the gripper reaches full closure.



A9. Gripper Angle at Full Closure